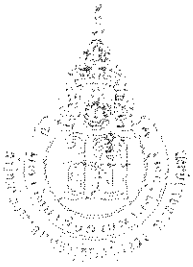

Modeling of Adsorption Isotherms for Supercritical Fluids on Microporous Adsorbents

Panita Sumanatrakul

A Thesis Submitted in Partial Fulfillment of the Requirements for the Degree of

Doctor of Engineering in Chemical Engineering

Prince of Songkla University

2010

Thesis Title	Modeling of Adsorption Isotherms for Supercritical Fluids on Microporous Adsorbents
Author	Miss Panita Sumanatrakul
Major Program	Chemical Engineering

Major Advisor:

.....

(Asst. Prof. Dr. Chayanoot Sangwichien)

Co-advisor:

.....

(Prof. Dr. Marc D. Donohue)

Examining Committee :

.....Chairperson

(Asst. Prof. Dr. Sukritthira Ratanawilai)

.....

(Asst. Prof. Dr. Chayanoot Sangwichien)

.....

(Prof. Dr. Marc D. Donohue)

.....

(Asst. Prof. Dr. Chairat Siripatana)

The Graduate School, Prince of Songkla University, has approved this thesis as partial fulfillment of the requirements for the Doctor of Engineering Degree in Chemical Engineering

.....

(Prof. Dr. Amornrat Phongdara)

Dean of Graduate School

Thesis Title	Modeling of Adsorption Isotherms for Supercritical Fluids on Microporous Adsorbents
Author	Miss Panita Sumanatrakul
Major Program	Chemical Engineering
Academic Year	2010

ABSTRACT

The Ono-Kondo lattice model is able to predict all known types of adsorption behavior including supercritical systems. In Chapter 1 is presented a brief review of adsorption models for supercritical fluids. It is interesting to respect on Ono-Kondo model because it features to describe both of monolayer and multilayer adsorption isotherms based on the physical properties of the adsorbate and accessible characterization of the adsorbents. And it also incorporates accurate density calculations which may reduce the correlative burden of the adsorption model.

In Chapter 2, adsorption behavior for supercritical fluids is analyzed in the framework of the Ono-Kondo lattice theory. By changing two energetic parameters as energies for adsorbate-adsorbent and adsorbate-adsorbate interactions, supercritical adsorption isotherms are sensitive to change with these interactions. Results show that increasing ε_s/kT (adsorbate-adsorbent interactions) leads to increase in the Henry's constant and the adsorption becoming stronger. On the other hand, for small values of ε/kT (adsorbate-adsorbate interactions) the adsorption isotherm is relatively independent of this parameter over a wide range of reduced densities. Moreover, the Gibbs adsorption isotherms for supercritical gases are calculated from equation (2.22) that are sensitive to change in ε_s/kT and ε/kT values. The Gibbs adsorption isotherms under supercritical conditions have a negative slope and decrease as the pressure (or density) increases. This is because the bulk density is increasing but the monolayer density is constant. Therefore, at supercritical region allow nearly complete monolayer coverage but there is not multilayer adsorption because the temperature is sufficiently above the critical temperature of the adsorbate and the pressures are high enough for a completely covered monolayer.

In Chapter 3, the Ono-Kondo approach is used for analysis of intermolecular interactions in adsorbed phases for supercritical systems. Experimental isotherms for adsorption of supercritical fluids (including nitrogen, methane, and carbon dioxide) are plotted in Ono-Kondo coordinates in two ways: with variable Henry's constant, H, and with the Henry's constant estimated based on results of modeling as well as calorimetric and chromatographic measurements. Linear sections of these graphs show the range of applicability of the classical Ono-Kondo model with constant energies of adsorbate-adsorbate interactions, U_m; the slopes of these lines are related to the adsorbate-adsorbate energies.

The generalized Ono-Kondo model is applied over a wide range of pressures - from Henry's law range to supercritical pressures. When this is done, U_m varies from positive at low pressures to negative at high pressures. The latter indicates adsorption compression with repulsive interactions in the adsorbed phase. The shape of isotherms in Ono-Kondo coordinates can help to understand adsorbate-adsorbate energies; the slope of the line in Ono-Kondo coordinates gives the sign and magnitude of the energy as a function of adsorbate density.

Chapter 4 is discussed for intermolecular interactions for binary adsorption above critical points of mixtures (including CH_4/CO_2, CH_4/N_2, and N_2/CO_2 systems). Using coordinates of equations (4.20) and (4.21) allow analyzing interactions in adsorbed layers. Results indicate adsorption compression can be occurs in binary systems where the one of component has a high affinity to the surface of adsorbent. The strong field of the adsorbent pulls adsorbate molecules into surface phase at the density higher than in normal liquid that indicates repulsions between molecules in adsorbed phase.

Finally, Chapter 5 is overall conclusions to summarize that the Ono-Kondo lattice theory has a potential to describe the adsorption compression phenomenon for pure gases and binary mixtures under supercritical conditions.

ACKNOWLEDGEMENTS

I would like to express my thanks and gratitude to everyone who offered me their help throughout this research. I would like to acknowledge to my honorable advisor, Asst. Prof. Dr. Chayanoot Sangwichien, Prof. Dr. Marc D. Donohue, and Prof. Dr. Gregory Aranovich for the support, guidance, and encouragement on this thesis. Appreciation is extended to my research committee, Asst. Prof. Dr. Sukritthira Ratanawilai, and Asst. Prof. Dr. Chairat Siripatana for efforts and many helpful suggestions.

I am very grateful to all my dear persons in Department of Chemical Engineering, Faculty of Engineering at Prince of Songkla University. And I would like to thank the faculty of Engineering and the Graduate School, Prince of Songkla University for providing me a scholarship to study and pursue this degree.

Thanks must be given to all members of Donohue research group in Department of Chemical and Biomolecular Engineering, Johns Hopkins University in USA, especially Miss Elizabeth Epps, for their friendship, assistance and support. I would like to acknowledge support by Department of Chemical and Biomolecular Engineering, Johns Hopkins University for their assistance during my time in the United States.

Many thanks to all my friends for their kind support over my years of study. I also would like to thank my dear uncles and aunts. My life wouldn't be the same without their love and support.

Finally, I wish to thank to my family: Mom, and twin sisters who are always giving my love, patience, and support which is a constant reminder that I pursued this degree for them as well as myself.

Panita Sumanatrakul

CONTENTS

CONTENTS (CONT'D)

LIST OF TABLES

LIST OF TABLES (CONT'D)

LIST OF TABLES (CONT'D)

LIST OF FIGURES

LIST OF FIGURES (CONT'D)

CHAPTER 1

INTRODUCTION

1.1 Background and Rationale

The global warming is a serious worldwide problem which is the result of the rapid buildup of greenhouse gases. Carbon dioxide and methane emissions represent the main problem, since they account for about 74% and 16%, respectively of the major greenhouse gases [1]. One of the ways to reduce greenhouse gas emissions is to capture them at their source and then store them in the earth. For many processes, this can be done with adsorption technology [2]. The adsorption and desorption processes are widely used for the separation of undesirable substances and recovery of desirable components. These technologies are widely used in the field of carbon capture and storage. One example in the capture of carbon dioxide using adsorption-desorption technologies is the injection of carbon dioxide at supercritical conditions into coal-bed methane reservoirs. The carbon dioxide displaces methane from the coal seam and is itself permanently stored. Thus, the recovery methane is enhanced while the carbon dioxide is sequestered [3].

Knowledge of the adsorption behavior at high pressure has long been important in processes involving high pressure gas adsorption such as: gas separation, fuel storage, and carbon dioxide sequestration. However, the applicability of the existing data at high pressures is limited by the discrepancies between the literature data and the lack of reliable theoretical models that can be used to interpret, interpolate and extrapolate the data. Generally, the thermodynamic properties, including phase behavior are not available for all components nor are they available at all operating conditions of interest at supercritical conditions. Hence, they need to be estimated by thermodynamic models. Accurate models which have a strong theoretical base can allow us to predict gas adsorption when experimental data are not available.

Adsorption behavior of supercritical fluids is fundamentally different from subcritical adsorption. This is reflected in a new classification of adsorption isotherms [4-5] and in numerous experimental and theoretical studies [6-13]. In this study, an equation for the adsorption isotherm of a supercritical gas adsorption is presented based on statistical thermodynamics. Adsorption at a fluid-solid interface is considered in the framework of a lattice

with boundaries using ideas proposed by Ono and Kondo. It has been shown that the Ono-Kondo model is able to predict all known types of adsorption behavior [14-18], including supercritical systems, by changing temperature and bulk pressure (or density), by changing the energetic parameters (i.e. energies for adsorbate - adsorbate and adsorbate - adsorbent interactions), and by choosing appropriate boundary conditions (in particular, for microporous adsorbents). Therefore, this research deals with the prediction of adsorption behavior for supercritical systems using Ono-Kondo lattice theory and testing of theoretical calculations with literature data to accurately predict supercritical fluid adsorption isotherms for systems of practical interest.

1.2 Review of Literature

1.2.1 Supercritical Fluid

A supercritical fluid is a substance at a temperature and pressure above its critical point (T_c and P_c, respectively). Figure 1 shows the supercritical fluid region for carbon dioxide on a pressure-temperature phase diagram. When increasing both temperature and pressure above the critical point, the liquid becomes less dense due to thermal expansion and the gas becomes denser as the pressure rises. Eventually, the densities of the two phases converge and become identical; the distinction between gas and liquid disappears. Once the critical temperature and pressure have been reached the two distinct phases of liquid and gas are no longer visible. The meniscus can no longer be seen. One homogenous phase called the "supercritical fluid" phase occurs which shows properties intermediate between these of liquids and gases [19-21].

Supercritical fluids have physicochemical properties as density; viscosity; and diffusivity which are intermediate between those of liquid and gas and which are continuously adjustable from gas to liquid with small pressure and temperature variations. Table 1 illustrates density and transport properties of a supercritical fluid near the critical point.

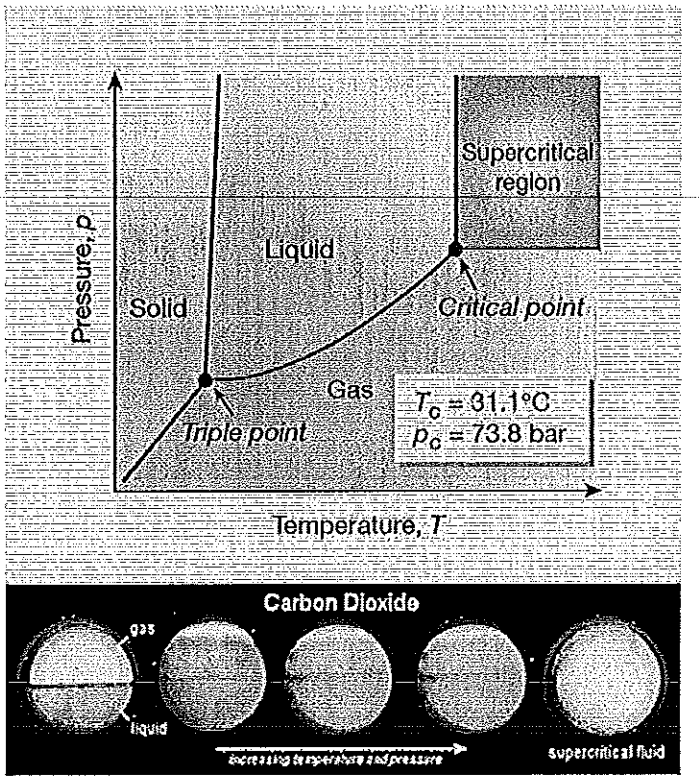

Figure 1.1 Pressure-temperature phase diagram of supercritical carbon dioxide [22-23].

Table 1.1 Comparison of the physical properties of gases, supercritical fluids, and liquids [24].

Physical property	Gases	Supercritical fluids	Liquids
Density (g/ml)	0.001	0.2-1.0	0.6-1.6
Dynamic viscosity (Pa.s)	10^{-5}	10^{-4}	10^{-3}
Diffusivity (cm^3/s)	10^{-1}	10^{-3}	10^{-5}

1.2.2 Supercritical Adsorption Model

Physical adsorption of fluids at conditions above the critical point is of growing importance in both engineering processes and potential industrial applications. For example, separation of several gases [25-30]; purification of drug in pharmaceuticals [31-32]; storage of fuel gases [33-34]; and adsorption for supercritical gases in extraction processes and chromatography [35-40]. Additionally, knowledge of the fluid-solid interface phenomenon at high pressures is fundamental to heterogeneous catalysis [41]. The utility of supercritical adsorption is summarized in Figure 1.2.

Physical adsorption of supercritical fluids at high pressures has interesting features compared to subcritical fluid adsorption, and these differences present challenges to theoretical modeling [42]. Over the past decade there have been major advances in the application of molecular simulation and statistical mechanical methods to the study of adsorption. Starting from the consideration of the adsorption potential theory was developed by many succeeding researchers, especially by Dubinin and Asktahov [42-46]. The Langmuir and Brunauer-Emmett-Teller (BET) isotherm equations were derived based on dynamic equilibrium between adsorption and desorption. The limiting adsorption of the Langmuir equation represents completion of the monolayer and may be used for the calculation of surface area. However, many isotherms do not stop with monolayer adsorption and several models have been proposed [37, 47-48]. Brunauer-Emmett-Teller (BET) derived a multilayer adsorption isotherm that is used widely to determine surface areas for dispersed and porous materials from multilayer adsorption isotherms [38, 49]. Another class of supercritical isotherm models is obtained through evaluating the density profile in the adsorbed phase for instance Grand Canonical Monte Carlo simulation [9, 11, 14, 17]; non-local or simplified local density functional theory [12-13]. Nevertheless, limitations in the knowledge of interactions at the molecular level and the assumptions made in these models mean that they are only a partially successful. In a similarly way, a lattice model was proposed to represent the adsorption system and the Ono-Kondo equation [14-18] has been used to relate the density in each adsorbed layer. In conclusion, Figure 1.3 provides a review of adsorption models for supercritical systems. However, the physical meaning of the parameters in these models may not always be reasonable due to the complexity of the interactions between adsorbed molecules and solid surfaces. Therefore, additional work still is needed.

1.3 Objective

1.3.1 To understand and predict adsorption behavior for supercritical systems including adsorption compression in the first adsorbed layer at supercritical conditions.

1.3.2 To compare theoretical calculations with literature data for the adsorption of supercritical fluids on microporous adsorbents.

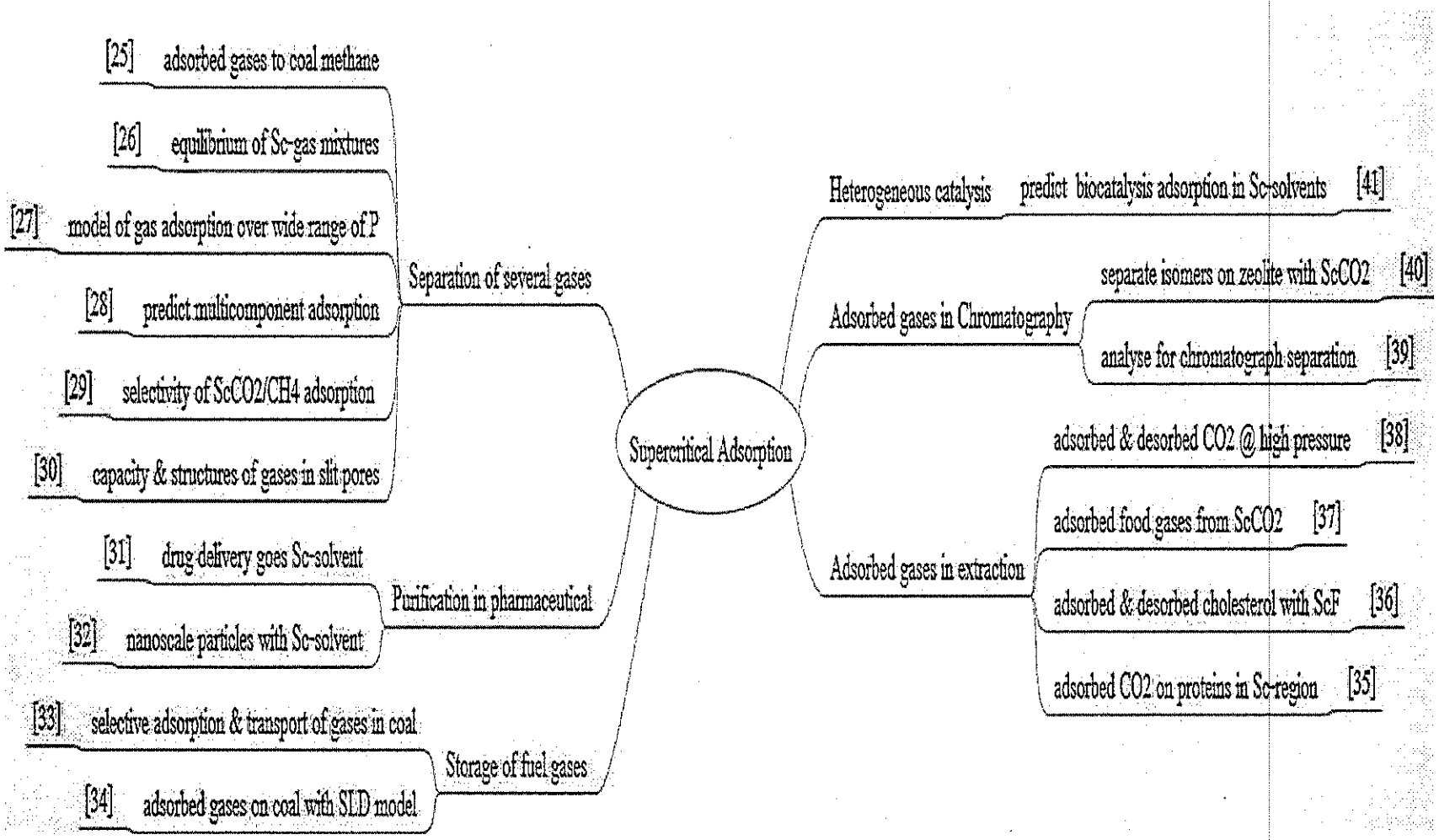

Figure 1.2 The summarization for supercritical adsorption utilities.

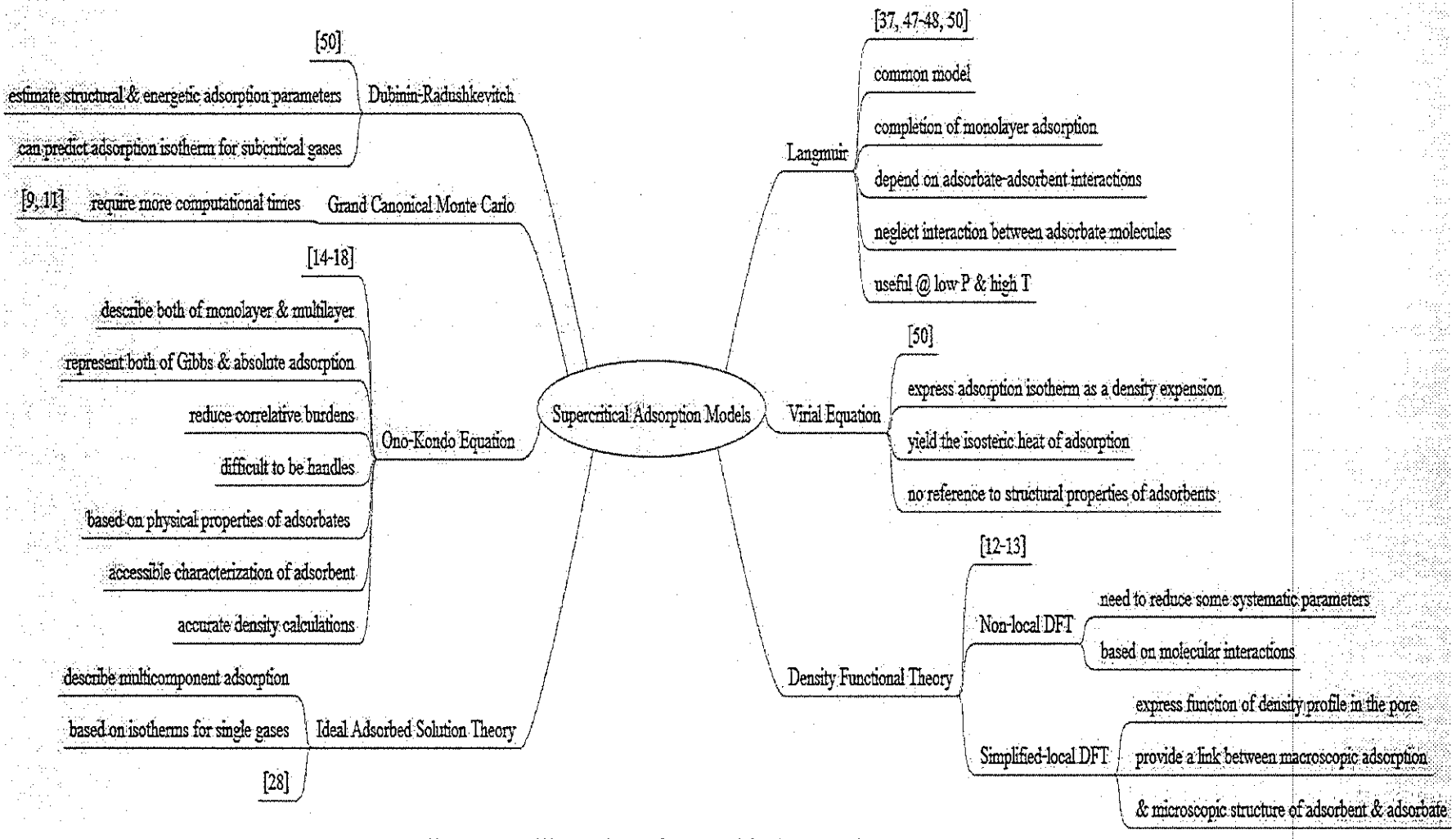

Figure 1.3 The review of supercritical adsorption models.

CHAPTER 2

RESEARCH METHODOLOGY

2.1 Introduction

The Ono-Kondo equation has been used to describe the thermodynamic theory of surface tension and adsorption by the method of the dividing surface of Gibbs. The thermodynamic method for defining surface tension based upon the second law is convenient but restricted only to systems in thermodynamic equilibrium. The thermodynamic quantities of a system in thermodynamic equilibrium can be given in terms of statistical thermodynamics which is based on the relationship between the Helmholtz free energy and the partition function. Surface tension can be derived through the relationship between the pressure tensor and distribution functions. Another case is physical adsorption. The amount adsorbed is defined as the density of molecules at the surface in excess of the density in the bulk. It is treated from the general statistical mechanical considerations.

In this work, adsorption at fluid-solid interface is considered in the framework of a lattice with boundaries using ideas proposed by Ono, S.; and Kondo, S [51]. The Ono-Kondo approach was originally derived to describe density gradients at a vapor-liquid interface, and it become a classical part of molecular theory for surface of liquids. Then it was applied to binary fluids. Additionally, this approach has been extended to enable prediction for adsorption on macro-, meso, and microporous adsorbents by imposing different boundary conditions. This model can predict steps in monolayer and multilayer adsorption isotherms, scaling behavior near saturation conditions, subcritical isotherms, supercritical isotherms with weak maxima, and adsorption hysteresis [4, 52-58]. Recently, the Ono-Kondo equation has been developed to determine of the adsorption isotherms over wide temperature and pressure ranges [59]. For these reasons, it is reasonable to use the Ono-Kondo lattice model for supercritical fluids. The physical basis of the model allows investigation of how energies of intermolecular interactions lead to different types of adsorption isotherms.

2.2 Classical Ono-Kondo Theory

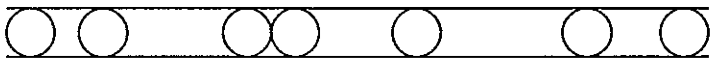

Figure 2.1 Cross section of monolayer between two walls.

Consider a one component lattice gas in contact with a surface (hard wall). There are interactions between the nearest neighbors with ε being the energy of adsorbate-adsorbate interactions and ε_s being the interaction energy for adsorbate molecules at the adsorbent surface. For attractive forces, both ε and ε_s are negative. For one layer between two walls (Figure 2.1), the Ono-Kondo equation can be written in the following form:

$$\ln\frac{x_1(1-x_b)}{x_b(1-x_1)}+\frac{z_1\varepsilon_s}{kT}+\frac{z_2\varepsilon}{kT}x_1-\frac{z_3\varepsilon}{kT}x_b=0 \qquad (2.1)$$

In equation (2.1), x_1 is the density or fraction of sites occupied by molecules in the adsorbed layer, x_b is the fraction of sites occupied with fluid molecules in the bulk, z_3 is the coordination number for tree-dimensional lattice ($z_3 = 6$ for cubic lattice [60]), z_2 is the monolayer coordination number ($z_2 = 4$ for square lattice), z_1 is the number of molecule-surface bonds ($z_1 = 2$ for one layer between two walls as shown in Figure 2.1), k is Boltzmann's constant, and T is the absolute temperature.

2.3 Analysis of Adsorption Isotherms

Deriving the adsorption isotherm at high pressure uses concepts first proposed for lattice systems by Ono and Kondo [51] and developed Aranovich-Donohue model [4, 14-18, 52-58, 60]. Consider taking an adsorbate molecule from the surface and moving it to an empty volume between molecules in the bulk (far from the surface). This is equivalent to the exchange of the molecule with a vacancy that it fills,

$$M_i + V_b \quad = \quad V_i + M_b \qquad (2.11)$$

If this exchange occurs at equilibrium, then;

$$\Delta H - T\Delta S = 0 \tag{2.12}$$

where ΔH and ΔS are the enthalpy and entropy changes and T is the absolute temperature. The value of ΔS can be represented in the form;

$$\Delta S = k \ln W_1 - k \ln W_2 \tag{2.13}$$

where W_1 is the number of configurations where a particular site in the layer i is occupied by an adsorbate molecule and the infinitely distant site is empty, W_2 is the number of configurations where the infinitely distant site is occupied by an adsorbate molecule and the particular site in the layer i is empty, and k is Boltzmann's constant.

If the overall number of configurations for the system is W_0, then in the mean-field lattice approximation

$$W_1/W_0 = x_i (1-x_b) \tag{2.14}$$

$$W_2/W_0 = (1-x_i)\, x_b \tag{2.15}$$

Where W_0 is the overall number of configurations for the system, x_i is the probability that the particular site in the layer i is occupied by an adsorbate molecule, and x_b is the density of adsorbate in the bulk.

Substituting equations (2.14) and (2.15) into equation (2.13)

$$\Delta S = k \ln (x_i (1-x_b) W_0) - k \ln (x_b (1-x_i) W_0)$$

$$\Delta S = k \ln \left[\frac{x_i (1-x_b) W_0}{(1-x_i) x_b W_0} \right]$$

$$\Delta S = k \ln \left[\frac{x_i (1-x_b)}{(1-x_i) x_b} \right] \tag{2.16}$$

The change in enthalpy can be calculated in the mean-field approximation for a slit-like pore (see figure 2.2) by considering the number of neighboring sites that are occupied in the pore compared to the bulk. Then,

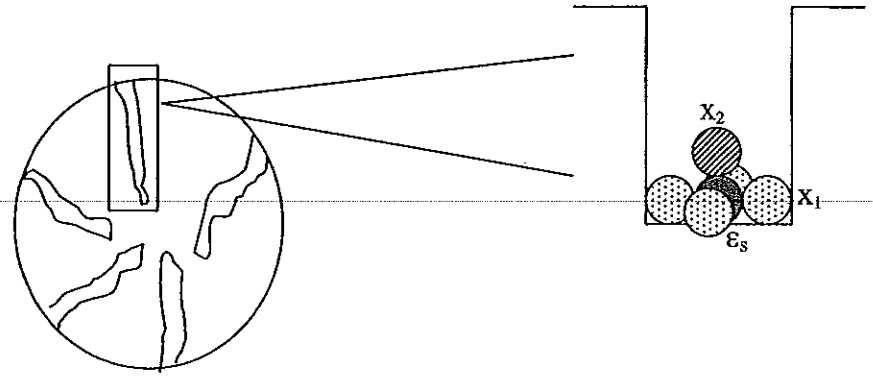

Figure 2.2 Adsorption in slit pores.

For $i = 1$, one can write

$$\Delta H = -\varepsilon_s - x_2\varepsilon - 4x_1\varepsilon + 6x_b\varepsilon \tag{2.17}$$

where x_1 is the probability that the certain site in the layer *1* is occupied by an adsorbate molecule, x_2 is the probability that the certain site in layer *2* is occupied by an adsorbate molecule, x_b is the density of adsorbate in the bulk, ε is adsorbate-adsorbate interactions, ε is adsorbate-adsorbent interactions. Note that, for attractive interactions, ε and ε_s are negative, and for repulsive interactions they are positive.

Substituting equations (2.17) and (2.16) into equation (2.12)

$$\ln\left[\frac{x_1(1-x_b)}{x_b(1-x_1)}\right] + \frac{\varepsilon_s}{kT} + (x_2 + 4x_1 - 6x_b)\frac{\varepsilon}{kT} = 0$$

This can be rewritten as

$$x_1 = \frac{x_b}{x_b + (1-x_b)e^{\frac{\varepsilon_s + (x_2 + 4x_1 - 6x_b)\varepsilon}{kT}}} \tag{2.18}$$

Figure 2.3 illustrates the adsorption isotherms calculated from equation (2.18) for nitrogen, methane, and carbon dioxide adsorbed on activated carbon at T = 318.2 K. Table 2.1 shows the different adsorbate-adsorbate (ε), and adsorbate-adsorbent (ε_s) interaction energies for each gas [61-62].

Table 2.1 Ono-Kondo parameters for pure components adsorbed on activated carbon at T = 318.2 K [62].

components	ε_s/k (K)	ε_s/kT	ε/k (K)	ε/kT
N_2	-1032	-3.24	41	0.13
CH_4	-1385	-4.35	64	0.20
CO_2	-1690	-5.31	82	0.26

As shown in Table 2.1 and Figure 2.3, nitrogen has the weakest surface interactions; hence it is the bottom curve, while carbon dioxide has the strongest surface of interactions and is the top curve. It should be noted that adsorption isotherms are sensitive to changes in ε_s/kT and ε/kT. Results show that increasing ε_s/kT (adsorbate-adsorbent interactions) leads to increase in the Henry's constant [56] and the adsorption becoming stronger. On the other hand, for small values of ε/kT (adsorbate-adsorbate interactions) the adsorption isotherm is relatively independent of this parameter over a wide range of reduced densities.

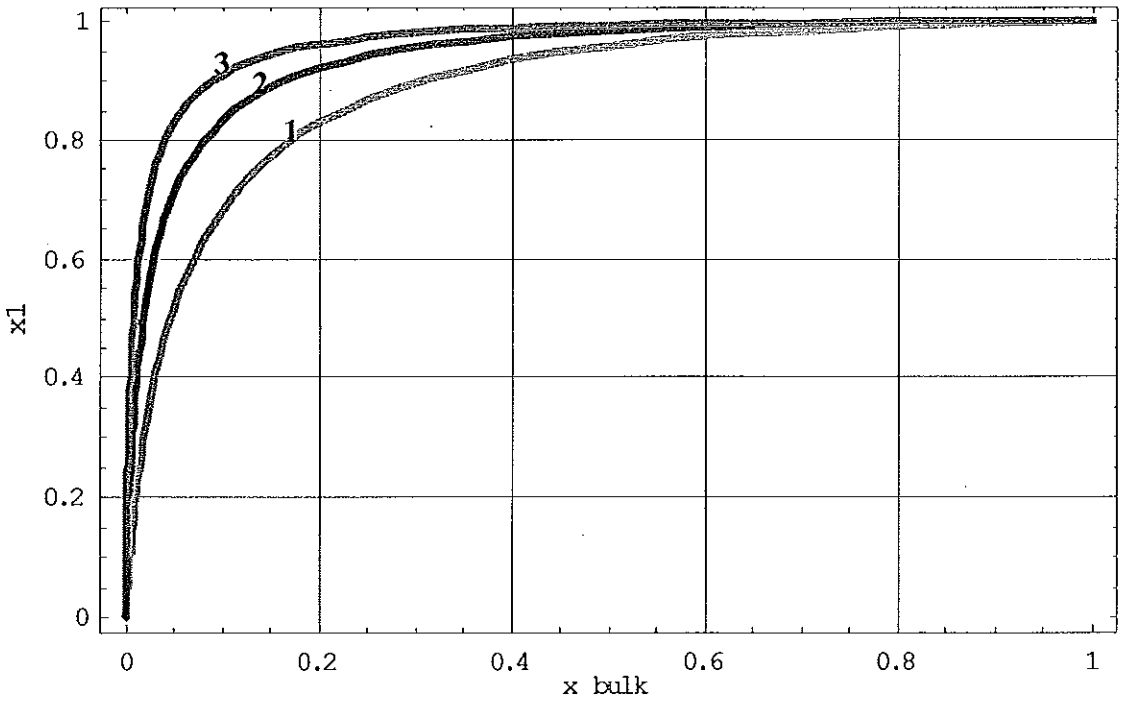

Figure 2.3 Dependence of x_1 on x_b obtained from equation (2.20) at different ε_s/kT and ε/kT values for (1) nitrogen, (2) methane, and (3) carbon dioxide adsorbed on activated carbon at T = 318.2 K.

2.4 Solution of Ono-Kondo Equation for Supercritical Adsorption

Physical meaning of Gibbs adsorption

$$\Gamma = \sum_i (x_i - x_b) \tag{2.19}$$

here absolute adsorption, $x_i = a/a_m$

By definition for monolayer adsorption, the Gibbs adsorption Γ can be calculated from the equation

$$\Gamma = c_m \sum_i (x_i - x_b) \tag{2.20}$$

where c_m is the monolayer capacity.

For monolayer adsorption, equation (2.18) can be easily solved, yielding the following expression:

$$x_1 = \frac{x_b}{x_b + (1-x_b)e^{\frac{\varepsilon_s + (4x_1 - 6x_b)\varepsilon}{kT}}} \tag{2.21}$$

An extension to adsorption of gaseous adsorbates on microporous adsorbents above critical temperatures proposed by Aranovich and Donohue [4] can be written as:

$$\Gamma = K\left(\frac{x_b}{x_b + (1-x_b)e^{\frac{\varepsilon_s + (4x_1 - 6x_b)\varepsilon}{kT}}}\right) - x_b/(1-\omega_1) \tag{2.22}$$

where ω_1 is the root which is smaller than unity and $K = 2c_m(1-\omega_1^n)/(1+\omega_1^{n-1})$.

Neglecting ω_1, the adsorption isotherm is given by

$$\Gamma = 2c_m\left(\frac{x_b}{x_b + (1-x_b)e^{\frac{\varepsilon_s + (4x_1 - 6x_b)\varepsilon}{kT}}}\right) - x_b \tag{2.23}$$

Figure 2.4 shows The Gibbs adsorption isotherms in the case of monolayer adsorption that gives theoretical predictions obtained from equation (2.23) at different ε_s/kT and ε/kT values for nitrogen, methane, and carbon dioxide adsorbed on activated carbon at T = 318.2

K. It is similar to Figure 2.3, the results show adsorption isotherms are also sensitive to change in ε_s/kT and ε/kT values for each of the components. It can be seen at a higher density that the Gibbs adsorption goes down as the density goes up. This is because the bulk density is increasing but the monolayer density is constant. Interestingly, carbon dioxide has similar trend when compared with the experimental data. This is consistent with the research of Gasem et al [70].

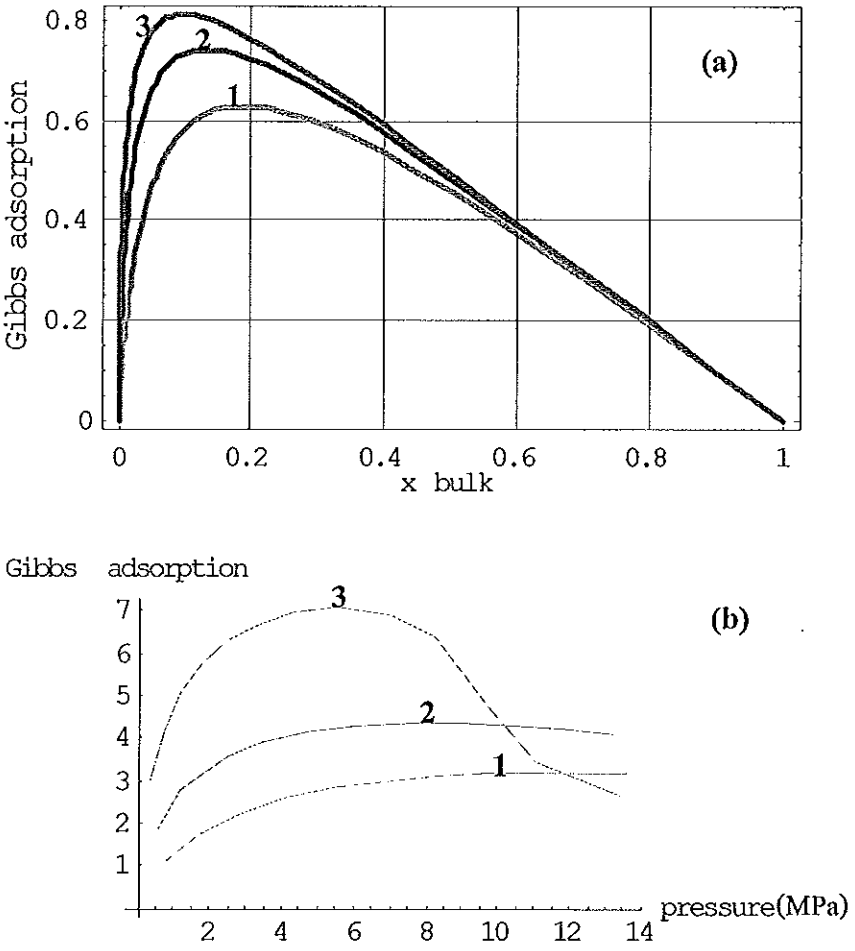

Figure 2.4 Isotherms of the Gibbs adsorption: (a) theoretical isotherms are obtained from equation (2.22) at different ε_s/kT and ε/kT values for (1) nitrogen, (2) methane, and (3) carbon dioxide; and (b) experimental isotherms [70] for (1) nitrogen, (2) methane, and (3) carbon dioxide adsorbed on activated carbon at T = 318.2 K.

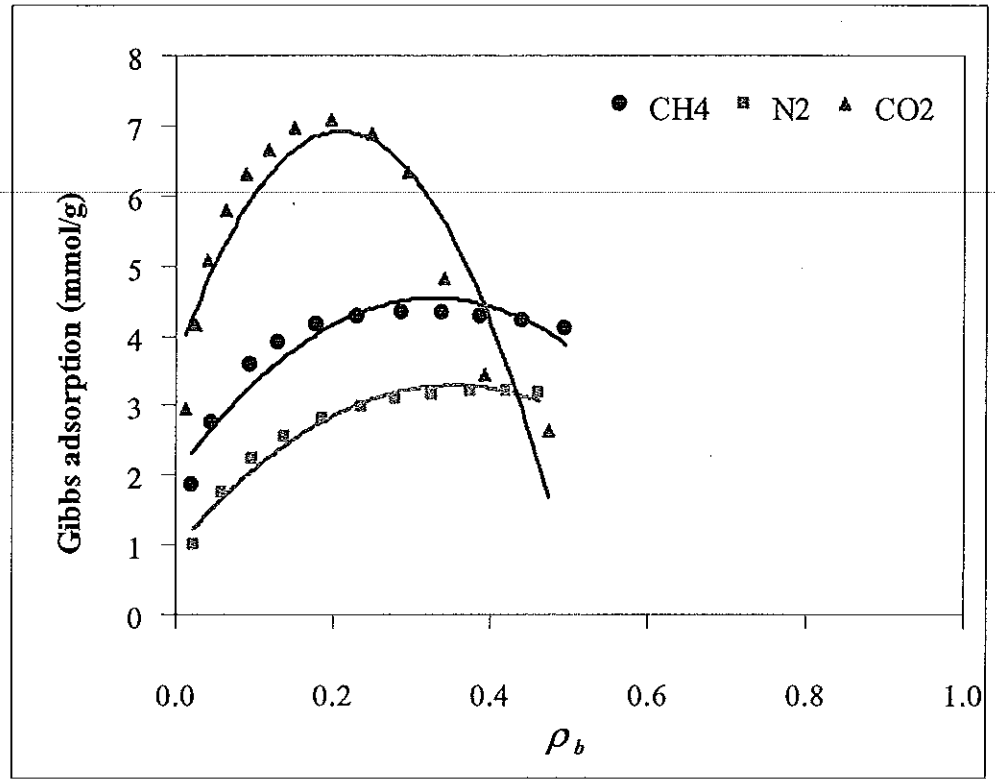

Figure 2.5 Gibbs adsorption isotherms under supercritical condition for nitrogen, methane, and carbon dioxide adsorbed on activated carbon at T = 318.2 K [experimental data from ref. 70].

Moreover, Figure 2.5 shows that similar behavior of the Gibbs adsorption isotherms occur under supercritical condition for nitrogen, methane, and carbon dioxide adsorbed on activated carbon at T = 318.2 K. These results can be confirmed the results in Figure 2.4 and the observation of Gasem [70] that presented the important point is that Ono-Kondo coordinates allow interpretation of intermolecular forces of adsorbate molecules.

2.5 Conclusions

Adsorption behavior for supercritical fluids is analyzed by using the Ono-Kondo lattice theory. Results indicate that isotherms are sensitive to changes of adsorbate-adsorbate and adsorbate-adsorbent interaction energies. Increasing ε_s/kT (adsorbate-adsorbent interactions) leads to increase in the Henry's constant and shows strong adsorption. On the other hand, for small values of ε/kT (adsorbate-adsorbate interactions) the adsorption isotherm is straight line over a wide range of reduced densities.

CHAPTER 3

ONO-KONDO ANALYSIS OF ADSORPTION COMPRESSION IN SUPERCRITICAL SYSTEMS

3.1 Introduction

Adsorption behavior of supercritical fluids is fundamentally different from subcritical systems. This is reflected in classification of adsorption isotherms [4-5] and in numerous experimental and theoretical studies [6-13]. In former publications [14-18], it was shown that Ono-Kondo density functional theory can predict all types of adsorption behavior, including supercritical, by varying the energetic parameters and by choosing appropriate boundary conditions for macro- /meso- and /micro- porous adsorbents. This is possible because Ono-Kondo density functional theory captures the essential physics of adsorption equilibria, including phase transitions and adsorption compression.

In prior work [14-18], the Ono-Kondo approach has been proven to be useful for analysis of adsorbate compression near surfaces. However, in previous studies, the scope of analysis was limited to subcritical temperatures and a relatively narrow range of pressures. In this study, we use the Ono-Kondo approach to analyze adsorbate-adsorbate interactions and adsorption compression in supercritical systems.

Adsorption compression arises from competition between attraction of the adsorbate to the adsorbent surface and repulsions between/among neighboring adsorbate molecules [14-15]. When there is a strong affinity to the adsorbent, the distance between adsorbate molecules can become less than in a normal liquid and nearest neighbors repel each other. This is possible because the decrease of free energy due to attraction to the adsorbent is greater than the increase of free energy due to repulsions between adsorbate molecules. In other words, a strong attraction to the adsorbent causes repulsions in the adsorbate layer. This phenomenon can be especially significant at supercritical conditions where the high temperature prevents classical multilayer adsorption [63], but saturation of nano-pores is possible due to the external field of the adsorbent.

In this work, experimental data for supercritical fluids are plotted in Ono-Kondo coordinates with variable Henry's constant, H, and with preliminary estimated H. This allows analysis of adsorbate-adsorbate interactions in the adsorbed phase from adsorption isotherms.

3.2 Ono-Kondo Model for Adsorption Equilibria

The Ono-Kondo model [51] has been applied to analyze adsorption equilibria for a wide variety of systems [53, 58, 64-65]. To apply the Ono-Kondo model, consider taking an adsorbate molecule from the surface and moving it to an empty volume between molecules in the bulk (far from the surface). This is equivalent to the exchange of the molecule with a vacancy that it fills

$$M_S + V_b = V_S + M_b \tag{3.1}$$

where M_s is the adsorbate molecule on the surface, M_b is the adsorbate molecule in the bulk, V_s is the vacancy on the surface, and V_b is the vacancy in the bulk. If this exchange occurs at equilibrium, then:

$$\Delta U - T\Delta S = 0 \tag{3.2}$$

where ΔU and ΔS are the configurational energy and entropy changes and T is the absolute temperature.

The value of ΔS can be represented in the form:

$$\Delta S = k \ln \frac{(a/a_m)(1-x_b)}{(1-a/a_m)x_b} \tag{3.3}$$

where k is Boltzmann's constant, x_b is the density of adsorbate in the bulk, a is the absolute adsorption ($a = a/a_m$) and a_m is the maximum density of adsorbate molecules that can be in the adsorbed monolayer.

Note that variables of the Ono-Kondo equation can be calculated in terms of classical thermodynamic parameters, such as pressure and temperature. In particular, the dimensionlesss density of adsorbate in the bulk can be calculated as $x_b = (\pi/6)n\sigma^3$ [66-67] where n is the number of particles per unit of volume, and σ is the distance between molecules (which can be determined, for example, from the Lennard-Jones potential). Assuming that deviations from ideal gas in the bulk are not significant, the value of n can be calculated as $n = \frac{n_m N_A}{V} = \frac{P}{kT}$, where P is pressure of the fluid [Pa], V is total volume of the fluid [m^3], n_m is the number of moles [mole], and N_A is Avogadro's number [molecules/mole].

The change in configurational energy due to adsorption, ΔU, can be represented as:

$$\Delta U = \varphi_s + U_m - U_g \tag{3.4}$$

where φ_s is the average energy of the molecule-surface interaction, U_m is the average energy of adsorbate-adsorbate interactions (between a central molecule and surrounding molecules in the adsorbed phase), and U_g is the average energy of interaction between a central molecule and surrounding molecules in the 3-D gas.

For a two-dimensional fluid in the monolayer, the value of U_m can be calculated as

$$U_m = \rho_{2D} \int_0^\infty \varphi(r) g(r) 2\pi r dr \tag{3.5}$$

where $\varphi(r)$ is the potential function for adsorbate molecules, $g(r)$ is the two-dimensional radial distribution function, and ρ_{2D} is the two-dimensional density. In the nearest neighbor approximation [18, 64]:

$$g(r) = g_0 \delta[(r - r^*)/r^*] \tag{3.6}$$

where r^* is the average distance between the central molecule and its nearest neighbors, δ is the delta function, and g_0 is a coefficient not depending on r.

Since $\rho_{2D} = C_{2D}\, a$ (where C_{2D} is the coefficient determining units of the two-dimensional density), then plugging $g(r)$ from equation (3.6) into equation (3.5) gives

$$U_m = \lambda_{2D} a \varphi(r^*) \tag{3.7}$$

where $\lambda_{2D} = 2\pi C_{2D}\, r^* g_0$. Equation (3.7) is consistent with the fact that U_m is linear with density at low and moderate densities [68-69]. Note that there are deviations from this linear behavior at high densities.

A three-dimensional version of equation (3.5) (with three-dimensional variables) can be written as

$$U_m = \rho_{3D} \int_0^\infty \varphi(r) g(r) 4\pi r^2 dr \tag{3.5a}$$

Using approximation (3.6) in this equation gives the same equation (3.7), but with $\lambda_{3D} = 4\pi C_{3D}\, r^{*2} g_0$ Instead of λ_{2D}. Since dimensionality influences only λ, it is reasonable to assume that equation (3.7) also is valid for phases with fractional dimensionality between 2 and 3, and equation (3.7) can be used for adsorbates in pores of adsorbent with some λ^* instead of λ_{2D}. For Lennard-Jones type of interactions, the value of r^* can be approximated as:

$$r^* = \begin{cases} 2^{1/6}\sigma & \text{for low densities} \\ r_0(a) & \text{for high densities} \end{cases} \tag{3.8}$$

where r_0 is the average distance between nearest molecules in the dense monolayer, and σ is the distance where potential function has minimum.

The energy of interaction, U_g , between a central molecule and surrounding molecules in the 3-D gas can be written in the form of equation (3.7):

$$U_g = \lambda_{3D} x_b \varphi(r^*) \tag{3.9}$$

Then, plugging equations (3.3) and (3.4) into equation (3.2) and using equations (3.7) and (3.9) gives:

$$\ln\frac{(a/a_m)(1-x_b)}{(1-a/a_m)x_b}+\frac{\varphi_s}{kT}+\lambda_{2D}\frac{a\varphi(r^*)}{kT}-\lambda_{3D}\frac{x_b\varphi(r^*)}{kT}=0 \tag{3.10}$$

Defining Henry's constant, H, as

$$H=\exp(-\varphi_S/kT) \tag{3.10a}$$

The first two terms of equation (3.10) can be combined to:

$$Y=\ln\frac{(a/a_m)(1-x_b)}{H(1-a/a_m)x_b} \tag{3.11}$$

Therefore, equation (3.10) can be represented in the following form:

$$\frac{Y}{x_b}=-\frac{\lambda_{2D}\varphi(r^*)}{kT}\frac{a}{x_b}+\frac{\lambda_{3D}\varphi(r^*)}{kT} \tag{3.12}$$

At constant $\varphi(r^*)/kT$, it follows from equation (3.12) that plotting Y/x_b versus a/x_b should give a straight line, and this can be a verification of the model itself. The slope of this line gives the value of $\lambda_{2D}\varphi(r^*)$ and the sign of $\lambda_{2D}\varphi(r^*)$ gives information about the character of adsorbate-adsorbate interactions – whether they are attractive or repulsive. Note that in low-pressure gas $x_b <<< 1$ and equation (3.12) can be simplified to:

$$Y=\ln\frac{(a/a_m)}{H(1-a/a_m)x_b} \tag{3.13}$$

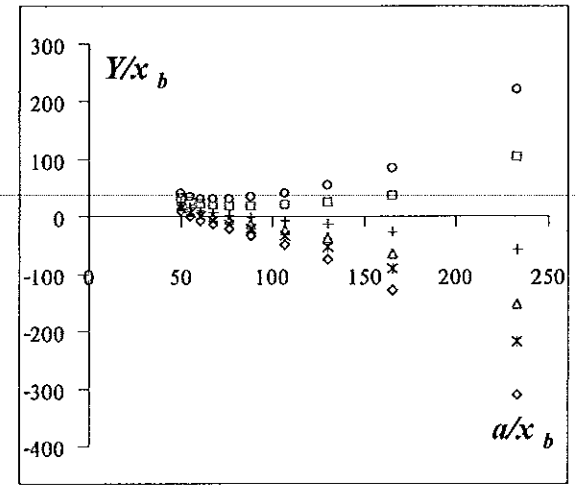

(a) N_2 adsorbed on activated carbon

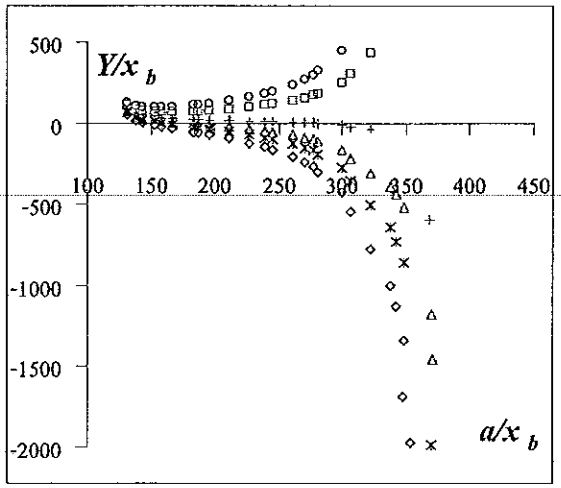

(d) N_2 adsorbed on zeolite

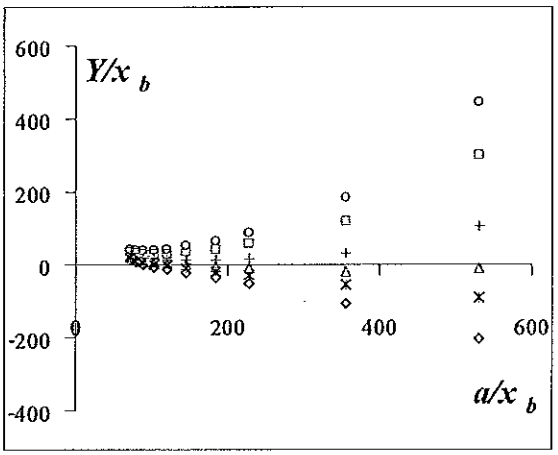

(b) CH_4 adsorbed on activated carbon

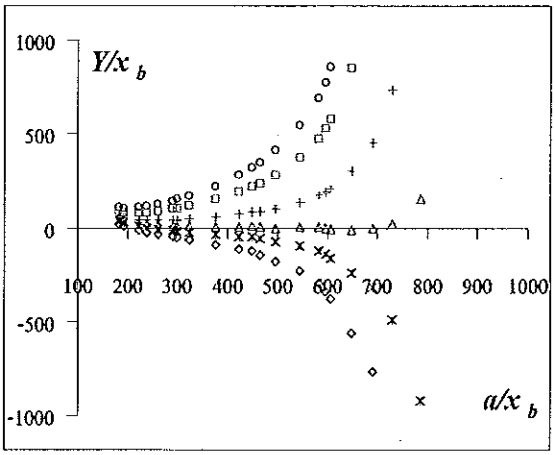

(e) CH_4 adsorbed on zeolite

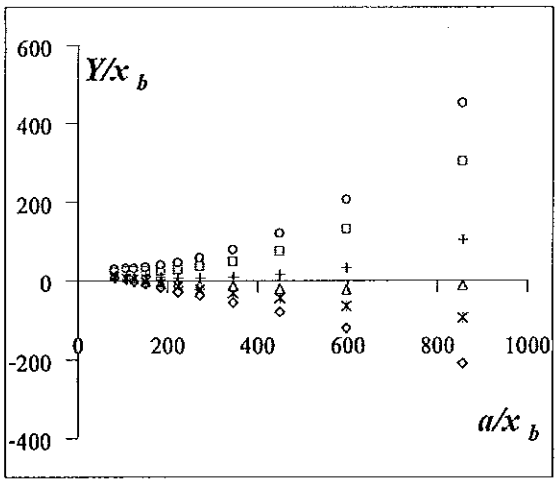

(c) CO_2 adsorbed on activated carbon

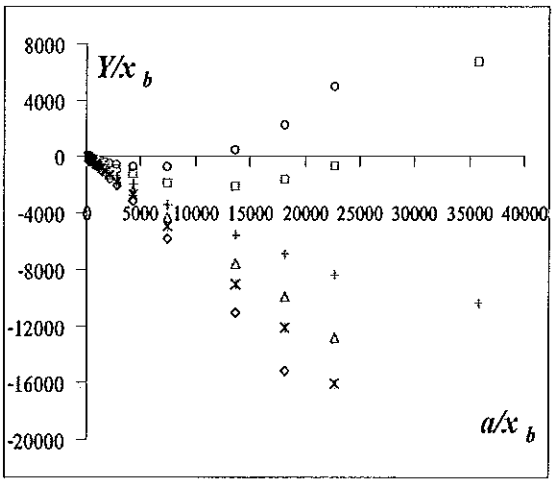

(f) CO_2 adsorbed on zeolite

Figure 3.1 Adsorption isotherms in Ono-Kondo coordinates with variable *H*: O for *H=30*, □ for *H=50*, + for *H=100*, △ for *H=150*, * for *H=200*, and ◊ for *H=300*; (a)-(c) for nitrogen, methane

and carbon dioxide on activated carbon Filtrasorb 400 at 318.2 K [experimental data from ref. 70], and (d)-(e) for nitrogen, methane on zeolite 13X at 308 K [experimental data from ref. 71]. Except (f) for carbon dioxide on zeolite 13X at 308 K is used variable H: O for $H=300$, □ for $H=500$, + for $H=1000$, △ for $H=1500$, * for $H=2000$, and ◊ for $H=3000$.

3.3 Plotting Adsorption Isotherms for Nitrogen, Methane, and Carbon Dioxide in Ono-Kondo Coordinates with Variable H

To analyze adsorption isotherms, we considered equation (3.12) with H being an adjustable parameter. In principle, the value of H can be estimated from the slope of the isotherm at small pressures. However, this adds significant error because of the lack of low pressure measurements for supercritical systems (at least in published data that we are aware of).

Figures 3.1 and 3.2 show adsorption isotherms for nitrogen, methane and carbon dioxide on activated carbon Filtrasorb 400 and on zeolite 13X in the coordinates of equation (3.12) for various (dimensionless) Henry's constants, H. In Figures 3.1 and 3.2, values of H for nitrogen and methane vary over the range from 30 to 300. For carbon dioxide on Filtrasorb 400, this range is also from 30 to 300; however, for carbon dioxide on zeolite 13X, H varies between 3000 and 30000, reflecting significantly stronger interactions with the adsorbent.

As shown by Figures 3.1 and 3.2, increasing of H from 30 to 300 for nitrogen, methane, and carbon dioxide on Filtrasorb 400 changes the shape of the isotherms in Ono-Kondo coordinates.; in particular, the slope at low pressure end changes from positive to negative. The same pattern in the same range of H is observed for nitrogen and methane on zeolite 13X. However, for carbon dioxide on zeolite 13X, switching from positive slope to negative at low pressure end occurs over significantly higher range of H – from 3000 to 30000. As mentioned earlier, this is because adsorption affinity of carbon dioxide to zeolite 13X is much larger than to Filtrasorb 400 and much larger than the affinity of nitrogen and methane to this adsorbent.

As seen from Figures 3.1 and 3.2, at the high pressure end (low values of a/x_m), all slopes become negative. This indicates that the adsorbate-adsorbate interactions become repulsive as pressure goes up, which is consistent with the concept of adsorption compression observed in subcritical systems [14-18]. To analyze the transition to adsorption compression, in the next section we plot isotherms in coordinates of equation (3.12) with estimated values of H.

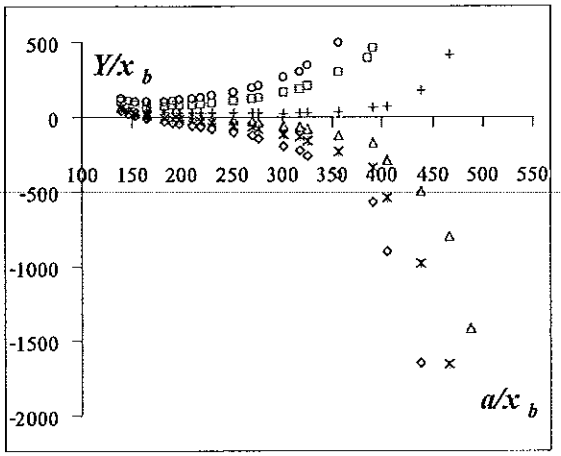

(a) N_2 adsorbed on zeolite at 298 K

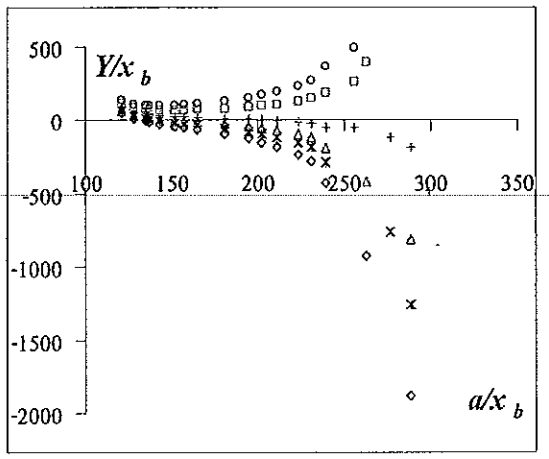

(b) N_2 adsorbed on zeolite at 323 K

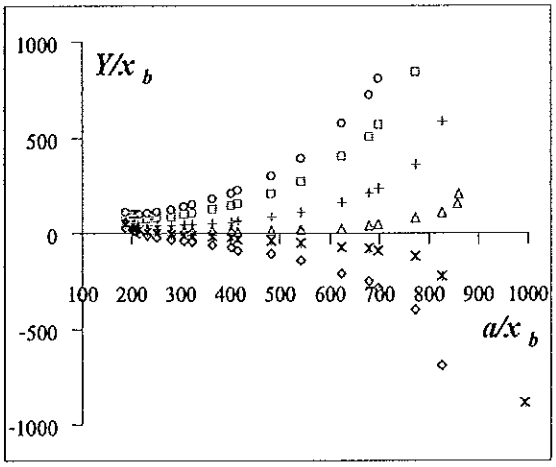

(c) CH_4 adsorbed on zeolite at 298 K

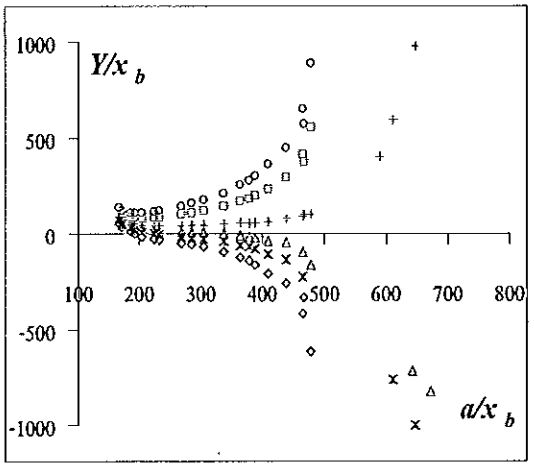

(d) CH_4 adsorbed on zeolite at 323 K

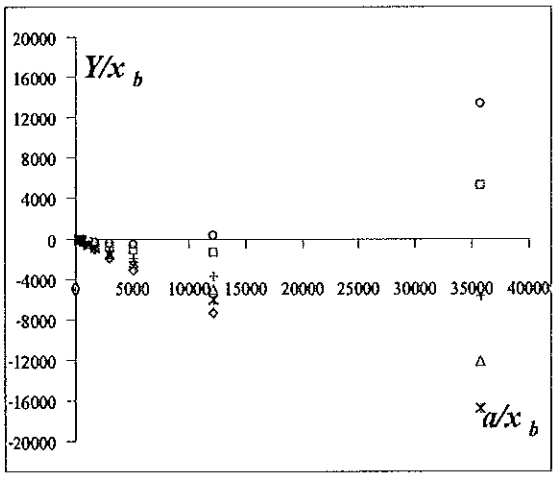

(e) CO_2 adsorbed on zeolite at 298 K

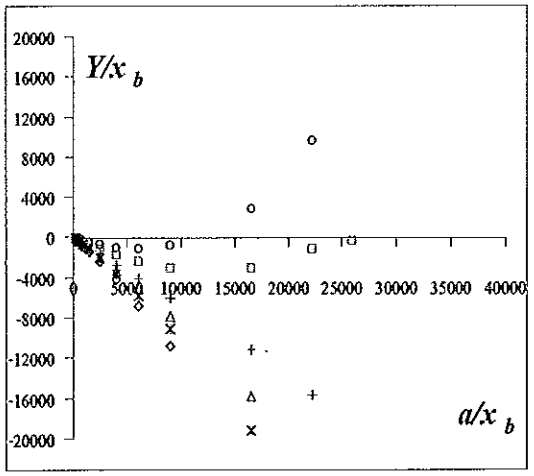

(f) CO_2 adsorbed on zeolite at 323 K

Figure 3.2 Adsorption isotherms in Ono-Kondo coordinates with variable *H*: O for *H=30*, □ for *H=50*, + for *H=100*, △ for *H=150*, * for *H=200*, and ◊ for *H=300*; (a)-(b) for nitrogen, and (c)-(d) methane on zeolite 13X at various temperatures [experimental data from ref. 71]. Except (e)-(f)

for carbon dioxide on zeolite 13X at various temperatures is used variable H: O for $H=300$, □ for $H=500$, + for $H=1000$, △ for $H=1500$, * for $H=2000$, and ◊ for $H=3000$.

3.4 Adsorption Isotherms in Ono-Kondo Coordinates with Estimated Henry's Constants

To our knowledge, there are not many publications with adsorption isotherms at supercritical conditions over a wide range of pressures. Moreover, where there are data at high pressures, there is a lack of measurements at very low pressures (such as in [70] and [71]) and this makes it difficult to evaluate Henry's constants with adequate accuracy. Independent estimates of Henry's constants [72] are limited to simplified models, and accurate independent measurements are reliable only for simple systems. In real adsorbents, there is a significant scatter depending on brand and on preliminary treatment which influences homogeneity and pores structure.

In Tables 3.1 and 3.2, we present estimates for normalized Henry's constants which are in a reasonable ranges in terms of results known from statistical modeling and from chromatographic and adsorption measurements [72 – 74]. Tables 3.1 and 3.2 also give values of $-\frac{\varphi_s}{RT}$ calculated from H by using equation (3.10a). These values can be related to differential heats of adsorption, though there could be a significant scatter in such estimates depending on pore heterogeneity and structure. Note that the simplest version of Ono-Kondo model uses average values of $-\frac{\varphi_s}{RT}$ which needs to be corrected for highly heterogeneous adsorbents in the limit of small pressures.

Table 3.1 Dimensionless Henry's constants for adsorption of nitrogen, methane, and carbon dioxide on activated carbon Filtrasorb 400 at T = 318.2 K [72].

Adsorbate	H	$-\frac{\varphi_s}{RT}$
Nitrogen	45	3.8
Methane	60	4.1
Carbon Dioxide	100	4.6

Table 3.2 Dimensionless Henry's constants for adsorption of nitrogen, methane, and carbon dioxideon zeolite 13X at T = 298 K, 308 K, and 323 K [72 – 74].

Adsorbate	H	$-\frac{\varphi_s}{RT}$
	T = 298 K	
Nitrogen	95	4.55
Methane	148	5
Carbon Dioxide	3905	8.27
	T = 308 K	
Nitrogen	80	4.4
Methane	120	4.8
Carbon Dioxide	3000	8
	T = 323 K	
Nitrogen	66	4.20
Methane	97	4.58
Carbon Dioxide	2056	7.63

Figures 3.3 and 3.4 show adsorption isotherms in Ono-Kondo coordinates for nitrogen, methane, and carbon dioxide on activated carbon Filtrasorb 400 and on zeolite 13X. As seen from Figures 3.3 and 3.4, in Ono-Kondo coordinates adsorption isotherms have similar shapes: going down to a minimum and then going up. This shape is consistent with interpretation of the derivative of this function representing potential function for adsorbate-adsorbate interactions. From this point of view, Figures 3.3 and 3.4 indicate that at small densities (high values of a/x_b) these interactions are attractive; as density goes up, they approach zero (neutral) point and switch to repulsions at higher density (low values of a/x_b).

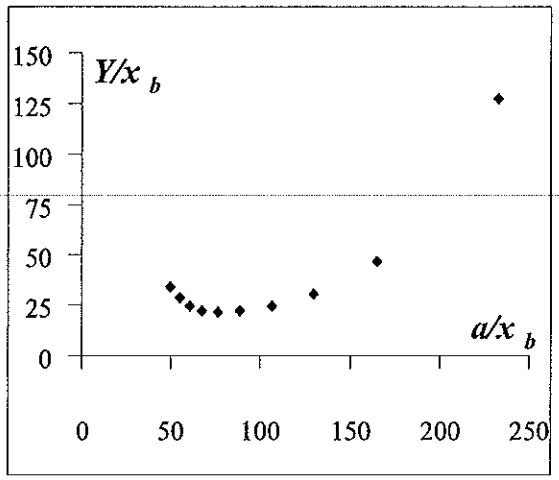

(a) N_2 adsorbed on activated carbon

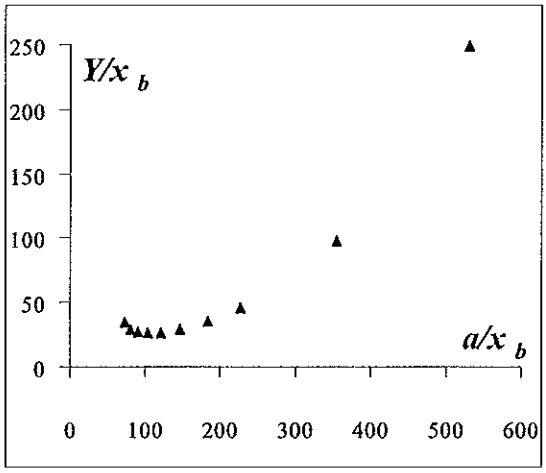

(b) CH_4 adsorbed on activated carbon

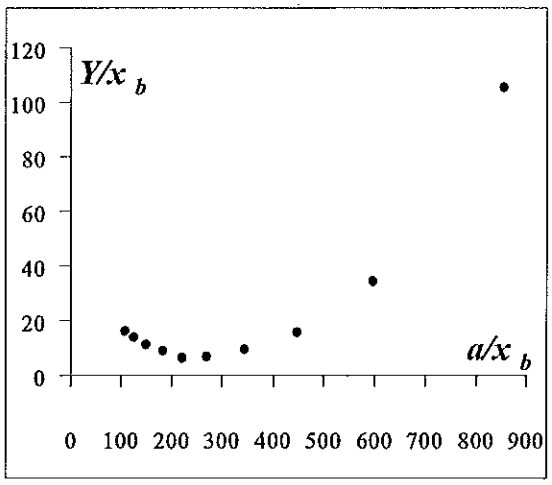

(c) CO_2 adsorbed on activated carbon

Figure 3.3 Adsorption isotherms for (a) nitrogen, (b) methane and (c) carbon dioxide on activated carbon Filtrasorb 400 at 318.2 K [experimental data from ref. 70] in Ono-Kondo coordinates with estimated *H* given in Table 3.1.

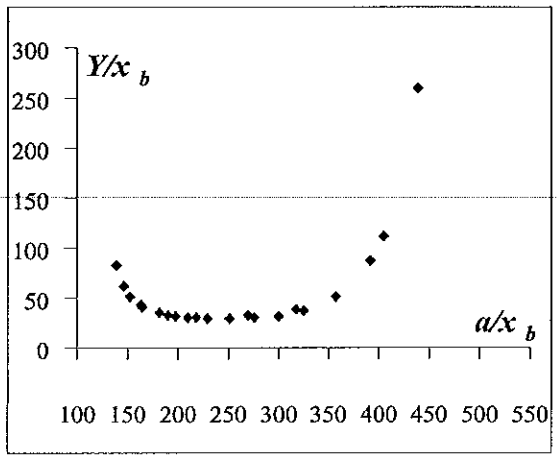

(a) N_2 adsorbed on zeolite at 298 K

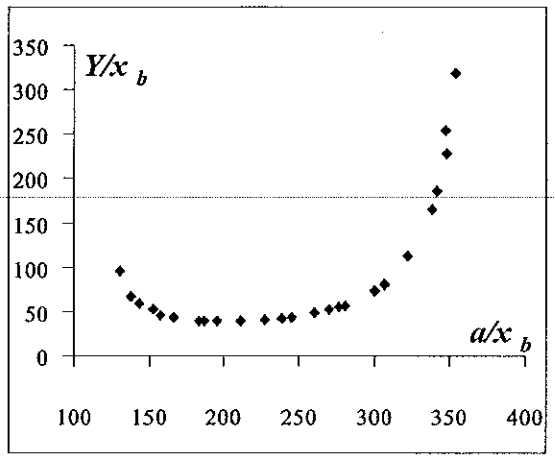

(b) N_2 adsorbed on zeolite at 308 K

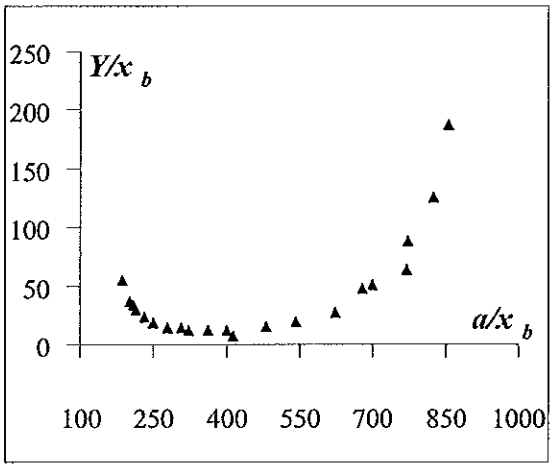

(c) CH_4 adsorbed on zeolite at 298 K

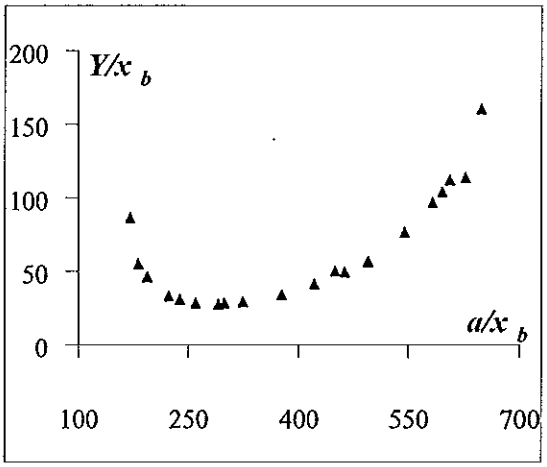

(d) CH_4 adsorbed on zeolite at 308 K

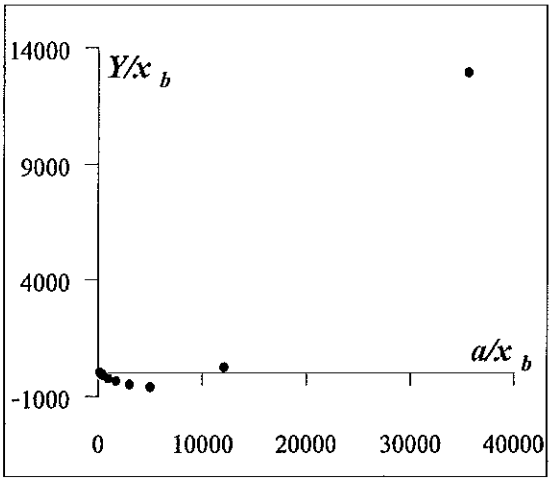

(e) CO_2 adsorbed on zeolite at 298 K

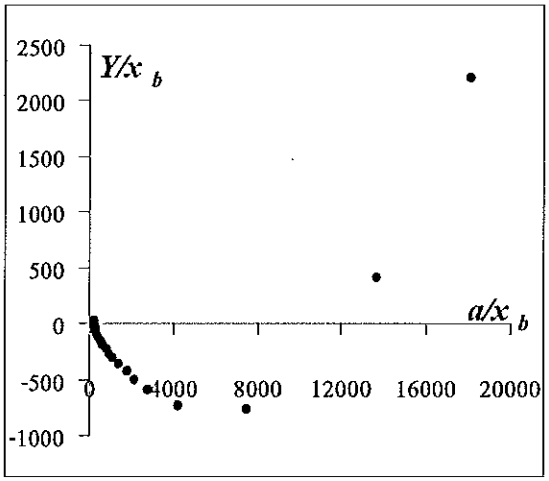

(f) CO_2 adsorbed on zeolite at 308 K

Figure 3.4 Adsorption isotherms for (a-b) nitrogen, (c-d) methane and (e-f) carbon dioxide on zeolite 13X [experimental data from ref. 71] at various temperatures in Ono-Kondo coordinates with estimated *H* given in Table 3.2.

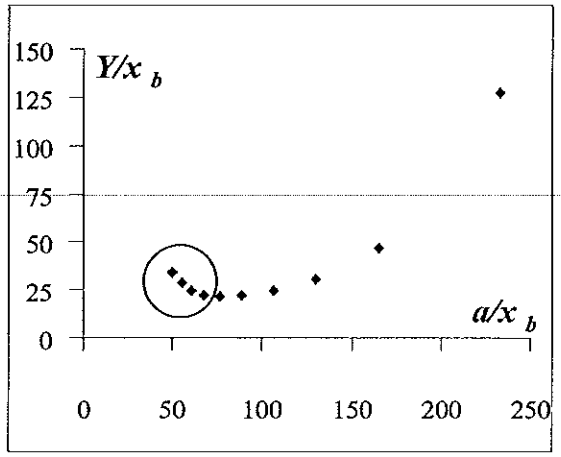

(a.1) N_2 adsorbed on activated carbon

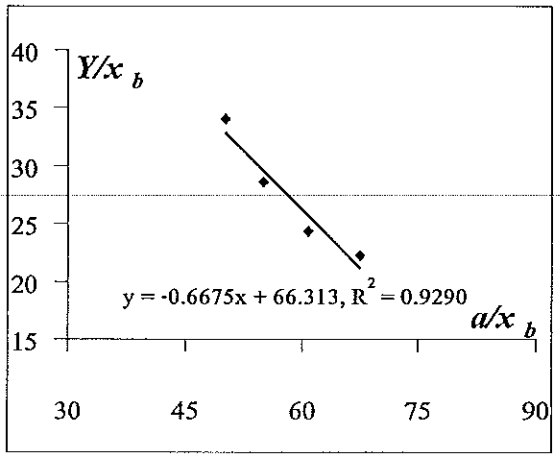

(a.2) large scale for adsorbed N_2

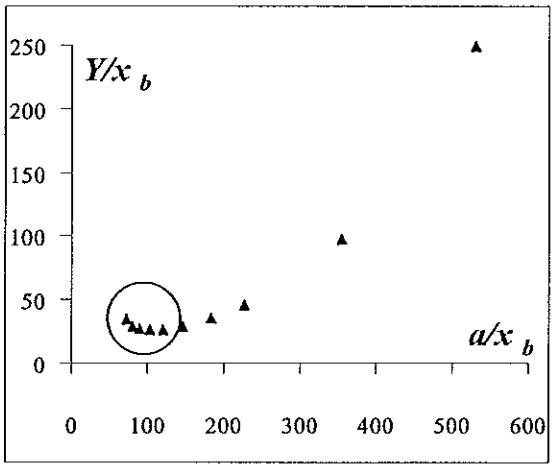

(b.1) CH_4 adsorbed on activated carbon

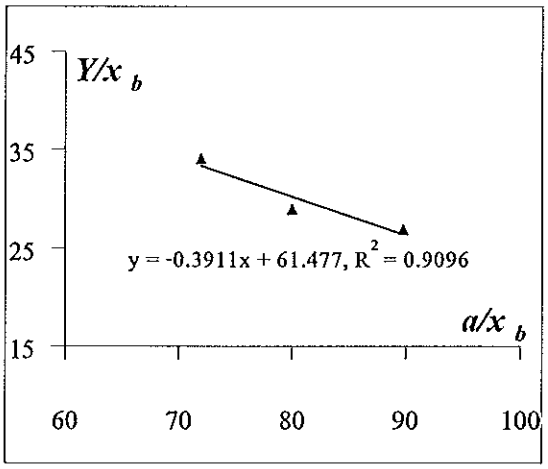

(b.2) large scale for adsorbed CH_4

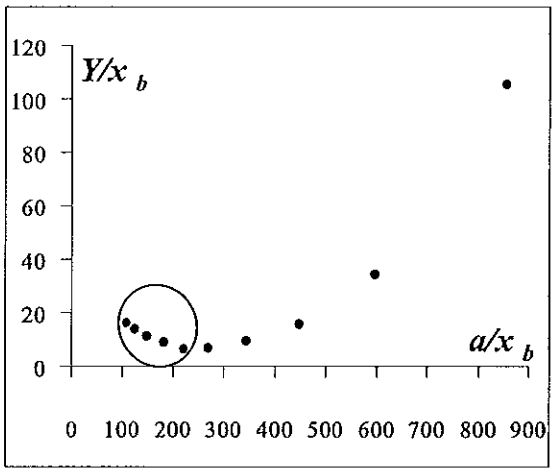

(c.1) CO_2 adsorbed on activated carbon

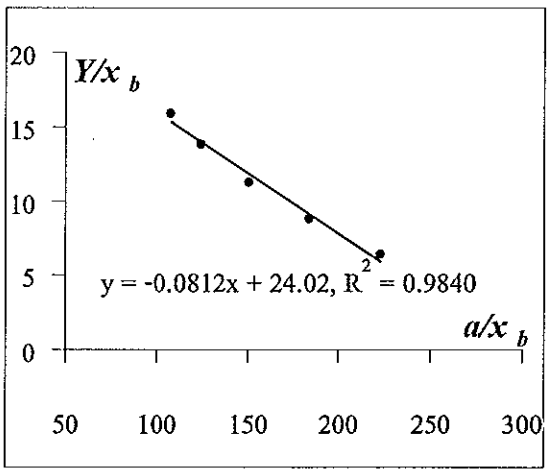

(c.2) large scale for adsorbed CO_2

Figure 3.5 Adsorption isotherms for (a) nitrogen, (b) methane and (c) carbon dioxide on activated carbon Filtrasorb 400 at 318.2 K [experimental data from ref. 70]. Circles indicate high pressure ends, and right frames show high pressure ends in larger scale.

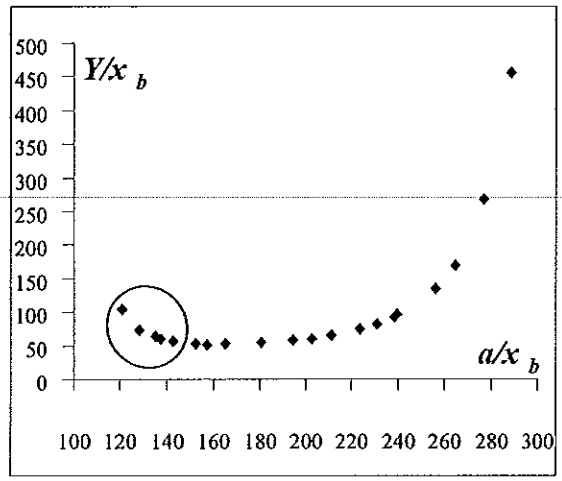

(a.1) N_2 adsorbed on zeolite

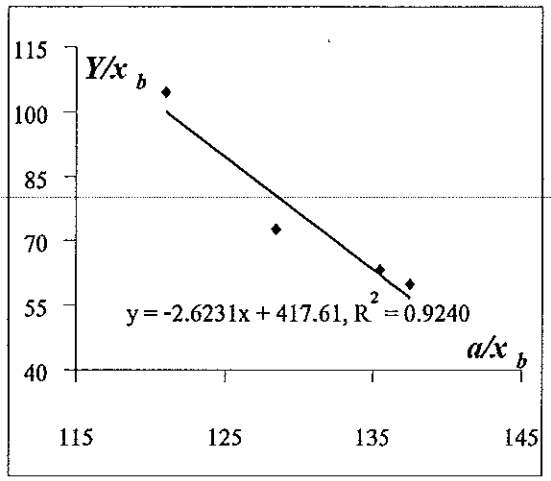

(a.2) large scale for adsorbed N_2

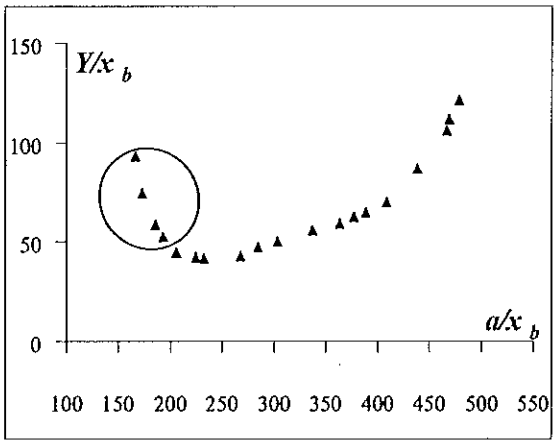

(b.1) CH_4 adsorbed on zeolite

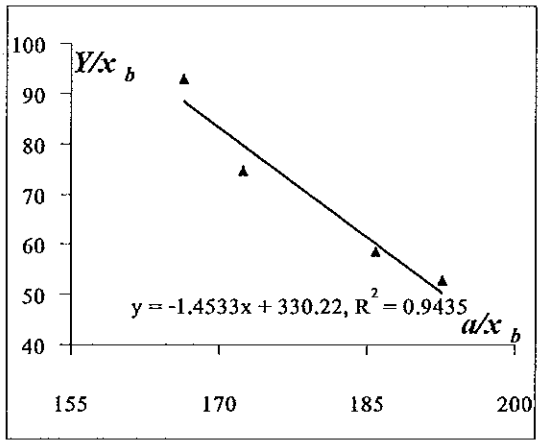

(b.2) large scale for adsorbed CH_4

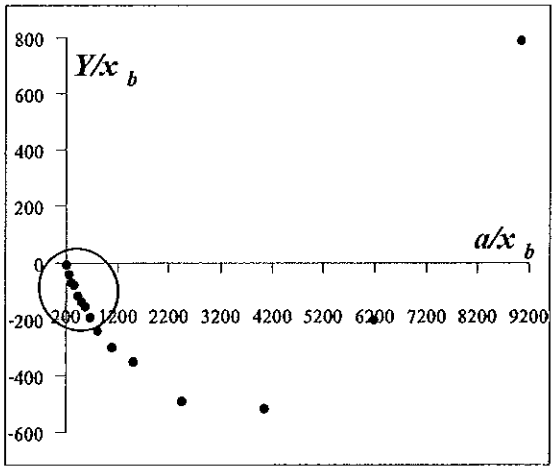

(c.1) CO_2 adsorbed on zeolite

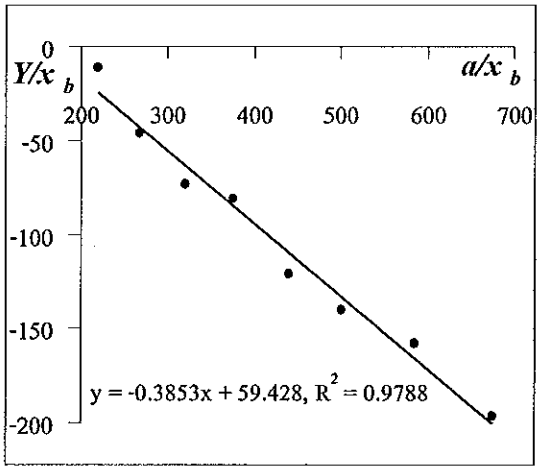

(c.2) large scale for adsorbed CO_2

Figure 3.6 Adsorption isotherms for (a) nitrogen, (b) methane and (c) carbon dioxide on zeolite 13X at 323 K [experimental data from ref. 71]. Circles indicate high pressure ends, and right frames show high pressure ends in larger scale.

Figures 3.5 and 3.6 show adsorption isotherms for nitrogen, methane, and carbon dioxide in Ono-Kondo coordinates at various scales. In these Figures, high pressure ends are marked by circles and the right frames give high pressure ends with much smaller scales. These graphs allow estimates of energies of adsorbate-adsorbate repulsions in supercritical systems. Comparison of Figures 3.5 and 3.6 indicates that adsorption compression of nitrogen, methane, and carbon dioxide in pores of zeolite is much stronger than in pores on Filtrasorb 400. This is to be expected.

Note that adsorption isotherms in Ono-Kondo coordinates shown in Figures 3.5 and 3.6 have minima. The reason for such a behavior is adsorption compression arising from competition between attraction of the adsorbate to the adsorbent surface and repulsions between/among neighboring adsorbate molecules [14-15]. At low pressure, neighbors in adsorbate attract each other. As pressure goes up, the distance between adsorbate molecules can become less than in a normal liquid and nearest neighbors repel each other. This is possible because the decrease of free energy due to attraction to the adsorbent is greater than the increase of free energy due to repulsions between adsorbate molecules. At the point where the adsorbate-adsorbate interactions go from attractive to repulsive, the average adsorbate-adsorbate energy is zero and this point corresponds to minimum in isotherms shown in Figures 3.5 and 3.6.

3.5 Conclusion

Ono-Kondo analysis of adsorption isotherms for supercritical systems (such as nitrogen, methane, and carbon dioxide on activated carbon Filtrasorb 400 and on zeolite 13X) indicates adsorption compression phenomenon at high pressure end just as in subcritical systems. The linear sections of these graphs show the range of applicability of the classical Ono-Kondo model with constant energies of interactions. The slopes of these linear sections represent values and signs of these energies: negative slopes indicate repulsive interactions in adsorbed phase due to adsorption compression. Switching interactions from attractive to repulsive with an increase in the pressure for supercritical adsorption suggests that adsorbed phase has two regions. One is an attractive region at low-pressures and the other is a repulsive region at high pressures.

With estimated or measured values of H, adsorption isotherms in Ono-Kondo coordinates show deviations from behavior of non-interacting particles. In these graphs, the slope (derivative) versus density characterizes the adsorbate-adsorbate interactions where the distance between nearest neighbors is a function of adsorbate density. It is important to note that the observation of a compressed adsorbed phase with repulsive adsorbate-adsorbate interactions at supercritical pressures can be made even from graphs with variable H, such as given in Figures 3.1 and 3.2.

CHAPTER 4

INTERMOLECULAR INTERACTIONS FOR BINARY ADSORPTION AT HIGH PRESSURE

4.1 Introduction

The utility of existing adsorption data at high pressures is limited by the discrepancies among the various data sets and also by the lack of reliable theoretical models that can be used to interpret, interpolate and extrapolate the data. Data on the behavior of supercritical fluids generally is neither available for all components nor available at all operating conditions of interest; thus this behavior needs to be estimated using thermodynamic models.

Although several theories have been developed for predicting the adsorption equilibria, no single theory can be used universally, especially for binary mixtures adsorbing at supercritical fluid conditions. Previously, several researchers have studied mixture adsorption over wide range of temperature and pressure and have tried to explain their data using the adsorption behavior for the pure components [11-13, 26, 28, and 75]. However, these references mainly focus on the fluid-solid interactions. Recently, we showed the applicability of the classical Ono-Kondo model with constant energies of adsorbate-adsorbate interactions to analyze intermolecular interactions in adsorbed phases for supercritical systems. The analysis indicates that there is adsorption compression with repulsive interactions in the adsorbed phase. In particular, the aim of this work is to extend the Ono-Kondo lattice gas model with adsorbate-adsorbate interactions to the treatment of binary component adsorption at high pressure. Experimental data for binary mixtures of methane/nitrogen, methane/carbon dioxide, and nitrogen/carbon dioxide supercritical fluids are plotted in Ono-Kondo coordinates with variable Henry's constant, H, and with preliminary estimated H. This allows analysis of adsorbate-adsorbate interactions in the adsorbed phase from adsorption isotherms.

4.2 Models

Consider a binary lattice with boundaries. Each site of the lattice can contain either an A molecule or a B molecule or it can be vacant. There are interactions between nearest neighbors with ε_{AA}, ε_{AB}, ε_{BB} being the energy of adsorbate-adsorbate interactions, and

ε_{AS}, ε_{BS} being the energy of adsorbate-adsorbent interactions. It can be assumed that the lattice fluid is in contact with a flat surface at the plane of *i=0* and that the first layer of adsorbed molecules is in the plane of *i=1*. Figure 4.1 illustrates the lattice model for both the adsorbate-adsorbate and adsorbate-adsorbent interactions in the monolayer adsorption.

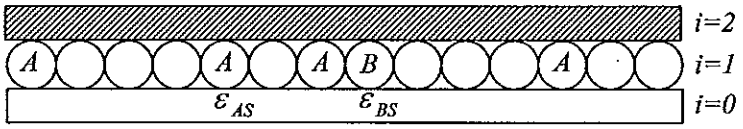

Figure 4.1 Schematic representation of the lattice model in the first layer for binary system.

In the model exhibited in Figure 1, *i=0* represents the surface plane, *i=1* defines the first layer of adsorbate molecules, *i=2* defines the second layer, and so on. The last layer, *i=N+1*, defines the bulk fluid. According to the Ono-Kondo model [51] and the Aranovich-Donohue model [54], can be represented as nonlinear finite difference equations of second order which relate the composition in each layer to the density in the bulk for *A* molecule as

$$kT\ln\frac{x_A(1-x_{A\infty}-x_{B\infty})}{(1-x_A-x_B)x_{A\infty}}+\frac{(z_3-z_2)}{2}\varepsilon_{As}+z_2x_A\varepsilon_{AA}+z_2x_B\varepsilon_{AB}+$$
$$\frac{(z_3-z_2)}{2}x_{A\infty}\varepsilon_{AA}+\frac{(z_3-z_2)}{2}x_{B\infty}\varepsilon_{AB}-[z_3x_{A\infty}\varepsilon_{AA}+z_3x_{B\infty}\varepsilon_{AB}]=0 \qquad (4.1)$$

where k_B is Boltzmann's constant, T is absolute temperature, z_1 is the number of connections between the surface and molecules in the first layer, z_2 is the coordination number in the monolayer, and z_3 is the coordination number for tree-dimensional lattice. Here, x_{∞} denotes the bulk concentration (or density), x_i is the concentration (or density) in the *i*-th adsorbed layer, ε represents the nearest-neighbor energy of the adsorbate-adsorbate interactions, and ε_s is the interaction energy between the adsorbate molecules on the adsorbent surface. Both ε and ε_s are negative for the attractive forces. Notice that the equations for *i*=1 and *i=N* define the boundary conditions on the lattice model.

Rearrangement equation (4.1) becomes to:

$$kT\ln\frac{x_A(1-x_{A\infty}-x_{B\infty})}{(1-x_A-x_B)x_{A\infty}}+\frac{(z_3-z_2)}{2}\varepsilon_{As}+z_2(x_A\varepsilon_{AA}+x_B\varepsilon_{AB})-\left(z_3-\frac{z_3-z_2}{2}\right)(x_{A\infty}\varepsilon_{AA}+x_{B\infty}\varepsilon_{AB})=0 \tag{4.2}$$

Equation (4.2) reduces to:

$$kT\ln\frac{x_A(1-x_{A\infty}-x_{B\infty})}{(1-x_A-x_B)x_{A\infty}}+\frac{(z_3-z_2)}{2}\varepsilon_{As}+z_2(x_A\varepsilon_{AA}+x_B\varepsilon_{AB})-\left(\frac{z_3+z_2}{2}\right)(x_{A\infty}\varepsilon_{AA}+x_{B\infty}\varepsilon_{AB})=0 \tag{4.3}$$

Similarly, for B molecules:

$$kT\ln\frac{x_B(1-x_{A\infty}-x_{B\infty})}{(1-x_A-x_B)x_{B\infty}}+\frac{(z_3-z_2)}{2}\varepsilon_{Bs}+z_2(x_A\varepsilon_{AB}+x_B\varepsilon_{BB})-\left(\frac{z_3+z_2}{2}\right)(x_{A\infty}\varepsilon_{AB}+x_{B\infty}\varepsilon_{BB})=0 \tag{4.4}$$

If $x_{A\infty}/x_{B\infty}=\alpha$, in the experiment ($x_{A\infty}$ changes due to change of pressure of A+B mixture) then; $x_{B\infty}=x_{A\infty}/\alpha$

$$kT\ln\frac{x_A(1-x_{A\infty}-\frac{x_{A\infty}}{\alpha})}{(1-x_A-x_B)x_{A\infty}}+\frac{(z_3-z_2)}{2}\varepsilon_{As}+z_2(x_A\varepsilon_{AA}+x_B\varepsilon_{AB})-\left(\frac{z_3+z_2}{2}\right)(x_{A\infty}\varepsilon_{AA}+\frac{x_{A\infty}}{\alpha}\varepsilon_{AB})=0 \tag{4.5}$$

In the limit of small $x_{A\infty}+x_{B\infty}$:

$$kT\ln\frac{x_A}{x_{A\infty}}+\frac{z_3-z_2}{2}\varepsilon_{As}=0 \tag{4.6}$$

Then: $x_A=x_{A\infty}H_A$

where $H_A = \exp\left[\frac{z_2 - z_3}{2}\varepsilon_{As}/kT\right]$

Same for H_B: $H_B = \exp\left[\frac{z_2 - z_3}{2}\varepsilon_{Bs}/kT\right]$

Therefore, equation (4.3) can be written as:

$$kT\ln\frac{x_A(1-x_{A\infty}-x_{B\infty})}{(1-x_A-x_B)x_{A\infty}} + kT\ln H_A + z_2(x_A\varepsilon_{AA} + x_B\varepsilon_{AB}) - \left(\frac{z_3+z_2}{2}\right)(x_{A\infty}\varepsilon_{AA} + x_{B\infty}\varepsilon_{AB}) = 0 \quad (4.7)$$

Also for B component:

$$kT\ln\frac{x_B(1-x_{A\infty}-x_{B\infty})}{(1-x_A-x_B)x_{B\infty}} + kT\ln H_B + z_2(x_A\varepsilon_{AB} + x_B\varepsilon_{BB}) - \left(\frac{z_3+z_2}{2}\right)(x_{A\infty}\varepsilon_{AB} + x_{B\infty}\varepsilon_{BB}) = 0 \quad (4.8)$$

Subtraction of equation (4.8) from (4.7) gives:

$$kT\ln\left(\frac{x_A}{x_B}\times\frac{x_{B\infty}}{x_{A\infty}}\right) - kT\frac{H_A}{H_B} + z_2[x_A(\varepsilon_{AA}-\varepsilon_{AB}) + x_B(\varepsilon_{AB}-\varepsilon_{BB})] - (\frac{z_3+z_2}{2})[x_{A\infty}(\varepsilon_{AA}-\varepsilon_{AB}) + x_{B\infty}(\varepsilon_{AB}-\varepsilon_{BB})] = 0 \quad (4.9)$$

Equation (4.9) can be written as:

$$\frac{kT}{x_{A\infty}}\ln\left(\frac{x_A}{\alpha x_B}\right) - kT\frac{H_A}{H_B} + z_2\frac{x_A}{x_{A\infty}}(\varepsilon_{AA}-\varepsilon_{AB}) + z_2\frac{x_B}{\alpha x_{B\infty}}(\varepsilon_{AB}-\varepsilon_{BB}) - (\frac{z_3+z_2}{2})[\varepsilon_{AA}-\varepsilon_{AB}+\frac{1}{\alpha}(\varepsilon_{AB}-\varepsilon_{BB})] = 0 \quad (4.10)$$

And:

$$\frac{kT\times\ln\left(\frac{x_A.H_A}{\alpha x_B.H_B}\right)}{x_{A\infty}}+z_2\frac{x_A}{x_{A\infty}}(\varepsilon_{AA}-\varepsilon_{AB})+z_2\frac{x_B}{x_{B\infty}}\frac{(\varepsilon_{AB}-\varepsilon_{BB})}{\alpha}- \tag{4.10a}$$
$$(\frac{z_3+z_2}{2})[\varepsilon_{AA}-\varepsilon_{AB}+(\frac{\varepsilon_{AB}-\varepsilon_{BB}}{\alpha})]=0$$

Equation (4.7) gives (dividing by $x_{A\infty}$):

$$\frac{kT}{x_{A\infty}}\ln\frac{x_A(1-x_{A\infty}-x_{B\infty})}{H_A(1-x_A-x_B)x_{A\infty}}+z_2\left(\frac{x_A}{x_{A\infty}}\varepsilon_{AA}+\frac{x_B}{\alpha x_{B\infty}}\varepsilon_{AB}\right)- \tag{4.11}$$
$$\left(\frac{z_3+z_2}{2}\right)\left(\varepsilon_{AA}+\frac{\varepsilon_{AB}}{\alpha}\right)=0$$

Equation (4.8) gives similar result for B component:

$$\frac{kT}{x_{B\infty}}\ln\frac{x_B(1-x_{A\infty}-x_{B\infty})}{H_B(1-x_A-x_B)x_{B\infty}}+z_2\left(\frac{x_B}{x_{B\infty}}\varepsilon_{BB}+\frac{\alpha x_A}{x_{A\infty}}\varepsilon_{AB}\right)- \tag{4.12}$$
$$\left(\frac{z_3+z_2}{2}\right)(\varepsilon_{BB}+\alpha\varepsilon_{AB})=0$$

Specifies:

$$z_2\varepsilon_{AA}=A \qquad z_2\varepsilon_{AB}=B$$
$$\left(\frac{z_3+z_2}{2}\right)\varepsilon_{AA}=C \qquad \left(\frac{z_3+z_2}{2}\right)\varepsilon_{AB}=C.\frac{B}{A}$$

Equation (4.11) becomes:

$$\frac{kT}{x_{A\infty}}\ln\frac{x_A(1-x_{A\infty}-x_{B\infty})}{H_A(1-x_A-x_B)x_{A\infty}}+A.\frac{x_A}{x_{A\infty}}+B.\frac{x_B}{\alpha x_{B\infty}}-C-\frac{C.B}{\alpha A}=0 \tag{4.13}$$

Defines:

$$z_2\varepsilon_{BB} = D \qquad z_2\varepsilon_{AB} = B$$

$$\left(\frac{z_3 + z_2}{2}\right)\varepsilon_{BB} = E \qquad \left(\frac{z_3 + z_2}{2}\right)\varepsilon_{AB} = E.\frac{B}{D}$$

Then, equation (4.12) becomes:

$$\frac{kT}{x_{B\infty}}\ln\frac{x_B(1-x_{A\infty}-x_{B\infty})}{H_B(1-x_A-x_B)x_{B\infty}} + D.\frac{x_B}{x_{B\infty}} + \alpha B.\frac{x_A}{x_{A\infty}} - E - \alpha E\frac{B}{D} = 0 \tag{4.14}$$

Equation (4.9) can be rewritten as:

$$kT\ln\left(\frac{x_A}{x_B}.\frac{H_B}{\alpha H_A}\right) + z_2(\varepsilon_{AA}-\varepsilon_{AB}).x_A + z_2(\varepsilon_{AB}-\varepsilon_{BB}).x_B -$$
$$\left(\frac{z_3 + z_2}{2}\right)(\varepsilon_{AA}-\varepsilon_{AB}).x_{A\infty} + \left(\frac{z_3 + z_2}{2}\right)(\varepsilon_{AB}-\varepsilon_{BB}).x_{B\infty} = 0 \tag{4.15}$$

Notations:

$$z_2\left(\frac{\varepsilon_{AA}-\varepsilon_{AB}}{kT}\right) = A \qquad z_2(\varepsilon_{AB}-\varepsilon_{BB}) = B$$

$$\left(\frac{z_3 + z_2}{2}\right)\left(\frac{\varepsilon_{AA}-\varepsilon_{AB}}{kT}\right) = C \qquad \left(\frac{z_3 + z_2}{2}\right)\left(\frac{\varepsilon_{AB}-\varepsilon_{BB}}{kT}\right) = C.\frac{B}{A}$$

And equation (4.15) becomes:

$$\ln\left(\frac{x_A.H_B}{x_B.\alpha H_A}\right) + Ax_A + Bx_B - Cx_{A\infty} - C\frac{B}{A}x_{B\infty} = 0 \tag{4.16}$$

When $x_{A\infty}/x_{B\infty} = \alpha$, then; $x_{B\infty} = x_{A\infty}/\alpha$, and equation (4.16) is:

$$\ln\left(\frac{x_A.H_B}{x_B.\alpha H_A}\right) + Ax_A + Bx_B - C\left(1+\frac{B}{\alpha A}\right)x_{A\infty} = 0 \tag{4.17}$$

In the range of small $x_{A\infty}$ and $x_{B\infty}$, equation (4.17) becomes:

$$\ln\left(\frac{x_A.H_B}{x_B.\alpha H_A}\right)+Ax_A+Bx_B=0 \tag{4.18}$$

This allows getting parameters for A and B components if data are measured at two points (different α or different x_A/x_B). For example (4.18) is:

$$\frac{1}{x_B}\ln\left(\frac{x_A.H_B}{x_B.\alpha H_A}\right)=-A\frac{x_A}{x_B}+B \tag{4.19}$$

Plotting $\frac{1}{x_B}\ln\left(\frac{x_AH_B}{x_B\alpha H_A}\right)$ vs $\frac{x_A}{x_B}$ gives A and B, in the range of small $x_{A\infty}$ and $x_{B\infty}$, equation (4.7) can be rewritten as:

$$\frac{1}{x_B}\ln\frac{x_A}{(1-x_A-x_B)x_{A\infty}H_A}=-\frac{z_2\varepsilon_{AA}}{kT}\frac{x_A}{x_B}-\frac{z_2\varepsilon_{AB}}{kT} \tag{4.20}$$

Plotting $\frac{1}{x_B}\ln\frac{x_A}{(1-x_A-x_B)x_{A\infty}H_A}$ vs $\frac{x_A}{x_B}$ gives $\frac{z_2\varepsilon_{AA}}{kT}$ and $\frac{z_2\varepsilon_{AB}}{kT}$, similar equation (4.8) can be written for B component:

$$\frac{1}{x_A}\ln\frac{x_B}{(1-x_A-x_B)x_{B\infty}H_B}=-\frac{z_2\varepsilon_{BB}}{kT}\frac{x_B}{x_A}-\frac{z_2\varepsilon_{AB}}{kT} \tag{4.21}$$

Plotting $\frac{1}{x_A}\ln\frac{x_B}{(1-x_A-x_B)x_{B\infty}H_B}$ vs $\frac{x_B}{x_A}$ gives $\frac{z_2\varepsilon_{BB}}{kT}$ and $\frac{z_2\varepsilon_{AB}}{kT}$, signs of $\frac{z_2\varepsilon_{AA}}{kT}$, $\frac{z_2\varepsilon_{BB}}{kT}$ and $\frac{z_2\varepsilon_{AB}}{kT}$ gives information about compression. Here values of $x_{A\infty}$ and $x_{B\infty}$ can be approximated by $x_{A\infty}=(\pi/6)n\sigma_A^3$, here n is the total number of particles per volume of the container, and σ is the distance between molecules. Note that n is calculated from the classical ideal gas law as $n=\frac{n_mN_A}{V}=\frac{P}{kT}$, where P is pressure of the fluid [Pa], V is total volume of the container containing the fluid [m^3], n_m is the number of moles [mole], N_A is Avogadro number [molecules/mole], k is Boltzmann's constant [J/K], and T is absolute temperature [K].

4.3 Plotting Adsorption Isotherms for Binary Mixtures (CH_4/CO_2, CH_4/N_2, and N_2/CO_2) in Ono-Kondo Coordinates with Estimated Henry's Constants

Plotting Y (the first term in equations 4.20 and 4.21) as a function of x_A/x_B, we can get the value of $\frac{z_2\varepsilon_{AA}}{kT}$ and $\frac{z_2\varepsilon_{BB}}{kT}$ from the slope of the graph. The sign of $\frac{z_2\varepsilon_{AA}}{kT}$ and $\frac{z_2\varepsilon_{BB}}{kT}$ give in formation about the sign of adsorbate-adsorbate interactions. These coordinates also gives the intercept, $\frac{z_2\varepsilon_{AB}}{kT}$ which can be used to that verify this simplistic model is reasonable for gas-solid systems.

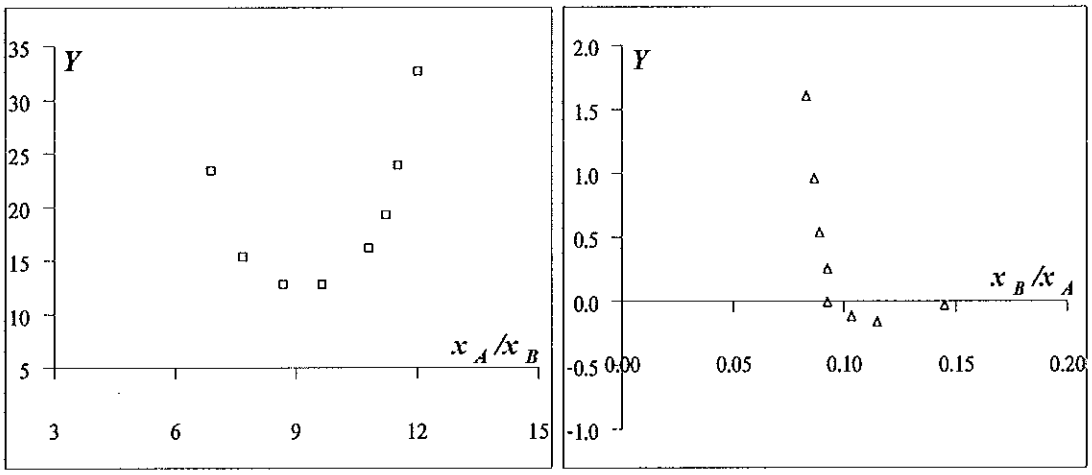

(a) coordinates of Eq. (4.20) for CH_4/N_2 (b) coordinates of Eq. (4.21) for CH_4/N_2

Figure 4.2 Adsorption isotherms for CH_4/N_2 binary system adsorbed on activated carbon Filtrasorb 400 at T = 318.2 K [experimental data from ref. 70] with ratio 81.7% : 18.3% ⇔ CH_4 : N_2 in coordinates of (a) equation (4.20), and (b) equation (4.21). Y is the first term for each of Eqs. (4.20) and (4.21). Specified CH_4 is A component and N_2 is B component.

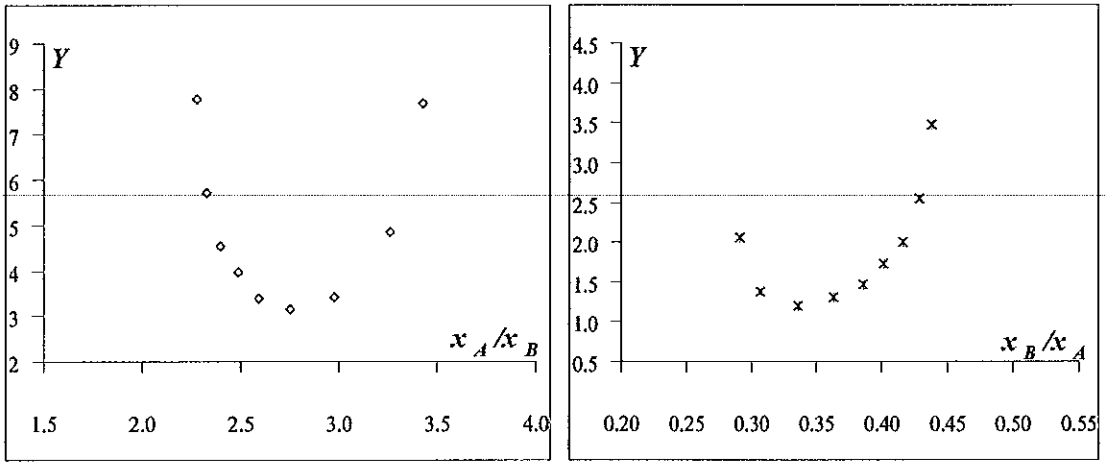

(a) coordinates of Eq. (4.20) for CH_4/CO_2 (b) coordinates of Eq. (4.21) for CH_4/CO_2

Figure 4.3 Adsorption isotherms for CH_4/CO_2 binary system adsorbed on activated carbon Filtrasorb 400 at T = 318.2 K [experimental data from ref. 70] with ratio 80.0% : 20.0% ⇔ CH_4 : CO_2 in coordinates of (a) equation (4.20), and (b) equation (4.21). *Y* is the first term for each of Eqs. (4.20) and (4.21). Specified CH_4 is *A* component and CO_2 is *B* component.

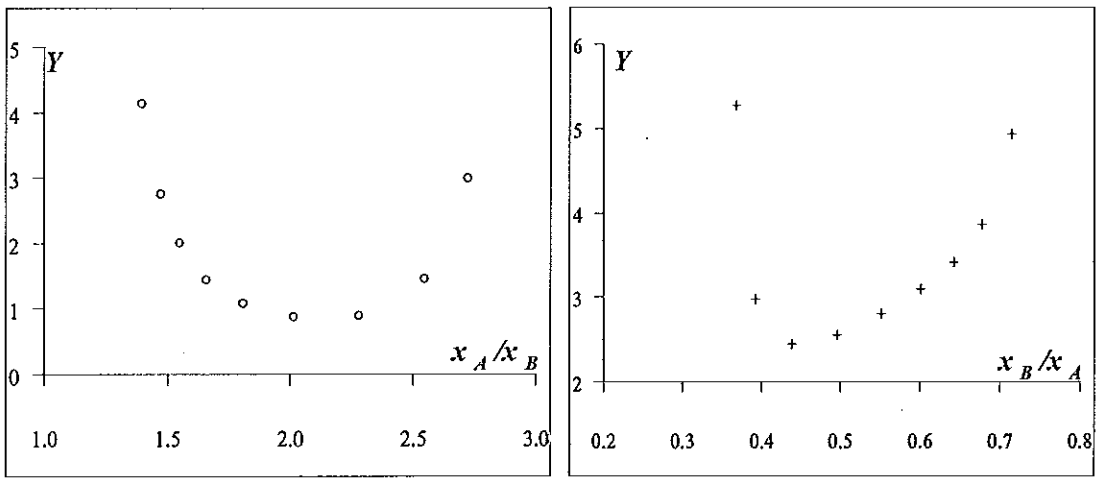

(a) coordinates of Eq. (4.20) for N_2/CO_2 (b) coordinates of Eq. (4.21) for N_2/CO_2

Figure 4.4 Adsorption isotherms for N_2/CO_2 binary system adsorbed on activated carbon Filtrasorb 400 at T = 318.2 K [experimental data from ref. 70] with ratio 80.0% : 20.0% ⇔ N_2 : CO_2 in coordinates of (a) equation (4.20), and (b) equation (4.21). *Y* is the first term for each of Eqs. (4.20) and (4.21). Specified N_2 is *A* component and CO_2 is *B* component.

We used the equilibrium adsorption data for binary mixtures on activated carbon at 318 K and pressures up to 13.6 MPa (data from [70]) to analyze adsorption isotherms. Figures 4.2-4.4 illustrate adsorption isotherms for different binary systems in coordinates of equations (4.20) and (4.21) with the estimated H values in Table 3.1 [72-74]. The results for the example of different systems have similar shapes: the change of adsorbate-adsorbate interactions for CH_4/N_2, CH_4/CO_2 and N_2/CO_2 mixtures is similarly going down to a certain minimum and then going up. These transitions indicate the competitive nature of the individual component adsorption from the mixtures. The relative adsorbate molecule size and pore structure may be effected to interacting change.

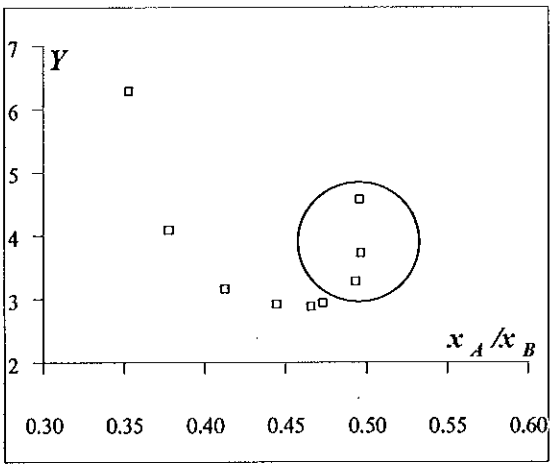

(a.1) coordinates of Eq. (4.20) for CH_4/N_2

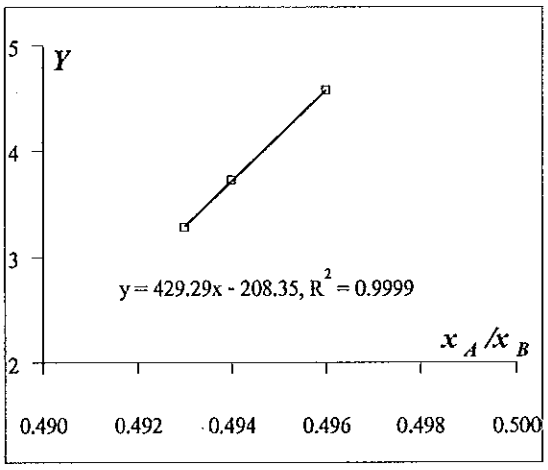

(a.2) larger scale for (a.1)

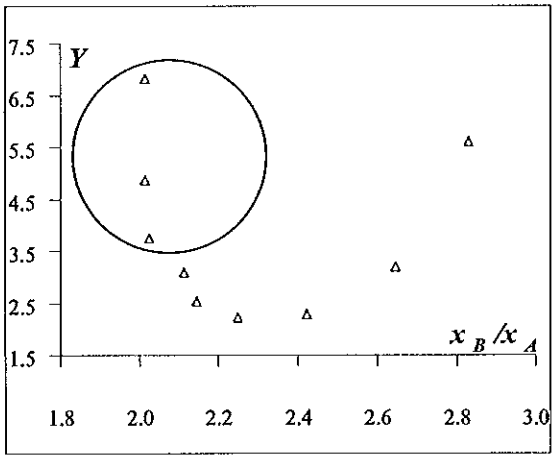

(b.1) coordinates of Eq. (4.21) for CH_4/N_2

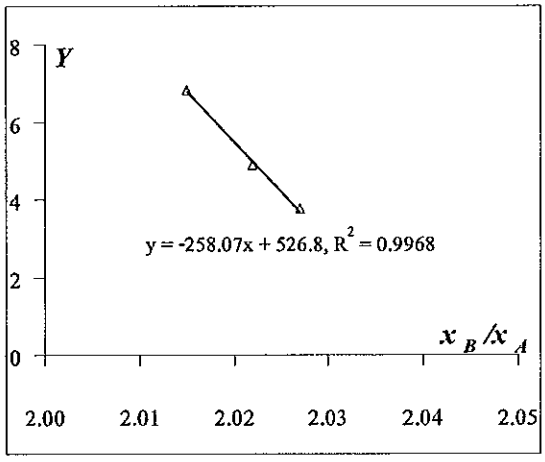

(b.2) larger scale for (b.1)

Figure 4.5 Adsorption isotherms for CH_4/N_2 binary system adsorbed on activated carbon Filtrasorb 400 at T = 318.2 K [experimental data from ref. 70] with ratio 20.0% : 80.0% ⇔ CH_4 :

N_2 in coordinates of (a) equation (4.20), and (b) equation (4.21). *Y* is the first term for each of Eqs. (4.20) and (4.21). Specified N_2 is *A* component and CO_2 is *B* component. Circles indicate high composition ends, and right frames show high pressure ends in larger scale.

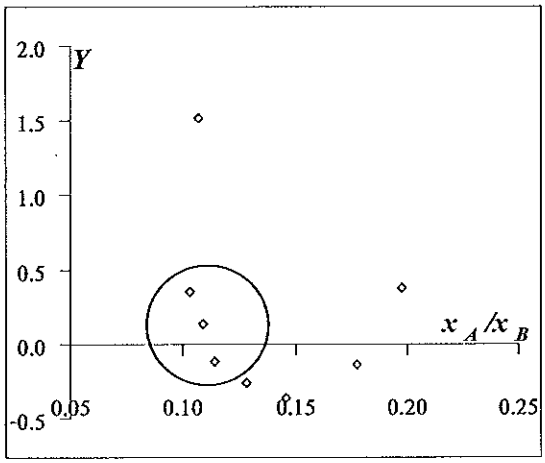

(a.1) coordinates of Eq. (4.20) for CH_4/CO_2

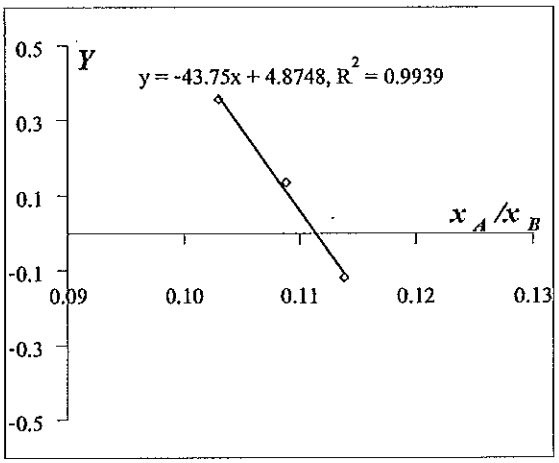

(a.2) larger scale for (a.1)

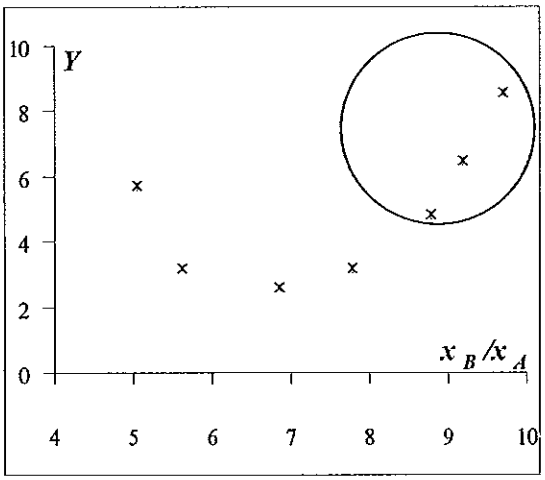

(b.1) coordinates of Eq. (4.21) for CH_4/CO_2

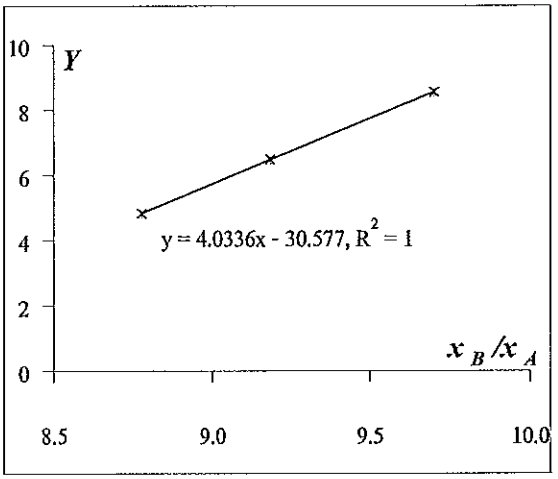

(b.2) larger scale for (b.1)

Figure 4.6 Adsorption isotherms for CH_4/CO_2 binary system adsorbed on activated carbon Filtrasorb 400 at T = 318.2 K [experimental data from ref. 70] with ratio 20.0% : 80.0% ⇔ CH_4 : CO_2 in coordinates of (a) equation (4.20), and (b) equation (4.21). *Y* is the first term for each of Eqs. (4.20) and (4.21). Specified CH_4 is *A* component and CO_2 is *B* component. Circles indicate high composition ends, and right frames show high pressure ends in larger scale.

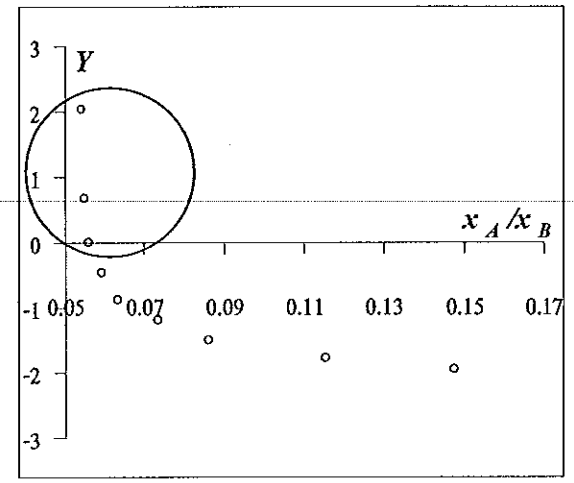

(a.1) coordinates of Eq. (4.20) for N_2/CO_2

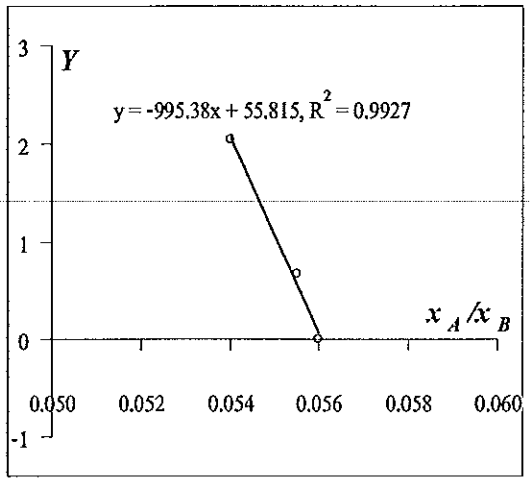

(a.2) larger scale for (a.1)

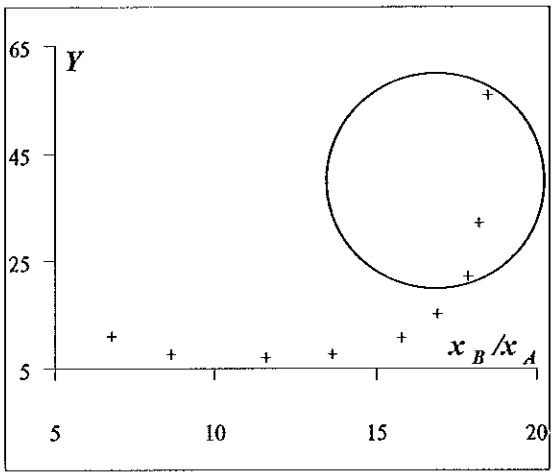

(b.1) coordinates of Eq. (4.21) for N_2/CO_2

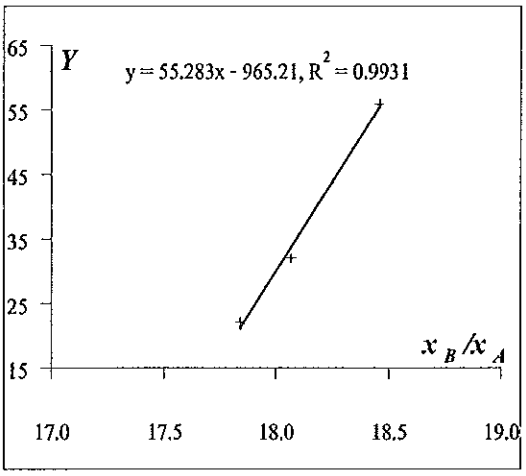

(b.2) larger scale for (b.1)

Figure 4.7 Adsorption isotherms for N_2/CO_2 binary system adsorbed on activated carbon Filtrasorb 400 at T = 318.2 K [experimental data from ref. 70] with ratio 20.0% : 80.0% $\Leftrightarrow$ N_2 : CO_2 in coordinates of (a) equation (4.20), and (b) equation (4.21). *Y* is the first term for each of Eqs. (4.20) and (4.21). Specified N_2 is *A* component and CO_2 is *B* component. Circles indicate high composition ends, and right frames show high pressure ends in larger scale.

From Figure 4.5-4.7, the results showed both negative and positive slopes. The negative slopes of lines (positive interaction energies) indicate repulsions between adsorbate molecules on the surface. These isotherms indicate the transition from attraction to repulsion between molecules of the adsorbate. The positive values of interaction energy are not surprising because of the very strong Lennard-Jones repulsion between adsorbed molecules on nearest neighbor adsorption sites. This also suggests that the repulsive part of adsorbate-adsorbate

interactions is the dominant contribution to the average intermolecular interaction at high densities.

4.4 Conclusions

Compressed molecules can be expected on any adsorbent at high concentrations where the adsorbed layer is nearly full. At high enough density, interactions in adsorbed layer become repulsive and $z_2\varepsilon_{AA}$, or $z_2\varepsilon_{BB}$ becomes positive, but the total change in energy still can be negative because of large negative ε_s. However, the repulsion of molecules in the full monolayer seems to be general behavior for high enough affinity to the adsorbent.

CHAPTER 5

CONCLUSIONS

This is the first time that supercritical data has been evaluated and shown to demonstrate adsorption compression. The Ono-Kondo model is used to correlate with experimental data from references for the adsorption of pure nitrogen, methane, and carbon dioxide on activated carbon Filtrasorb 400 and zeolite 13X and their binary mixtures on activated carbon Filtrasorb 400 at 318.2 K. Results indicate that the adsorption isotherms in Ono-Kondo coordinates show adsorption compression with repulsive interactions in the adsorbed phase for single gases and binary systems at supercritical conditions. For pure gases, the adsorbate-adsorbate interaction energies vary from positive at low pressures to negative at high pressures when considered from Henry's law range to supercritical pressures. For binary mixtures, compressed molecules can be expected on any adsorbent at high concentrations where the adsorbed layer is nearly full. At high enough density, interactions in adsorbed layer become repulsive and $z_2\varepsilon_{AA}$, or $z_2\varepsilon_{BB}$ becomes positive, but the total change in energy still can be negative because of large negative of ε_s. However, the repulsion of molecules in the full monolayer seems to be general behavior for high enough affinity to the adsorbent.

Moreover, the Gibbs adsorption isotherms for supercritical gases are calculated from equation (2.23) that are sensitive to change in ε_s/kT and ε/kT values. The Gibbs adsorption isotherms under supercritical conditions have a negative slope and decrease as the pressure (or density) increases. This is because the bulk density is increasing but the monolayer density is constant. Therefore, at supercritical region allow nearly complete monolayer coverage but there is not multilayer adsorption because the temperature is sufficiently above the critical temperature of the adsorbate and the pressures are high enough for a completely covered monolayer [76].

REFERENCES

[1] United States Environmental Protection Agency: Global Greenhouse Gas Data. http://www.epa.gov/climatechange/emissions/globalghg.html (Accessed August 7, 2008)

[2] Davis, M. L., and Masten, S. J. 2004. *Principles of Environmental Engineering and Science*. McGraw-Hill.

[3] Mazzotti, M., Pini, R., and Storti, G. 2009. Enhanced coalbed methane recovery. *J. of Supercritical Fluids* 47: 619-627.

[4] Aranovich, G. L., Donohue, M. D. 1996. Adsorption of supercritical fluids. *J. Colloid. Interface. Sci.* 180: 537-541.

[5] Zhou, L. 2002. Adsorption Isotherms for the Supercritical Region. In *Adsorption; Theory, Modeling, and Analysis*. Marcel Dekker, Inc. USA.

[6] Myers, A. L., and Monson, P. A. 2002. Adsorption in Porous Materials at High Pressure: Theory and Experiment. *Langmuir* 18: 10261-10273.

[7] Monsalvo, M. A., and Shapiro, A. A. 2009. Study of high-pressure adsorption from supercritical fluids by the potential theory. *Fluid Phase Equilibria* 283: 56-64.

[8] Nitta, T, and Shigeta, T. 1998. Computer simulation studies of adsorption characteristics in supercritical fluids. *Fluid Phase Equilibria* 144: 245-256.

[9] Egorov, S. A. 2001. Adsorption of supercritical fluids and fluid mixtures: inhomogeneous integral equation study. *J. Phys. Chem. B* 105: 6583-6591.

[10] Nguyen, T. X., Bhatia, S. K., and Nicholson, D. 2005. Prediction of high-pressure adsorption equilibrium of supercritical gases using density functional theory. *Langmuir* 21: 3187-3197.

[11] Kurniawan, Y., Bhatia, S. K., and Rudolph, V. 2006. Simulation of binary mixture adsorption of methane and CO_2 at supercritical conditions in carbons. *AIChE J.* 52: 957-967.

[12] Yan, B., and Yang, X. 2005. Adsorption prediction for three binary supercritical gas mixtures on activated carbon based on a NDFT/PSD approach. *Chem. Eng. Sci.* 60: 3267-3277.

[13] Yang, X., and Lira, C. T. 2006. Theoretical study of adsorption on activated carbon from a supercritical fluid by the SLD-ESD approach. *J. Supercrit Fluids* 37: 191-200.

[14] Charniak, C. L., Wetzel, T. E., Aranovich, G. L., and Donohue, M. D. 2008. Monte Carlo simulations of phase transitions and adsorption isotherm discontinuities on surface compression. *J. Colloid. Interface. Sci.* 324: 9-14.

[15] Aranovich, G. L., and Donohue, M. D. 2005. The role of adsorption compression in nanocapillarity. *J. Colloid. Interface. Sci.* 292: 202-209.

[16] Aranovich, G. L., Wetzel, T. E., and Donohue, M. D. 2008. Adsorption Behavior of Repulsive Molecules. *J. Phys. Chem. B* 109: 10189-10193.

[17] Wetzel, T. E., Erickson, J. S., Donohue, P. S., Charniak, C. L., Aranovich, G. L., and Donohue, M. D. 2004. Monte Carlo simulations on the effect of substrate geometry on adsorption and compression. *J. Chem. Phys.* 120: 11765-11774.

[18] Aranovich, G. L.; Donohue, M. D. 2003. Adsorption Compression: An Important New Aspect of Adsorption Behavior and Capillarity. *Langmuir* 19: 2722-2735.

[19] Brunner, G. 2005. Supercritical fluids: technology and application to food processing. *Journal of Food Engineering* 67: 21-33.

[20] Pasquali, I., Bettini, R., and Giordano, F. 2006. Solid-state chemistry and particle engineering with supercritical fluids in pharmaceutics. *European Journal of Pharmaceutical Sciences* 27: 299-310.

[21] Nalawade, S. P., Picchioni, F., and Janssen, L. P. B. M. 2006. Supercritical carbon dioxide as a green solvent for processing polymer melts: Processing aspects and applications. *Progress in Polymer Science* 31: 19-43.

[22] Leitner, W. 2000. Green chemistry: Designed to dissolve. *Nature* 405 (May): 129-130. http://www.nature.com/nature/journal/v405/n6783/fig_tab/405129a0_F1.html (Accessed November 16, 2008)

[23] Phillips, T. 2003. Harvesting Mars. NASA. http://www.nasa.gov/vision/earth/technologies/harvestingmars_prt.htm (Accessed November 16, 2008)

[24] Sun, Y. P. 2002. Supercritical Fluid Technology in Materials Science and Engineering: syntheses, properties, and applications, Marcel Dekker, USA.

[25] Clarkson, C. R., Bustin, R. M., and Levy, J. H. 1997. Application of the mono/multilayer and adsorption potential theories to coal methane adsorption isotherms at elevated temperature and pressure. *Carbon* 35: 1689-1705.

[26] Wu, et al. 2004. Prediction of the adsorption equilibrium of mixtures composed of supercritical gases. *J J. Colloid. Interface. Sci.* 276: 277–283.

[27] Ustinov, et al. 2002. Modeling of Gas Adsorption Equilibrium over a Wide Range of Pressure: A Thermodynamic Approach Based on Equation of State. *J. Colloid. Interface. Sci.* 250: 49–62.

[28] Zhou, et al. 2005. Prediction of multicomponent adsorption equilibrium of gas mixtures including supercritical components. *Chem. Eng. Sci.* 60: 2833-2844.

[29] Humayun, R. and Tomasko, D. L. 2000. High-Resolution Adsorption Isotherms of Supercritical Carbon Dioxide on Activated Carbon. *AIChE J.* 46: 2065-2075.

[30] Bhatia, et al. 2004. High-pressure adsorption capacity and structure of CO_2 in carbon slit pores: theory and simulation. *Langmuir* 20: 9612-9620.

[31] Ginty, et al. 2005. Drug delivery goes supercritical. *Materials Today* 8: 42-48.

[32] Meziani, et al. 2006. Supercitical fluid processing of nanoscale particles from biodegradable and biocompatible polymers. *Ind. Eng. Chem. Res.* 45: 3402-3424.

[33] Perrut, M. 2000. Supercitical fluid application: industrial developments and economic issues. *Ind. Eng. Chem. Res.* 39: 4531-4535.

[34] Fitzgerald, et al. 2003. Modeling the adsorption of pure gases on coals with the SLD model. *Carbon* 41: 2203-2216.

[35] Nakamura, K., Hoshino, T., and Ariyama, H. 1991. Adsorption of carbon dioxide on proteins in the supercritical region. *Agric. Biol. Chem.* 55: 2341-2347.

[36] Lim, S., and Rizvi, S. S. H. 1996. Adsorption and desorption of cholesterol in continuous supercritical fluid processing of anhydrous milk fat. *J. Food. Sci.* 61: 817-820.

[37] Lucas, et al. 2004. Adsorption isotherms for ethylacetate and furfural on activated carbon from supercritical carbon dioxide. *Fluid Phase Equilibria* 219: 171-179.

[38] Chen, J. H., Wong, D. S. H., Subramanian, C. S. T., Lira, C. T., and Orth, M. 1997. Adsorption and Desorption of Carbon Dioxide onto and from Activated Carbon at High Pressures. *Ind. Eng. Chem. Res.* 36(7): 2808–2815.

[39] Cross, W. M., and Akgerman, A. 1998. Adsorption separations using supercritical frontal analysis chromatography. *AIChE J.* 44: 1542-1554.

[40] Iwair, et al. 2003. Adsorption of supercritical carbon dioxide + 2,6- and 2,7- dimethyl naphthalene isomers on NaY zeolite. *Ind. Eng. Chem. Res.* 42: 5261-5267.

[41] Condoret, et al. 1997. Prediction of water adsorption curves for heterogeneous biocatalysis in organic and supercritical solvents. *Chem. Eng. Sci.* 52: 213-220.

[42] Myers, A. L. 2002. Thermodynamics of adsorption in porous materials. *AIChE J.* 48: 145-160.

[43] Li, M., Gu, A., Lu, X., and Wang, R. 2004. Supercritical Methane Adsorption Equilibrium Data on Activated Carbon with Prediction by the Adsorption Potential Theory. *J. Chem. Eng. Data 49*(1): 73–76.

[44] Zhou, L., and Zhou, Y. A. 1996. Comprehensive Model for the Adsorption of Supercritical Hydrogen on Activated Carbon. *Ind. Eng. Chem. Res. 35*(11): 4166–4168.

[45] Czerny, A. M., Benard, P., and Chahine, R. 2005. Adsorption of Nitrogen on Granular Activated Carbon: Experiment and Modeling. *Langmuir* 21(7): 2871–2875.

[46] Zhan, L., Li, K. X., Zhang, R., Liu, Q. F., Lu, CH. X., Ling, L. CH. 2004. Improvements of the DA equation for application in hydrogen adsorption at supercritical conditions. *The Journal of Supercritical Fluids* 28(1): 37-45.

[47] Tan, C. S., and Liou, D. C. 1990. Adsorption equilibrium of toluene from supercritical carbon dioxide on activated carbon. *Ind. Eng. Chem. Res.* 29: 1412-1415.

[48] Ryu, Y. K., Kim, K. L., and Lee, C. H. 2000. Adsorption and desorption of n-Hexane, methyl ethyl ketone, and toluene on activated carbon fiber from supercritical carbon dioxide. *Ind. Eng. Chem. Res.* 39: 2510-2518.

[49] Gathitu, B. B., Chen, W. Y., and McClure, M. 2009. Effects of Coal Interaction with Supercritical CO_2: Physical Structure. *Ind. Eng. Chem. Res. 48*(10): 5024–5034.

[50] Benard, P., and Chahine, R. 1997. Modeling of high-pressure adsorption isotherms above the critical temperature on microporous adsorbents: Application to methane. *Langmuir* 13: 808-813.

[51] Ono, S., and Kondo, S. 1960. *Molecular theory of surface tension in liquids*, Flugge, S., Ed., Encyclopedia of Physics, 10: 134. Berlin: Springer-Verlag.

[52] Aranovich, G. L., and Donohue, M. D. 1995. Adsorption isotherms for microporous adsorbents. *Carbon* 33: 1369-1375.

[53] Aranovich, G. L., and Donohue, M. D. 1997. Predictions of multilayer adsorption using lattice theory. *J. Colloid. Interface. Sci.* 189: 101-108.

[54] Aranovich, G. L., and Donohue, M. D. 1998. Analysis of adsorption isotherms: lattice theory predictions, classification of isotherms for gas-solid equilibria, and similarities in gas and liquid adsorption behavior. *J. Colloid. Interface. Sci.* 200: 273-290.

[55] Donohue, M. D., and Aranovich, G. L. 1998. Adsorption hysteresis in porous solids. *J. Colloid. Interface. Sci.* 205: 121-130.

[56] Donohue, M. D., and Aranovich, G. L. 1999. A new classification of isotherms for Gibbs adsorption of gases on solids. *Fluid Phase Equilibria* 158-160: 557-563.

[57] Hacher, T., Aranovich, G. L., and Donohue, M. D. 1999. Monolayer adsorption for the subcritical lattice gas and partially miscible binary mixtures. *J. Colloid. Interface. Sci.* 211: 61-80.

[58] Aranovich, G. L., and Donohue, M. D. 2000. Vapor adsorption on microporous adsorbents. *Carbon* 38: 701-708.

[59] Benard, P., and Chahine, R. 2001. Determination of the adsorption isotherms of hydrogen on activated carbons above the critical temperature of the Adsorbate over wide temperature and pressure ranges. *Langmuir* 17: 1950-1955.

[60] Aranovich, G. L., and Donohue, M. D. 2003. Critical point corrections for two- and three- dimensional systems. *Langmuir* 19: 2162-2168.

[61] Do, D. D. 1998. *Adsorption analysis: Equilibrium and kinetics*, vol. 2, Imperial College Press. London.

[62] Sudibandriyo, et al. 2003. Extension of the Ono-Kondo lattice model to high-pressure mixture adsorption. *Proceeding of the AIChE Spring National Meeting*, New Orleans, LA, March 30-April 3.

[63] Everett, D. H., and Radke, C. J. 1975. *Thermodynamics of Adsorption and Interparticle Forces*. In Adsorption at Interface: ACS Symposium Series. USA.

[64] Benard, et al. 2007. Comparison of hydrogen adsorption on nanoporous materials. *Journal of Alloys and Compounds* 446-447: 380-384.

[65] Kowalczyk, K., Tanaka, H., Kanoh, H., and Kaneko, K. 2004. Adsorption energy distribution from the Aranovich-Donohue lattice density functional theory. *Langmuir* 20: 2324-2332.

[66] Aranovich, G. L., Sangwichien, C., and Donohue, M. D. 2000. Intermolecular repulsions in adsorbed layers. *J. Colloid. Interface. Sci.* 227: 553-560.

[67] Aranovich, G. L., and Donohue, M. D. 2001. Surface compression in adsorption systems. *Colloid and Surfaces A: Physicochemical and Engineering Aspects* 187-188: 95-108.

[68] Bokis, C. P., and Donohue, M. D. 1995. A closed-form equation of state for Lennard-Jones molecules based on perturbation theory. *Journal of Physical Chemistry* 99, 12655-12660.

[69] Lee, L. L. 1988. Molecular Thermodynamics in Nonideal Fluids; Butterworths: Boston, p. 254.

[70] Sudibandriyo, M., Pan, Z., Fitzgerald, J. E., Robinson, R. L., and Gasem, K. A. M. 2003. Adsorption of methane, nitrogen, carbon dioxide, and their binary mixtures on dry activated carbon at 318.2 K and pressure up to 13.6 MPa, *Langmuir* 19: 5323-5331.

[71] Cavenati, S., Grande, C. A., and Rodrigues, A. E. 2004. Adsorption equilibrium of methane, carbon dioxide, and nitrogen on Zeolite 13X at high pressures, *J. Chem. Eng. Data.* 49: 1095-1101.

[72] Kiselev, A.V. 1986. Intermolecular Interactions in Adsorption and Chromatography: Vysshaya Shkola, Moscow.

[73] McNair, H. M., and Bonelli, E. J. 1968. Basic Gas Chromatography: Varian Aerograph, USA.

[74] Cowper, C. J., and DeRose, A. J. 1983. The Analysis of Gases by Chromatography: Pergamon Press, Oxford.

[75] Ustinov, et al. 2004. Multicomponent adsorption on activated carbons under supercritical conditions. *J. Colloid. Interface. Sci.* 275: 376-385.

[76] Aranovich, G. L., and Donohue, M. D. 1997. Determining surface areas from linear adsorption isotherms at supercritical conditions. *J. Colloid. Interface. Sci.* 194: 392-397.

APPENDIX

APPENDIX A

COMPUTER CODE FOR SOLVING THE ONO-KONDO EQUATIONS

The following codes in the MATHEMATICA language solve the Ono-Kondo equations (2.20) and (2.22). For equation (2.20), the output is a relation of values for x_1 vs x_b. Input the values of all fixed parameters (ε_s/kT, ε/kT, z_0, z_1, z_2, and n_1) for each gas adsorption in the MATHEMATICA language. For example, input data for methane adsorption, we get result in Figure A.1;

```
ePsilonmethane=0.20;ePsilon=0.20; ePsilonS=-4.35; z0=6; z1=1; z2=4; n1=1;

Calculate x1 for 1 layer case →x1  (by define function H1 to calculate

fH1[x11_,xb_]:=ePsilonS+z2*x11*ePsilonmethane-z0*xb*ePsilon;

fX1[x11_,xb_]:=(xb/(xb+(1-xb)*Exp[fH1[x11,xb]]))-x11;

x11Series=Table[{10^xb,x11/.FindRoot[fX1[x11,10^xb]==0,{x11,1}]},{xb,-
5,0,0.05}];
(*TableForm[x11Series]*)

graph1=ListPlot[x11Series,PlotJoined->True,PlotStyle\[Rule]{Thickness[0.01],
RGBColor[0.25,0.5,0]},GridLines->Automatic,Frame->True,FrameLabel\[Rule]{"x
bulk","x1"},PlotRange->All];
```

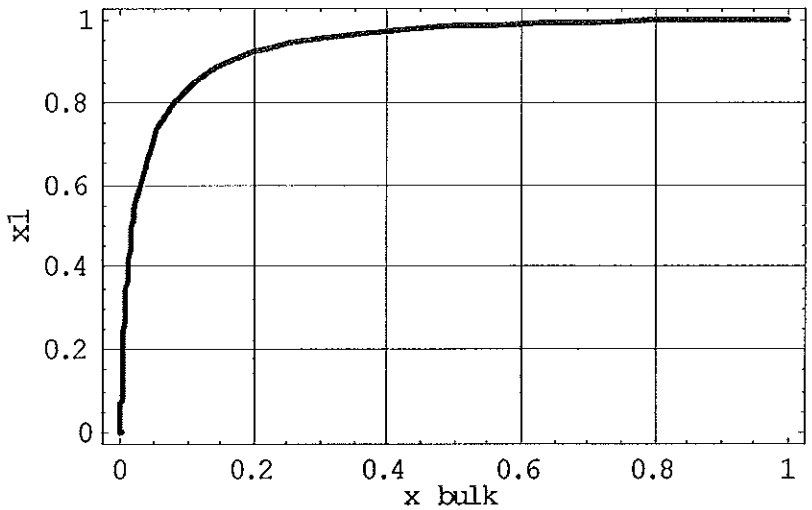

Figure A.1 Relation of x_1 vs x_b obtained from equation (2.20) for methane adsorption.

For equation (2.20), the output is a relation of values for Gibbs adsorption vs x_b. Calculated isotherm of methane adsorption data, we result in Figure A.2;

```
gibbsSeries1=Table[{Part[x11Series,i,1], Part[x11Series,i,2]-
Part[x11Series,i,1]},{i,1,Part[Dimensions[x11Series],1]}];

gibbsPlot1=ListPlot[gibbsSeries1, \PlotJoined->True,PlotStyle-
>{Thickness[0.01],RGBColor[0.25,0.5,0]},GridLines->Automatic,Frame-
>True,FrameLabel->{"x bulk","Gibbs adsorption"},PlotRange->All];
```

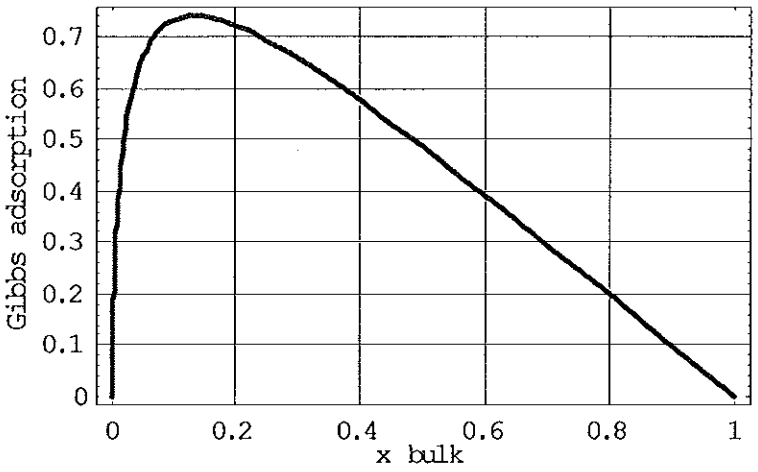

Figure A.2 Theoretical isotherm of the Gibbs adsorption for methane.

It can be calculated Gibbs adsorption isotherms for nitrogen and carbon dioxide in these similar ways as illustrate in Figures A.3, and A.4, respectively.

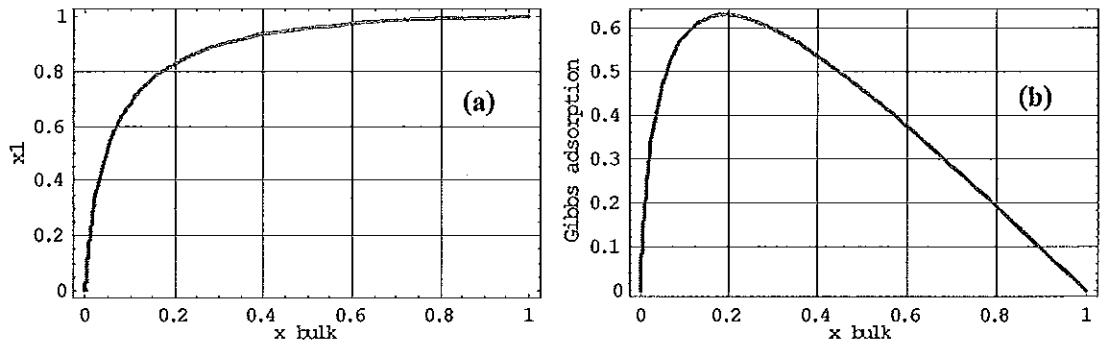

Figure A.3 Adsorption isotherms for nitrogen (a) dependence of x_1 vs x_b, and (b) theoretical isotherm of the Gibbs adsorption.

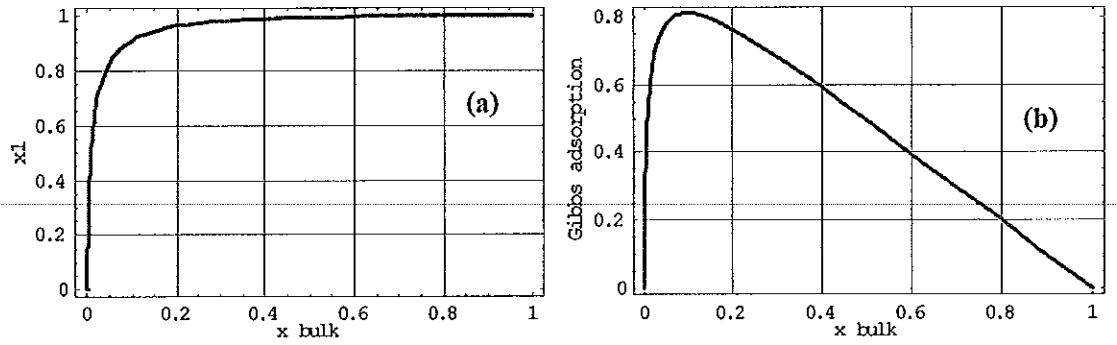

Figure A.4 Adsorption isotherms for carbon dioxide (a) dependence of x_1 vs x_b, and (b) theoretical isotherm of the Gibbs adsorption.

APPENDIX B

CALCULATIONS FOR ONO-KONDO PARAMETERS FOR PURE GASES

1. Calculation of the total number of particles per volume (nN_A/V) from the classical ideal gas law equation;

$$
\begin{aligned}
PV &= nRT \\
PV &= n(N_A k)T \\
\frac{nN_A}{V} &= \frac{P}{kT} \\
\frac{[mole][\frac{molecules}{mole}]}{[m^3]} &= \frac{[Pa]}{[\frac{J}{K}][K]} \\
\frac{[\text{molecules}]}{[\text{m}^3]} &= \frac{\frac{[\text{N}]}{[\text{m}^2]}}{[\frac{\text{N,m}}{\text{K}}][K]} \\
\frac{[\text{molecules}]}{[\text{m}^3]} &= \frac{[\text{values}]}{[m^3]}
\end{aligned}
$$

where P is pressure of the gases [Pa], V is total volume of the container containing the gases [m^3], n is the number of moles [mole], N_A is Avogadro number [molecules/mole], k is Boltzmann's constant [J/K], and T is absolute temperature [K].

2. In order to plot $\frac{Y}{x_b} = \ln\frac{(a/a_m)}{H(1-a/a_m)x_b}$ vs $\frac{a}{x_b}$, it must be calculated $\frac{a}{a_m}$, x_b, and Y by using data from [70]. Here, it can be defined $\frac{a}{a_m} = \frac{\text{absolute adsorption}}{\text{max absolute adsorption}}$, and $x_b = \frac{\pi}{6}n\sigma^3$, where $\sigma_{N_2} = 3.745\times10^{-10}$ m, $\sigma_{CH_4} = 3.7838\times10^{-10}$ m, and $\sigma_{CO_2} = 4.328\times10^{-10}$ m. For example, calculated all parameters for methane adsorption on activated carbon at T = 318.2 K show in Table B.1.

Table B.1 All parameters for methane adsorption on activated carbon at $T = 318.2$ K.

pressure (MPa)	nN_A/V (molecules/m^3)	x_b (dimenssionless)	absolute adsorption (mmol/g)	a/a_m (dimenssionless)
0.55	1.25E+26	0.004	1.888	0.340
1.23	2.80E+26	0.008	2.822	0.509
2.55	5.81E+26	0.016	3.755	0.677
3.48	7.93E+26	0.022	4.149	0.748
4.80	1.09E+27	0.031	4.541	0.818
6.18	1.41E+27	0.040	4.835	0.871
7.64	1.74E+27	0.049	5.066	0.913
9.03	2.06E+27	0.058	5.238	0.944
10.37	2.36E+27	0.067	5.357	0.965
11.76	2.68E+27	0.076	5.459	0.984
13.25	3.02E+27	0.086	5.549	1.000

It can be calculated all parameters for nitrogen and carbon dioxide in these similar ways as illustrate in Tables B.2, and B.3, respectively.

Table B.2 All parameters for nitrogen adsorption on activated carbon at $T = 318.2$ K.

pressure (MPa)	nN_A/V (molecules/m^3)	x_b (dimenssionless)	absolute adsorption (mmol/g)	a/a_m (dimenssionless)
0.69	1.57E+26	0.004	1.007	0.252
1.73	3.94E+26	0.011	1.788	0.448
2.86	6.51E+26	0.018	2.324	0.582
4.10	9.34E+26	0.026	2.735	0.685
5.53	1.26E+27	0.035	3.078	0.771
6.97	1.59E+27	0.044	3.338	0.836
8.31	1.89E+27	0.052	3.522	0.882
9.66	2.20E+27	0.060	3.683	0.922
11.10	2.53E+27	0.070	3.826	0.958
12.46	2.84E+27	0.078	3.916	0.980
13.66	3.11E+27	0.086	3.994	1.000

Table B.3 All parameters for carbon dioxide adsorption on activated carbon at $T = 318.2$ K.

pressure (MPa)	nN_A/V (molecules/m^3)	x_b (dimenssionless)	absolute adsorption (mmol/g)	a/a_m (dimenssionless)
0.36	8.20E+25	0.003	2.982	0.334
0.73	1.66E+26	0.007	4.223	0.473
1.19	2.71E+26	0.012	5.172	0.580
1.79	4.08E+26	0.017	5.976	0.670
2.52	5.74E+26	0.024	6.611	0.741
3.30	7.52E+26	0.032	7.106	0.796
4.29	9.77E+26	0.041	7.641	0.856
5.56	1.27E+27	0.054	8.101	0.908
7.01	1.60E+27	0.068	8.434	0.945
8.30	1.89E+27	0.080	8.623	0.966
9.64	2.20E+27	0.093	8.577	0.961
11.06	2.52E+27	0.107	8.781	0.984
13.36	3.04E+27	0.129	8.924	1.000

3. Calculated data for nitrogen, methane, and carbon dioxide on activated carbon Filtrasorb 400 at T = 318.2 K in Ono-Kondo coordinates (equation 3.12) with variable H can be shown in Tables B.4, B.5, and B.6, respectively.

It can be calculated all parameters for adsorbed nitrogen, methane and carbon dioxide on zeolite 13X at various temperatures by using data from [71] in similar methods with adsorbed gases on activated carbon.

Table B.4 Calculated data for adsorbed nitrogen on activated carbon Filtrasorb 400 at 318.2 K in Ono-Kondo coordinates with variable *H*.

variable *H*											
X axis	Y axis	X axis	Y axis	X axis	Y axis	X axis	Y axis	X axis	Y axis	X axis	Y axis
H = 30		H = 50		H = 100		H = 150		H = 200		H = 300	
233	221	233	103	233	-57	233	-151	233	-218	233	-312
165	84	165	37	165	-27	165	-64	165	-91	165	-128
130	53	130	25	130	-14	130	-37	130	-53	130	-75
107	40	107	20	107	-7	107	-22	107	-34	107	-49
89	34	89	19	89	-1	89	-13	89	-21	89	-33
76	31	76	19	76	4	76	-6	76	-12	76	-22
68	30	68	20	68	7	68	-1	68	-6	68	-14
61	31	61	23	61	11	61	4	61	0	61	-7
55	34	55	27	55	17	55	11	55	7	55	1
50	39	50	33	50	24	50	19	50	15	50	10

Table B.5 Calculated data for adsorbed methane on activated carbon Filtrasorb 400 at 318.2 K in Ono-Kondo coordinates with variable *H*.

variable *H*											
X axis	Y axis	X axis	Y axis	X axis	Y axis	X axis	Y axis	X axis	Y axis	X axis	Y axis
H = 30		H = 50		H = 100		H = 150		H = 200		H = 300	
531	444	531	300	531	105	531	-9	531	-90	531	-204
355	185	355	120	355	33	355	-18	355	-54	355	-105
228	88	228	57	228	15	228	-10	228	-28	228	-52
185	66	185	43	185	12	185	-6	185	-19	185	-37
146	51	146	34	146	12	146	-1	146	-10	146	-23
121	43	121	31	121	13	121	3	121	-4	121	-14
103	40	103	29	103	15	103	7	103	1	103	-7
90	39	90	30	90	18	90	11	90	6	90	-1
80	39	80	32	80	21	80	15	80	11	80	5
72	43	72	36	72	27	72	22	72	18	72	13

Table B.6 Calculated data for adsorbed carbon dioxide on activated carbon Filtrasorb 400 at 318.2 K in Ono-Kondo coordinates with variable *H*.

Variable *H*											
X axis	Y axis	X axis	Y axis	X axis	Y axis	X axis	Y axis	X axis	Y axis	X axis	Y axis
H = 30		H = 50		H = 100		H = 150		H = 200		H = 300	
857	451	857	304	857	105	857	-11	857	-94	857	-210
598	205	598	132	598	34	598	-23	598	-64	598	-121
450	120	450	76	450	16	450	-20	450	-45	450	-80
345	79	345	49	345	9	345	-14	345	-31	345	-54
271	56	271	35	271	7	271	-10	271	-22	271	-39
223	44	223	28	223	6	223	-6	223	-15	223	-28
184	38	184	25	184	9	184	-1	184	-8	184	-18
151	34	151	24	151	11	151	4	151	-2	151	-9
124	32	124	24	124	14	124	8	124	4	124	-2
107	31	107	25	107	16	107	11	107	7	107	2
92	23	92	18	92	10	92	6	92	3	92	-1
82	28	82	23	82	16	82	13	82	10	82	6

4. Calculated data for nitrogen, methane, and carbon dioxide on zeolite 13X at T = 298 K in Ono-Kondo coordinates (equation 3.12) with variable *H* can be shown in Tables B.7, B.8, and B.9, respectively.

5. Calculated data for nitrogen, methane, and carbon dioxide on zeolite 13X at T = 308 K in Ono-Kondo coordinates (equation 3.12) with variable *H* can be shown in Tables B.10, B.11, and B.12, respectively.

6. Calculated data for nitrogen, methane, and carbon dioxide on zeolite 13X at T = 323 K in Ono-Kondo coordinates (equation 3.12) with variable *H* can be shown in Tables B.13, B.14, and B.15, respectively.

Table B.7 Calculated data for adsorbed nitrogen on zeolite 13X at T = 298 K in Ono-Kondo coordinates with variable *H*.

Variable *H*													
X axis	Y axis	X axis	Y axis	X axis	Y axis	X axis	Y axis	X axis	Y axis	X axis	Y axis	X axis	Y axis
H = 30		H = 50		H = 100		H = 150		H = 200		H = 300		H = 500	
585	37530	585	25069	585	8160	585	-1731	585	-8748	585	-18639	585	-31100
514	19110	514	12197	514	2817	514	-2670	514	-6563	514	-12050	514	-18963
488	8165	488	5123	488	995	488	-1420	488	-3133	488	-5548	488	-8590
469	5116	469	3167	469	523	469	-1024	469	-2121	469	-3668	469	-5617
466	4014	466	2487	466	415	466	-797	466	-1657	466	-2868	466	-4395
439	2174	439	1325	439	174	439	-500	439	-978	439	-1651	439	-2500
405	1125	405	676	405	66	405	-291	405	-544	405	-900	405	-1350
391	751	391	457	391	58	391	-175	391	-340	391	-574	391	-867
386	640	386	393	386	59	386	-136	386	-275	386	-471	386	-717
357	493	357	297	357	32	357	-124	357	-234	357	-390	357	-586
325	339	325	205	325	24	325	-83	325	-158	325	-265	325	-399
317	301	317	185	317	27	317	-66	317	-132	317	-224	317	-341
301	262	301	160	301	21	301	-61	301	-118	301	-200	301	-302
276	204	276	127	276	22	276	-39	276	-82	276	-144	276	-221
270	190	270	120	270	26	270	-30	270	-69	270	-124	270	-194
251	164	251	104	251	23	251	-24	251	-58	251	-105	251	-165
229	137	229	89	229	24	229	-14	229	-42	229	-80	229	-128
219	127	219	84	219	25	219	-9	219	-33	219	-67	219	-111
210	119	210	80	210	26	210	-5	210	-27	210	-59	210	-98
197	110	197	75	197	28	197	1	197	-19	197	-46	197	-81
191	106	191	73	191	29	191	4	191	-15	191	-40	191	-73
182	101	182	72	182	32	182	8	182	-8	182	-32	182	-61
165	96	165	72	165	39	165	20	165	6	165	-13	165	-37
163	96	163	72	163	40	163	21	163	8	163	-11	163	-34
153	98	153	78	153	49	153	33	153	21	153	5	153	-16
146	105	146	86	146	60	146	45	146	34	146	19	146	0
139	121	139	104	139	80	139	67	139	57	139	43	139	26

Table B.8 Calculated data for adsorbed methane on zeolite 13X at T = 298 K in Ono-Kondo coordinates with variable *H*.

Variable *H*											
X axis	Y axis	X axis	Y axis	X axis	Y axis	X axis	Y axis	X axis	Y axis	X axis	Y axis
H = 30		H = 50		H = 100		H = 150		H = 200		H = 300	
859	57819	859	39533	859	14719	859	205	859	-10094	859	-24608
1073	22278	1073	16122	1073	7768	1073	2881	1073	-586	1073	-5472
994	13514	994	9636	994	4375	994	1297	994	-887	994	-3965
857	4383	857	3040	857	1218	857	152	857	-605	857	-1670
826	1977	826	1384	826	580	826	110	826	-224	826	-694
771	1466	771	1017	771	408	771	52	771	-201	771	-557
773	1190	773	837	773	359	773	79	773	-120	773	-400
698	806	698	564	698	236	698	44	698	-93	698	-285
680	718	680	503	680	212	680	42	680	-79	680	-250
624	572	624	398	624	161	624	23	624	-75	624	-213
542	386	542	269	542	110	542	16	542	-50	542	-143
483	298	483	207	483	85	483	13	483	-38	483	-110
415	223	415	154	415	60	415	5	415	-34	415	-89
401	208	401	145	401	60	401	10	401	-25	401	-75
363	176	363	123	363	52	363	10	363	-19	363	-61
323	147	323	104	323	45	323	11	323	-13	323	-47
306	136	306	97	306	44	306	13	306	-9	306	-40
280	121	280	87	280	41	280	14	280	-6	280	-33
250	107	250	79	250	40	250	18	250	2	250	-21
231	101	231	76	231	42	231	22	231	8	231	-11
215	98	215	76	215	46	215	29	215	17	215	-1
208	99	208	78	208	50	208	33	208	21	208	5
201	98	201	79	201	52	201	36	201	25	201	9
186	109	186	92	186	68	186	55	186	45	186	31

Table B.9 Calculated data for adsorbed carbon dioxide on zeolite 13X at T = 298 K in Ono-Kondo coordinates with variable *H*.

Variable *H*											
X axis	Y axis	X axis	Y axis	X axis	Y axis	X axis	Y axis	X axis	Y axis	X axis	Y axis
H = 3000		H = 5000		H = 10000		H = 15000		H = 20000		H = 30000	
94171	132835	94171	90895	94171	33986	94171	697	94171	-22922	94171	-56212
35719	13394	35719	5281	35719	-5728	35719	-12167	35719	-16736	35719	-23176
12203	304	12203	-1399	12203	-3711	12203	-5063	12203	-6023	12203	-7375
5063	-598	5063	-1173	5063	-1953	5063	-2409	5063	-2733	5063	-3189
3064	-495	3064	-804	3064	-1224	3064	-1469	3064	-1643	3064	-1889
1744	-352	1744	-511	1744	-728	1744	-855	1744	-945	1744	-1071
1115	-236	1115	-330	1115	-458	1115	-533	1115	-586	1115	-661
622	-135	622	-184	622	-250	622	-288	622	-316	622	-355
464	-72	464	-106	464	-153	464	-180	464	-199	464	-226
348	-63	348	-89	348	-124	348	-144	348	-158	348	-179
301	-44	301	-66	301	-95	301	-112	301	-124	301	-142
263	-20	263	-39	263	-64	263	-79	263	-89	263	-104

Table B.10 Calculated data for adsorbed nitrogen on zeolite 13X at T = 308 K in Ono-Kondo coordinates with variable *H*.

Variable *H*													
X axis	Y axis	X axis	Y axis	X axis	Y axis	X axis	Y axis	X axis	Y axis	X axis	Y axis	X axis	Y axis
H = 30		H = 50		H = 100		H = 150		H = 200		H = 300		H = 500	
386	35573	386	20419	386	-143	386	-12171	386	-20705	386	-32733	386	-47886
368	14696	368	8209	368	-593	368	-5743	368	-9396	368	-14545	368	-21032
384	9229	384	5311	384	-6	384	-3116	384	-5322	384	-8432	384	-12350
371	4065	371	2312	371	-67	371	-1459	371	-2446	371	-3838	371	-5591
370	3335	370	1902	370	-41	370	-1178	370	-1985	370	-3122	370	-4554
354	2020	354	1133	354	-69	354	-773	354	-1272	354	-1976	354	-2862
347	1699	347	947	347	-74	347	-670	347	-1094	347	-1691	347	-2443
348	1394	348	787	348	-38	348	-520	348	-862	348	-1344	348	-1951
342	1165	342	655	342	-36	342	-440	342	-727	342	-1131	342	-1641
338	1032	338	581	338	-31	338	-390	338	-644	338	-1002	338	-1453
323	772	323	429	323	-37	323	-309	323	-503	323	-775	323	-1118
307	546	307	303	307	-26	307	-219	307	-356	307	-549	307	-792
307	496	307	280	307	-13	307	-185	307	-307	307	-479	307	-695
300	443	300	250	300	-11	300	-164	300	-273	300	-425	300	-618
281	322	281	183	281	-4	281	-114	281	-192	281	-302	281	-441
277	296	277	171	277	1	277	-99	277	-169	277	-269	277	-394
270	270	270	157	270	2	270	-88	270	-152	270	-242	270	-356
261	237	261	139	261	6	261	-72	261	-127	261	-205	261	-303
245	197	245	117	245	9	245	-54	245	-99	245	-162	245	-242
239	183	239	109	239	10	239	-48	239	-89	239	-147	239	-220
227	161	227	98	227	13	227	-37	227	-72	227	-122	227	-185
211	137	211	86	211	17	211	-24	211	-53	211	-94	211	-145
196	121	196	78	196	20	196	-13	196	-37	196	-71	196	-114
187	112	187	74	187	22	187	-8	187	-30	187	-60	187	-98
184	110	184	73	184	24	184	-5	184	-26	184	-55	184	-91
167	100	167	70	167	31	167	7	167	-9	167	-32	167	-62
158	96	158	70	158	34	158	13	158	-2	158	-22	158	-49
153	98	153	74	153	42	153	23	153	9	153	-10	153	-34
144	100	144	78	144	50	144	33	144	21	144	4	144	-17
138	105	138	85	138	59	138	43	138	32	138	16	138	-3
131	130	131	112	131	88	131	74	131	64	131	50	131	32

Table B.11 Calculated data for adsorbed methane on zeolite 13X at T = 308 K in Ono-Kondo coordinates with variable *H*.

Variable H											
X axis	Y axis	X axis	Y axis	X axis	Y axis	X axis	Y axis	X axis	Y axis	X axis	Y axis
H = 30		H = 50		H = 100		H = 150		H = 200		H = 300	
628	39681	628	25101	628	5317	628	-6256	628	-14467	628	-26040
860	23021	860	16156	860	6841	860	1392	860	-2475	860	-7924
801	12121	801	8368	801	3277	801	299	801	-1814	801	-4793
785	6173	785	4263	785	1670	785	154	785	-922	785	-2438
730	2850	730	1951	730	731	730	18	730	-488	730	-1202
692	1786	692	1219	692	450	692	0	692	-320	692	-770
649	1254	649	851	649	305	649	-15	649	-242	649	-562
606	854	606	580	606	209	606	-8	606	-162	606	-379
596	774	596	527	596	192	596	-4	596	-143	596	-339
582	690	582	471	582	174	582	1	582	-122	582	-296
545	543	545	371	545	138	545	2	545	-95	545	-232
495	412	495	281	495	103	495	0	495	-74	495	-178
464	348	464	238	464	89	464	1	464	-61	464	-148
450	316	450	218	450	85	450	7	450	-48	450	-126
422	279	422	191	422	72	422	3	422	-46	422	-116
377	221	377	152	377	59	377	4	377	-35	377	-90
324	169	324	117	324	47	324	6	324	-23	324	-64
300	150	300	105	300	44	300	8	300	-17	300	-53
291	143	291	100	291	42	291	9	291	-16	291	-49
261	124	261	88	261	40	261	12	261	-7	261	-35
239	112	239	82	239	41	239	17	239	0	239	-24
224	106	224	79	224	43	224	21	224	6	224	-15
194	103	194	82	194	53	194	36	194	25	194	8
182	107	182	87	182	62	182	46	182	36	182	21

Table B.12 Calculated data for adsorbed carbon dioxide on zeolite 13X at T = 308 K in Ono-Kondo coordinates with variable *H*.

Variable *H*											
X axis	Y axis	X axis	Y axis	X axis	Y axis	X axis	Y axis	X axis	Y axis	X axis	Y axis
H = 3000		H = 5000		H = 10000		H = 15000		H = 20000		H = 30000	
65562	101476	65562	60881	65562	5797	65562	-26425	65562	-49287	65562	-81509
35870	19275	35870	6708	35870	-10345	35870	-20321	35870	-27398	35870	-37374
22792	4943	22792	-709	22792	-8378	22792	-12864	22792	-16047	22792	-20533
18137	2198	18137	-1663	18137	-6901	18137	-9965	18137	-12139	18137	-15203
13640	412	13640	-2136	13640	-5594	13640	-7617	13640	-9053	13640	-11075
7496	-773	7496	-1905	7496	-3443	7496	-4342	7496	-4980	7496	-5879
4267	-740	4267	-1278	4267	-2008	4267	-2435	4267	-2739	4267	-3166
2810	-597	2810	-916	2810	-1350	2810	-1604	2810	-1784	2810	-2038
2157	-505	2157	-737	2157	-1053	2157	-1237	2157	-1368	2157	-1553
1774	-429	1774	-611	1774	-859	1774	-1004	1774	-1107	1774	-1252
1398	-358	1398	-497	1398	-684	1398	-794	1398	-872	1398	-982
1097	-305	1097	-411	1097	-554	1097	-638	1097	-697	1097	-781
948	-276	948	-366	948	-487	948	-559	948	-609	948	-680
799	-230	799	-304	799	-403	799	-461	799	-502	799	-560
654	-195	654	-254	654	-333	654	-379	654	-412	654	-459
572	-174	572	-225	572	-293	572	-333	572	-361	572	-401
496	-148	496	-191	496	-249	496	-283	496	-307	496	-340
407	-118	407	-152	407	-199	407	-225	407	-245	407	-272
344	-93	344	-121	344	-159	344	-181	344	-197	344	-219
292	-64	292	-87	292	-118	292	-137	292	-149	292	-168
266	-47	266	-68	266	-96	266	-112	266	-123	266	-140
237	-23	237	-41	237	-65	237	-79	237	-89	237	-103
225	25	225	8	225	-14	225	-28	225	-37	225	-50

Table B.13 Calculated data for adsorbed nitrogen on zeolite 13X at T = 323 K in Ono-Kondo coordinates with variable *H*.

Variable *H*													
X axis	Y axis	X axis	Y axis	X axis	Y axis	X axis	Y axis	X axis	Y axis	X axis	Y axis	X axis	Y axis
H = 30		H = 50		H = 100		H = 150		H = 200		H = 300		H = 500	
269	17279	269	8111	269	-4331	269	-11608	269	-16772	269	-24050	269	-33218
288	8785	288	4455	288	-1421	288	-4858	288	-7296	288	-10733	288	-15064
299	4395	299	2328	299	-476	299	-2117	299	-3281	299	-4921	299	-6988
288	3104	288	1601	288	-437	288	-1630	288	-2476	288	-3668	288	-5170
289	1673	289	885	289	-185	289	-811	289	-1255	289	-1881	289	-2670
277	998	277	525	277	-117	277	-493	277	-759	277	-1135	277	-1608
263	769	263	393	263	-118	263	-416	263	-628	263	-927	263	-1303
265	627	265	331	265	-70	265	-305	265	-471	265	-706	265	-1002
256	490	256	260	256	-52	256	-234	256	-364	256	-546	256	-776
240	368	240	192	240	-47	240	-187	240	-286	240	-426	240	-602
238	317	238	172	238	-25	238	-141	238	-222	238	-338	238	-483
231	271	231	149	231	-16	231	-113	231	-182	231	-278	231	-400
224	235	224	131	224	-9	224	-91	224	-149	224	-232	224	-335
211	193	211	110	211	-2	211	-68	211	-114	211	-180	211	-263
202	171	202	99	202	2	202	-55	202	-95	202	-152	202	-224
195	153	195	91	195	7	195	-42	195	-76	195	-125	195	-187
181	130	181	81	181	14	181	-25	181	-53	181	-92	181	-141
165	112	165	73	165	21	165	-9	165	-31	165	-61	165	-99
157	105	157	70	157	24	157	-4	157	-23	157	-50	157	-85
152	102	152	70	152	27	152	2	152	-16	152	-41	152	-72
143	99	143	72	143	35	143	14	143	-2	143	-23	143	-50
138	98	138	73	138	40	138	20	138	6	138	-14	138	-38
135	100	135	76	135	44	135	25	135	12	135	-7	135	-31
128	105	128	84	128	55	128	39	128	27	128	10	128	-11
121	133	121	114	121	89	121	75	121	64	121	50	121	31

Table B.14 Calculated data for adsorbed methane on zeolite 13X at T = 323 K in Ono-Kondo coordinates with variable *H*.

Variable H											
X axis	Y axis	X axis	Y axis	X axis	Y axis	X axis	Y axis	X axis	Y axis	X axis	Y axis
H = 30		H = 50		H = 100		H = 150		H = 200		H = 300	
443	29217	443	15904	443	-2159	443	-12726	443	-20223	443	-30790
673	19994	673	13387	673	4422	673	-822	673	-4543	673	-9787
643	10777	643	7128	643	2177	643	-720	643	-2774	643	-5671
666	7401	666	4970	666	1671	666	-259	666	-1628	666	-3558
668	5347	668	3607	668	1245	668	-136	668	-1117	668	-2498
648	4413	648	2955	648	976	648	-181	648	-1002	648	-2160
612	2958	612	1956	612	596	612	-200	612	-764	612	-1560
590	2047	590	1349	590	402	590	-152	590	-545	590	-1099
848	1876	848	1390	848	730	848	343	848	69	848	-317
479	890	479	555	479	102	479	-164	479	-352	479	-618
466	649	466	412	466	92	466	-95	466	-228	466	-416
469	573	469	372	469	100	469	-60	469	-173	469	-332
438	449	438	291	438	78	438	-47	438	-136	438	-261
409	361	409	234	409	63	409	-38	409	-109	409	-209
389	301	389	199	389	59	389	-23	389	-81	389	-162
377	276	377	183	377	57	377	-16	377	-69	377	-142
364	252	364	168	364	54	364	-13	364	-60	364	-127
337	211	337	144	337	52	337	-2	337	-40	337	-94
304	174	304	120	304	47	304	5	304	-26	304	-68
284	156	284	109	284	44	284	7	284	-20	284	-58
268	142	268	99	268	40	268	6	268	-18	268	-52
232	118	232	85	232	40	232	14	232	-5	232	-31
224	114	224	83	224	40	224	16	224	-2	224	-27
205	106	205	79	205	43	205	22	205	7	205	-14
193	106	193	83	193	51	193	33	193	19	193	1
186	109	186	87	186	57	186	40	186	27	186	10
172	119	172	99	172	73	172	58	172	47	172	32
166	134	166	116	166	92	166	77	166	67	166	53

Table B.15 Calculated data for adsorbed carbon dioxide on zeolite 13X at T = 323 K in Ono-Kondo coordinates with variable *H*.

Variable *H*											
X axis	Y axis	X axis	Y axis	X axis	Y axis	X axis	Y axis	X axis	Y axis	X axis	Y axis
H = 3000		H = 5000		H = 10000		H = 15000		H = 20000		H = 30000	
35267	76955	35267	26350	35267	-42316	35267	-82482	35267	-110981	35267	-151148
25958	24675	25958	-391	25958	-34403	25958	-54298	25958	-68415	25958	-88311
22217	9521	22217	-1185	22217	-15714	22217	-24212	22217	-30242	22217	-38740
16556	2803	16556	-3111	16556	-11136	16556	-15830	16556	-19161	16556	-23855
9058	-848	9058	-3062	9058	-6066	9058	-7823	9058	-9070	9058	-10827
6196	-1145	6196	-2416	6196	-4141	6196	-5150	6196	-5866	6196	-6875
4059	-1049	4059	-1764	4059	-2734	4059	-3301	4059	-3704	4059	-4271
2462	-766	2462	-1135	2462	-1637	2462	-1931	2462	-2139	2462	-2433
1523	-502	1523	-701	1523	-971	1523	-1128	1523	-1240	1523	-1398
1104	-406	1104	-544	1104	-730	1104	-839	1104	-917	1104	-1026
834	-316	834	-414	834	-548	834	-626	834	-681	834	-760
675	-253	675	-329	675	-432	675	-493	675	-536	675	-596
586	-205	586	-268	586	-353	586	-403	586	-439	586	-489
501	-180	501	-233	501	-305	501	-347	501	-377	501	-419
441	-155	441	-201	441	-263	441	-299	441	-325	441	-361
375	-108	375	-145	375	-195	375	-225	375	-245	375	-275
320	-97	320	-128	320	-170	320	-195	320	-213	320	-238
268	-65	268	-90	268	-124	268	-144	268	-159	268	-179
219	-26	219	-46	219	-73	219	-89	219	-100	219	-116

Moreover, adsorption isotherms in Ono-Kondo Coordinates with estimated Henry's constants are also investigated for adsorbed nitrogen, methane and carbon dioxide both on activated carbon Filtrasorb 400 at 318.2 K and on zeolite 13X at various temperatures by using data from [70] and [71]. The calculated data of adsorption isotherms for adsorbed nitrogen, methane and carbon dioxide both on activated carbon Filtrasorb 400 at 318.2 K and on zeolite 13X at various temperatures with estimated Henry's constants are illustrated in Tables B.16-B.27.

Table B.16 Calculated data for adsorbed nitrogen on activated carbon Filtrasorb 400 at 318.2 K in Ono-Kondo coordinates with estimated Henry's constants.

pressure (MPa)	absolute (mmol/g)	a/a_m	x_b	X axis	Y axis
0.69	1.007	0.252	0.004	233.03	127.325
1.73	1.788	0.448	0.011	165.02	46.909
2.86	2.324	0.582	0.018	129.75	30.488
4.10	2.735	0.685	0.026	106.51	24.585
5.53	3.078	0.771	0.035	88.87	22.183
6.97	3.338	0.836	0.044	76.47	21.804
8.31	3.522	0.882	0.052	67.67	22.265
9.66	3.683	0.922	0.060	60.88	24.300
11.10	3.826	0.958	0.070	55.04	28.555
12.46	3.916	0.980	0.078	50.18	34.088
13.66	3.994	1.000	0.086	46.69	#DIV/0!

Table B.17 Calculated data for adsorbed methane on activated carbon Filtrasorb 400 at 318.2 K in Ono-Kondo coordinates with estimated Henry's constants.

pressure (MPa)	absolute (mmol/g)	a/a_m	x_b	X axis	Y axis
0.55	1.888	0.340	0.004	531.42	248.670
1.23	2.822	0.509	0.008	355.18	97.552
2.55	3.755	0.677	0.016	227.96	45.556
3.48	4.149	0.748	0.022	184.57	35.019
4.80	4.541	0.818	0.031	146.46	28.524
6.18	4.835	0.871	0.040	121.12	26.034
7.64	5.066	0.913	0.049	102.65	25.627
9.03	5.238	0.944	0.058	89.80	26.936
10.37	5.357	0.965	0.067	79.97	28.925
11.76	5.459	0.984	0.076	71.86	34.073
13.25	5.549	1.000	0.086	64.83	#DIV/0!

Table B.18 Calculated data for adsorbed carbon dioxide on activated carbon Filtrasorb 400 at 318.2 K in Ono-Kondo coordinates with estimated Henry's constants.

pressure (MPa)	absolute (mmol/g)	a/a_m	x_b	X axis	Y axis
0.36	2.982	0.334	0.003	856.89	105.198
0.73	4.223	0.473	0.007	598.44	34.205
1.19	5.172	0.580	0.012	449.60	15.726
1.79	5.976	0.670	0.017	345.36	9.148
2.52	6.611	0.741	0.024	271.38	6.561
3.30	7.106	0.796	0.032	222.76	6.369
4.29	7.641	0.856	0.041	184.25	8.727
5.56	8.101	0.908	0.054	150.72	11.258
7.01	8.434	0.945	0.068	124.46	13.756
8.30	8.623	0.966	0.080	107.47	15.862
9.64	8.577	0.961	0.093	92.04	10.468
11.06	8.781	0.984	0.107	82.13	16.350
13.36	8.924	1.000	0.129	69.10	#DIV/0!

Table B.19 Calculated data for adsorbed nitrogen on zeolite 13X at T = 298 K in Ono-Kondo coordinates with estimated Henry's constants.

pressure (MPa)	absolute adsorption (mol/kg)	a/a_m	x_b	X axis	Y axis
0.01105	0.038	0.009	0.0002	514	3511
0.02511	0.082	0.019	0.0003	488	1300
0.03920	0.123	0.029	0.0003	469	719
0.05003	0.156	0.037	0.0006	466	568
0.09002	0.264	0.063	0.0011	439	259
0.170	0.460	0.109	0.0017	405	111
0.260	0.680	0.161	0.0021	391	88
0.310	0.800	0.190	0.0026	386	84
0.390	0.930	0.221	0.0038	357	51
0.570	1.240	0.294	0.0044	325	37
0.655	1.390	0.330	0.0050	317	38
0.745	1.500	0.356	0.0066	301	31
0.990	1.830	0.434	0.0073	276	30
1.095	1.976	0.469	0.0086	270	33
1.280	2.151	0.510	0.0106	251	29
1.585	2.432	0.577	0.0118	229	29
1.770	2.592	0.615	0.0129	219	30
1.935	2.717	0.645	0.0147	210	30
2.205	2.909	0.690	0.0158	197	32
2.360	3.011	0.715	0.0174	191	32
2.595	3.161	0.750	0.0212	182	35
3.170	3.491	0.828	0.0216	165	41
3.230	3.528	0.837	0.0246	163	43
3.685	3.763	0.893	0.0268	153	52
4.010	3.923	0.931	0.0294	146	62
4.400	4.084	0.969	0.0316	139	82
4.725	4.214	1.000	0.0273	133	#DIV/0!

Table B.20 Calculated data for adsorbed nitrogen on zeolite 13X at T = 308 K in Ono-Kondo coordinates with estimated Henry's constants.

pressure (MPa)	absolute adsorption (mol/kg)	a/a_m	x_b	X axis	Y axis
0.01217	0.029	0.007	0.0001	368	2240
0.02015	0.050	0.013	0.0001	384	1706
0.04503	0.108	0.028	0.0003	371	699
0.05512	0.132	0.034	0.0004	370	584
0.08907	0.204	0.052	0.0006	354	318
0.105	0.236	0.061	0.0007	347	255
0.130	0.293	0.075	0.0008	348	228
0.155	0.343	0.088	0.0010	342	187
0.175	0.383	0.099	0.0011	338	166
0.230	0.480	0.123	0.0015	323	113
0.325	0.645	0.166	0.0021	307	80
0.365	0.724	0.186	0.0024	307	81
0.410	0.796	0.205	0.0027	300	73
0.570	1.035	0.266	0.0037	281	56
0.630	1.129	0.290	0.0041	277	56
0.695	1.215	0.313	0.0045	270	52
0.805	1.359	0.350	0.0052	261	49
0.990	1.572	0.404	0.0064	245	44
1.080	1.667	0.429	0.0070	239	42
1.255	1.844	0.474	0.0081	227	40
1.540	2.101	0.540	0.0100	211	39
1.855	2.352	0.605	0.0120	196	39
2.070	2.501	0.643	0.0134	187	39
2.160	2.568	0.660	0.0140	184	40
2.695	2.909	0.748	0.0174	167	43
3.010	3.075	0.791	0.0195	158	46
3.295	3.260	0.838	0.0213	153	52
3.710	3.451	0.888	0.0240	144	59
4.015	3.588	0.923	0.0260	138	67
4.465	3.785	0.974	0.0289	131	96
4.705	3.888	1.000	0.0304	128	#DIV/0!

Table B.21 Calculated data for adsorbed nitrogen on zeolite 13X at T = 323 K in Ono-Kondo coordinates with estimated Henry's constants.

pressure (MPa)	absolute adsorption (mol/kg)	a/a_m	x_b	X axis	Y axis
0.00903	0.015	0.004	0.0001	269	3127
0.01912	0.034	0.010	0.0001	288	2102
0.04006	0.074	0.021	0.0002	299	1205
0.05511	0.098	0.028	0.0003	288	785
0.10500	0.187	0.054	0.0006	289	456
0.17500	0.299	0.087	0.0011	277	268
0.22000	0.357	0.104	0.0014	263	189
0.28000	0.457	0.133	0.0017	265	171
0.36000	0.569	0.165	0.0022	256	135
0.47000	0.695	0.202	0.0029	240	96
0.57000	0.838	0.243	0.0035	238	93
0.68000	0.969	0.282	0.0042	231	83
0.80000	1.104	0.321	0.0049	224	75
1.00000	1.303	0.379	0.0062	211	65
1.15500	1.443	0.419	0.0071	202	60
1.34000	1.610	0.468	0.0083	195	58
1.68000	1.875	0.545	0.0104	181	54
2.16000	2.201	0.639	0.0133	165	53
2.40500	2.335	0.678	0.0148	157	52
2.62000	2.460	0.715	0.0162	152	53
3.06500	2.704	0.786	0.0189	143	57
3.34000	2.834	0.823	0.0206	138	60
3.49000	2.916	0.847	0.0215	135	63
3.92000	3.106	0.902	0.0242	128	73
4.47000	3.339	0.970	0.0276	121	104
4.72000	3.442	1.000	0.0291	118	#DIV/0!

Table B.22 Calculated data for adsorbed methane on zeolite 13X at T = 298 K in Ono-Kondo coordinates with estimated Henry's constants.

pressure (MPa)	absolute adsorption (mol/kg)	a/a_m	x_b	X axis	Y axis
0.00405	0.024	0.0042	0.00003	859	685
0.01203	0.089	0.0156	0.00008	1073	3043
0.01910	0.131	0.0229	0.00013	994	1399
0.05515	0.326	0.0570	0.00038	857	187
0.12500	0.712	0.1245	0.00086	826	126
0.16500	0.877	0.1533	0.00114	771	64
0.21000	1.120	0.1958	0.00145	773	88
0.30600	1.474	0.2577	0.00211	698	50
0.34500	1.617	0.2827	0.00238	680	47
0.42500	1.830	0.3200	0.00293	624	28
0.63100	2.357	0.4121	0.00435	542	19
0.81900	2.726	0.4767	0.00565	483	15
1.07000	3.060	0.5351	0.00738	415	7
1.18000	3.260	0.5700	0.00814	401	12
1.41000	3.530	0.6172	0.00973	363	12
1.72000	3.834	0.6704	0.01186	323	12
1.89000	3.991	0.6978	0.01304	306	14
2.17500	4.198	0.7340	0.01500	280	15
2.61000	4.506	0.7879	0.01800	250	18
2.98500	4.750	0.8306	0.02059	231	23
3.36500	4.987	0.8720	0.02321	215	30
3.56000	5.103	0.8923	0.02455	208	34
3.74500	5.191	0.9077	0.02583	201	37
4.26000	5.469	0.9563	0.02938	186	55
4.72500	5.719	1.0000	0.03259	175	#DIV/0!

Table B.23 Calculated data for adsorbed methane on zeolite 13X at T = 308 K in Ono-Kondo coordinates with estimated Henry's constants.

pressure (MPa)	absolute adsorption (mol/kg)	a/a_m	x_b	X axis	Y axis
0.00525	0.022	0.0042	0.00004	628	113
0.01115	0.064	0.0122	0.00007	860	4390
0.02040	0.109	0.0208	0.00014	801	1938
0.04007	0.210	0.0401	0.00027	785	989
0.08516	0.415	0.0793	0.00057	730	411
0.13500	0.623	0.1190	0.00090	692	247
0.19000	0.823	0.1572	0.00127	649	161
0.28000	1.133	0.2165	0.00187	606	112
0.31000	1.232	0.2354	0.00207	596	104
0.35000	1.360	0.2598	0.00234	582	96
0.44500	1.618	0.3091	0.00297	545	77
0.58500	1.931	0.3689	0.00390	495	57
0.69500	2.154	0.4115	0.00464	464	49
0.78000	2.342	0.4475	0.00521	450	50
0.87500	2.466	0.4712	0.00584	422	41
1.11000	2.792	0.5334	0.00741	377	34
1.48000	3.201	0.6116	0.00988	324	29
1.70000	3.409	0.6513	0.01134	300	28
1.79000	3.480	0.6649	0.01195	291	27
2.17000	3.781	0.7224	0.01448	261	28
2.53000	4.038	0.7715	0.01688	239	30
2.84000	4.236	0.8093	0.01895	224	33
3.64000	4.702	0.8984	0.02429	194	46
4.01500	4.884	0.9331	0.02679	182	55
4.49000	5.127	0.9796	0.02996	171	86
4.72000	5.234	1.0000	0.03150	166	#DIV/0!

Table B.24 Calculated data for adsorbed methane on zeolite 13X at T = 323 K in Ono-Kondo coordinates with estimated Henry's constants.

pressure (MPa)	absolute adsorption (mol/kg)	a/a_m	x_b	X axis	Y axis
0.00603	0.017	0.0035	0.00004	443	-1366
0.01215	0.052	0.0108	0.00008	673	4816
0.02200	0.090	0.0186	0.00014	643	2394
0.03302	0.140	0.0290	0.00021	666	1816
0.04612	0.196	0.0406	0.00029	668	1349
0.05505	0.227	0.0470	0.00035	648	1063
0.08010	0.312	0.0646	0.00051	612	655
0.11500	0.432	0.0894	0.00073	590	444
0.16500	0.890	0.1843	0.00105	848	759
0.24000	0.731	0.1513	0.00153	479	121
0.34000	1.009	0.2089	0.00216	466	106
0.40000	1.193	0.2470	0.00255	469	112
0.51000	1.423	0.2946	0.00325	438	87
0.63500	1.653	0.3422	0.00404	409	70
0.78000	1.929	0.3994	0.00496	389	65
0.86500	2.077	0.4300	0.00550	377	63
0.95500	2.211	0.4578	0.00608	364	59
1.18500	2.545	0.5269	0.00754	337	56
1.49500	2.890	0.5983	0.00951	304	50
1.69500	3.067	0.6350	0.01079	284	47
1.86000	3.169	0.6561	0.01184	268	43
2.42500	3.577	0.7406	0.01543	232	42
2.57000	3.670	0.7598	0.01635	224	42
3.01500	3.933	0.8143	0.01919	205	45
3.42500	4.199	0.8694	0.02180	193	53
3.67000	4.341	0.8988	0.02335	186	58
4.18000	4.585	0.9493	0.02660	172	74
4.44500	4.706	0.9743	0.02829	166	93
4.74500	4.830	1.0000	0.03020	160	#DIV/0!

Table B.25 Calculated data for adsorbed carbon dioxide on zeolite 13X at T = 298 K in Ono-Kondo coordinates with estimated Henry's constants.

pressure (MPa)	absolute adsorption (mol/kg)	a/a_m	x_b	X axis	Y axis
0.00118	1.147	0.1556	0.00001	94171	130275
0.00610	2.249	0.3051	0.00006	35719	12898
0.02905	3.659	0.4963	0.00030	12203	200
0.08610	4.500	0.6104	0.00089	5063	-633
0.16000	5.060	0.6864	0.00165	3064	-514
0.31000	5.580	0.7569	0.00320	1744	-362
0.52500	6.040	0.8193	0.00542	1115	-241
1.01500	6.520	0.8844	0.01048	622	-138
1.44500	6.920	0.9387	0.01492	464	-74
1.93500	6.960	0.9441	0.01997	348	-65
2.28000	7.090	0.9617	0.02353	301	-45
2.66000	7.220	0.9794	0.02746	263	-21
3.20000	7.372	1.0000	0.03303	223	#DIV/0!

Table B.26 Calculated data for adsorbed carbon dioxide on zeolite 13X at T = 308 K in Ono-Kondo coordinates with estimated Henry's constants.

pressure (MPa)	absolute adsorption (mol/kg)	a/a_m	x_b	X axis	Y axis
0.00126	0.825	0.1192	0.00001	65562	101476
0.00407	1.458	0.2107	0.00004	35870	19275
0.00905	2.060	0.2977	0.00009	22792	4943
0.01325	2.400	0.3468	0.00013	18137	2198
0.02007	2.734	0.3951	0.00020	13640	412
0.04515	3.380	0.4884	0.00045	7496	-773
0.09503	4.050	0.5853	0.00095	4267	-740
0.16000	4.490	0.6488	0.00160	2810	-597
0.22000	4.740	0.6850	0.00220	2157	-505
0.28000	4.960	0.7168	0.00280	1774	-429
0.37000	5.167	0.7467	0.00370	1398	-358
0.48500	5.315	0.7681	0.00484	1097	-305
0.57000	5.399	0.7802	0.00569	948	-276
0.70000	5.586	0.8072	0.00699	799	-230
0.87500	5.718	0.8263	0.00874	654	-195
1.01500	5.803	0.8386	0.01014	572	-174
1.20000	5.942	0.8587	0.01198	496	-148
1.50500	6.116	0.8838	0.01503	407	-118
1.83000	6.291	0.9091	0.01828	344	-93
2.23500	6.510	0.9408	0.02232	292	-64
2.50000	6.631	0.9582	0.02497	266	-47
2.86000	6.769	0.9782	0.02856	237	-23
3.06500	6.885	0.9949	0.03061	225	25
3.36500	6.920	1.0000	0.03361	206	#DIV/0!

Table B.27 Calculated data for adsorbed carbon dioxide on zeolite 13X at T = 323 K in Ono-Kondo coordinates with estimated Henry's constants.

pressure (MPa)	absolute adsorption (mol/kg)	a/a_m	x_b	X axis	Y axis
0.00106	0.356	0.0618	0.00001	35267	114386
0.00214	0.529	0.0918	0.00002	25958	43216
0.00501	1.060	0.1840	0.00005	22217	17441
0.00907	1.430	0.2482	0.00009	16556	7177
0.02423	2.090	0.3627	0.00023	9058	789
0.04220	2.490	0.4321	0.00040	6196	-205
0.07503	2.900	0.5033	0.00071	4059	-520
0.14500	3.400	0.5901	0.00138	2462	-492
0.27000	3.915	0.6795	0.00257	1523	-355
0.39000	4.100	0.7116	0.00371	1104	-304
0.54500	4.329	0.7513	0.00519	834	-243
0.70500	4.532	0.7865	0.00671	675	-197
0.85000	4.740	0.8226	0.00809	586	-158
1.01000	4.820	0.8365	0.00962	501	-141
1.17500	4.930	0.8556	0.01119	441	-121
1.45500	5.200	0.9025	0.01386	375	-81
1.72000	5.240	0.9094	0.01638	320	-74
2.12500	5.430	0.9424	0.02024	268	-46
2.69500	5.620	0.9754	0.02566	219	-11
3.39500	5.762	1.0000	0.03233	178	#DIV/0!

APPENDIX C

CALCULATIONS FOR ONO-KONDO PARAMETERS FOR BINARY MIXTURES

1. Calculation of the total number of particles per volume (nN_A/V) for binary mixtures from the classical ideal gas law equation;

$$
\begin{aligned}
(x_i P)V &= nRT \\
(x_i P)V &= n(N_A k)T \\
\frac{nN_A}{V} &= \frac{(x_i P)}{kT} \\
\frac{[mole][\frac{molecules}{mole}]}{[m^3]} &= \frac{[Pa]}{[\frac{J}{K}][K]} \\
\frac{[\text{molecules}]}{[\text{m}^3]} &= \frac{\frac{[\text{N}]}{[\text{m}^2]}}{[\frac{\text{N.m}}{\text{K}}][K]} \\
\frac{[\text{molecules}]}{[\text{m}^3]} &= \frac{[\text{values}]}{[m^3]}
\end{aligned}
$$

where x_i is mole fraction of any individual gas component in a gas mixtures, P is pressure of the gases [Pa], V is total volume of the container containing the gases [m^3], n is the number of moles [mole], N_A is Avogadro number [molecules/mole], k is Boltzmann's constant [J/K], and T is absolute temperature [K].

2. In order to plot $\frac{1}{x_B}\ln\frac{x_A}{(1-x_A-x_B)x_{A\infty}H_A}$ vs $\frac{x_A}{x_B}$, and $\frac{1}{x_A}\ln\frac{x_B}{(1-x_A-x_B)x_{B\infty}H_B}$ vs $\frac{x_B}{x_A}$, it must be calculated $\frac{x_A}{x_B}$, $\frac{x_B}{x_A}$, $x_{A\infty}$, and $x_{B\infty}$ by using data from [70]. Here, it can be defined x_A or $x_B = \frac{\text{absolute adsorption}}{\text{max absolute adsorption}}$, and $x_{A\infty}$ or $x_{B\infty} = \frac{\pi}{6}n\sigma^3$, where $\sigma_{N_2} = 3.745\times10^{-10}$ m, $\sigma_{CH_4} = 3.7838\times10^{-10}$ m, and $\sigma_{CO_2} = 4.328\times10^{-10}$ m. For example, calculated all parameters for CH_4/CO_2 binary

system adsorbed on activated carbon Filtrasorb 400 at T = 318.2 K with ratio 80.0%: 20.0% ⇔ CH_4: CO_2 show in Table C.1.

Table C.1 All parameters for CH_4/CO_2 binary system adsorbed on activated carbon Filtrasorb 400 at T = 318.2 K with ratio 80.0%: 20.0% ⇔ CH_4: CO_2. Specified CH_4 is *A* component and CO_2 is *B* component.

pressure (MPa)	composition 80% CH_4	absolute adsorption of CH_4 (mol/kg)	x_A	$x_{A\infty}$	composition 20% CO_2	absolute adsorption of CO_2 (mol/kg)	x_B	$x_{B\infty}$
0.77	0.890	1.960	0.319	0.004	0.110	0.571	0.093	0.001
1.46	0.886	2.591	0.422	0.008	0.114	0.794	0.129	0.002
2.81	0.884	3.225	0.525	0.016	0.116	1.082	0.176	0.003
4.12	0.883	3.556	0.579	0.023	0.117	1.291	0.210	0.005
5.55	0.877	3.789	0.617	0.031	0.123	1.462	0.238	0.007
6.92	0.871	3.951	0.643	0.039	0.129	1.588	0.258	0.009
8.30	0.866	4.042	0.658	0.046	0.134	1.684	0.274	0.011
9.67	0.861	4.127	0.672	0.054	0.139	1.771	0.288	0.013
11.04	0.856	4.194	0.683	0.061	0.144	1.839	0.299	0.015
12.41	0.852	4.253	0.692	0.068	0.148	1.892	0.308	0.018

3. Calculated data for binary mixtures (CH_4/CO_2, CH_4/N_2, and N_2/CO_2) on activated carbon Filtrasorb 400 at T = 318.2 K in Ono-Kondo coordinates (equations 4.20 and 4.21) with estimated Henry's constants can be shown in Tables C.2, C.3, and C.4, respectively.

Table C.2 Calculated data for CH_4/CO_2 binary mixtures on activated carbon Filtrasorb 400 at 318.2 K in Ono-Kondo coordinates with estimated Henry's constants (CH_4 is *A*, and CO_2 is *B* component).

				Coordinated Eq. (4.20)		Coordinated Eq. (4.21)	
x_A	$x_{A\infty}$	x_B	$x_{B\infty}$	X axis	Y axis	X axis	Y axis
				80.0% CH_4		20.0% CO_2	
0.319	0.004	0.093	0.001	3.433	7.683	0.291	2.061
0.422	0.008	0.129	0.002	3.263	4.855	0.306	1.378
0.525	0.016	0.176	0.003	2.981	3.409	0.336	1.191
0.579	0.023	0.210	0.005	2.754	3.162	0.363	1.310
0.617	0.031	0.238	0.007	2.592	3.402	0.386	1.472
0.643	0.039	0.258	0.009	2.488	3.972	0.402	1.728
0.658	0.046	0.274	0.011	2.400	4.532	0.417	2.005
0.672	0.054	0.288	0.013	2.330	5.706	0.429	2.543
0.683	0.061	0.299	0.015	2.281	7.768	0.438	3.471
x_A	$x_{A\infty}$	x_B	$x_{B\infty}$	60.0% CH_4		40.0% CO_2	
0.220	0.003	0.175	0.001	1.262	3.294	0.793	3.074
0.295	0.007	0.253	0.003	1.164	1.681	0.859	2.024
0.355	0.014	0.342	0.006	1.038	1.035	0.963	1.657
0.384	0.020	0.406	0.010	0.945	0.995	1.059	1.752
0.399	0.027	0.456	0.014	0.876	1.178	1.142	2.061
0.413	0.033	0.488	0.018	0.846	1.537	1.183	2.382
0.413	0.039	0.520	0.022	0.793	1.878	1.260	3.001
0.418	0.044	0.541	0.027	0.773	2.489	1.293	3.755
x_A	$x_{A\infty}$	x_B	$x_{B\infty}$	40.1% CH_4		59.9% CO_2	
0.141	0.003	0.256	0.003	0.551	1.419	1.815	3.733
0.184	0.006	0.368	0.005	0.501	0.514	1.996	2.246
0.211	0.011	0.486	0.011	0.434	0.161	2.307	1.984
0.221	0.016	0.570	0.017	0.389	0.203	2.573	2.158
0.227	0.020	0.626	0.024	0.362	0.397	2.759	2.603
0.225	0.024	0.676	0.030	0.333	0.649	3.001	3.626
0.228	0.028	0.707	0.038	0.322	1.021	3.109	4.652
0.228	0.032	0.735	0.046	0.311	1.581	3.219	6.435
0.231	0.036	0.752	0.053	0.307	2.423	3.261	9.062
x_A	$x_{A\infty}$	x_B	$x_{B\infty}$	20.0% CH_4		80.0% CO_2	
0.069	0.0017	0.347	0.004	0.198	0.376	5.054	5.732
0.084	0.0033	0.470	0.008	0.178	-0.139	5.625	3.192
0.090	0.0065	0.619	0.017	0.146	-0.365	6.851	2.597
0.091	0.0092	0.711	0.027	0.129	-0.259	7.781	3.176
0.088	0.0116	0.773	0.037	0.114	-0.120	8.779	4.827
0.089	0.0136	0.814	0.047	0.109	0.134	9.186	6.488
0.087	0.0154	0.843	0.057	0.103	0.356	9.703	8.555
0.086	0.0168	0.856	0.068	0.101	0.442	9.940	8.901

Table C.3 Calculated data for CH_4/N_2 binary mixtures on activated carbon Filtrasorb 400 at 318.2 K in Ono-Kondo coordinates with estimated Henry's constants (CH_4 is *A*, and N_2 is *B* component).

				Coordinated Eq. (4.20)		Coordinated Eq. (4.21)	
x_A	$x_{A\infty}$	x_B	$x_{B\infty}$	X axis	Y axis	X axis	Y axis
				81.7% CH_4		18.3% N_2	
0.292	0.003	0.042	0.001	6.89	23.30	0.145	-0.03
0.438	0.006	0.057	0.003	7.69	15.27	0.130	-0.29
0.601	0.013	0.069	0.005	8.68	12.77	0.115	-0.16
0.692	0.020	0.072	0.007	9.65	12.73	0.104	-0.12
0.763	0.027	0.071	0.009	10.81	14.90	0.093	-0.01
0.804	0.033	0.074	0.011	10.81	16.11	0.093	0.25
0.843	0.041	0.075	0.013	11.25	19.28	0.089	0.54
0.874	0.048	0.076	0.015	11.52	23.89	0.087	0.95
0.901	0.054	0.075	0.016	12.02	32.62	0.083	1.61
x_A	$x_{A\infty}$	x_B	$x_{B\infty}$	60.0% CH_4		40.0% N_2	
0.225	0.002	0.097	0.003	2.31	11.57	0.433	0.34
0.332	0.004	0.132	0.005	2.51	7.88	0.398	0.02
0.557	0.012	0.184	0.014	3.03	5.84	0.330	0.16
0.617	0.017	0.194	0.018	3.18	6.09	0.314	0.35
0.668	0.022	0.201	0.023	3.32	6.77	0.301	0.61
0.711	0.027	0.203	0.027	3.51	8.10	0.285	0.94
0.738	0.031	0.206	0.030	3.57	9.43	0.280	1.35
0.764	0.036	0.209	0.034	3.65	12.25	0.274	2.13
x_A	$x_{A\infty}$	x_B	$x_{B\infty}$	40.0% CH_4		60.0% N_2	
0.153	0.001	0.154	0.004	0.99	8.35	1.008	1.65
0.242	0.002	0.228	0.008	1.06	5.09	0.944	0.89
0.337	0.004	0.283	0.014	1.19	4.26	0.840	0.58
0.409	0.007	0.315	0.020	1.30	4.12	0.769	0.63
0.457	0.010	0.343	0.025	1.33	4.00	0.751	0.91
0.499	0.013	0.362	0.031	1.38	4.27	0.725	1.24
0.536	0.016	0.371	0.037	1.44	4.88	0.692	1.63
0.565	0.019	0.378	0.042	1.49	5.78	0.670	2.21
0.586	0.022	0.387	0.048	1.52	7.29	0.659	3.23
x_A	$x_{A\infty}$	x_B	$x_{B\infty}$	20.0% CH_4		80.0% N_2	
0.074	0.0005	0.211	0.004	0.353	6.28	2.832	5.61
0.119	0.0010	0.315	0.008	0.378	4.08	2.646	3.19
0.174	0.0019	0.421	0.016	0.413	3.15	2.423	2.28
0.219	0.0030	0.492	0.023	0.445	2.91	2.248	2.23
0.274	0.0057	0.580	0.038	0.473	2.93	2.114	3.09
0.298	0.0071	0.605	0.045	0.493	3.28	2.027	3.74
0.312	0.0086	0.629	0.052	0.497	3.72	2.014	4.87
0.323	0.0102	0.650	0.059	0.496	4.57	2.015	6.82

Table C.4 Calculated data for N_2/CO_2 binary mixtures on activated carbon Filtrasorb 400 at 318.2 K in Ono-Kondo coordinates with estimated Henry's constants (N_2 is *A*, and CO_2 is *B* component).

				Coordinated Eq. (4.20)		Coordinated Eq. (4.21)	
x_A	$x_{A\infty}$	x_B	$x_{B\infty}$	X axis	Y axis	X axis	Y axis
				80.0% N_2		20.0% CO_2	
0.198	0.005	0.073	0.0004	2.723	2.984	0.367	5.271
0.294	0.009	0.115	0.001	2.549	1.451	0.392	2.974
0.387	0.017	0.170	0.001	2.283	0.880	0.438	2.446
0.452	0.026	0.224	0.002	2.017	0.865	0.496	2.552
0.490	0.034	0.271	0.003	1.811	1.069	0.552	2.810
0.516	0.042	0.311	0.004	1.661	1.435	0.602	3.099
0.537	0.051	0.345	0.005	1.555	1.990	0.643	3.413
0.552	0.059	0.373	0.006	1.477	2.746	0.677	3.866
0.563	0.067	0.402	0.007	1.401	4.135	0.714	4.925
x_A	$x_{A\infty}$	x_B	$x_{B\infty}$	58.1% N_2		41.9% CO_2	
0.138	0.005	0.158	0.001	0.873	-0.862	1.146	6.058
0.182	0.008	0.228	0.002	0.798	-0.928	1.254	4.250
0.227	0.015	0.329	0.003	0.690	-0.846	1.450	3.438
0.251	0.023	0.429	0.006	0.585	-0.649	1.708	3.543
0.267	0.037	0.560	0.011	0.476	-0.127	2.101	4.198
0.269	0.043	0.611	0.014	0.440	0.238	2.271	4.926
0.271	0.049	0.654	0.017	0.415	0.742	2.410	6.001
0.269	0.056	0.698	0.021	0.385	1.669	2.597	8.647
x_A	$x_{A\infty}$	x_B	$x_{B\infty}$	40.0% N_2		60.0% CO_2	
0.085	0.004	0.207	0.002	0.410	-1.799	2.437	7.461
0.112	0.007	0.306	0.003	0.365	-1.607	2.740	4.862
0.131	0.013	0.448	0.006	0.293	-1.418	3.418	4.216
0.134	0.019	0.563	0.010	0.239	-1.210	4.189	4.559
0.134	0.025	0.646	0.015	0.207	-0.961	4.827	5.124
0.134	0.030	0.711	0.021	0.188	-0.647	5.312	5.917
0.134	0.035	0.762	0.026	0.176	-0.252	5.694	7.739
0.136	0.039	0.800	0.035	0.170	0.231	5.875	9.441
0.134	0.044	0.834	0.041	0.161	0.910	6.229	13.746
x_A	$x_{A\infty}$	x_B	$x_{B\infty}$	20.0% N_2		80.0% CO_2	
0.042	0.0024	0.284	0.003	0.148	-1.949	6.772	10.908
0.052	0.0052	0.451	0.006	0.116	-1.769	8.655	7.613
0.053	0.0122	0.720	0.021	0.073	-1.187	13.614	7.706
0.051	0.0150	0.798	0.030	0.063	-0.883	15.793	10.862
0.051	0.0172	0.853	0.041	0.059	-0.462	16.885	15.237
0.050	0.0191	0.892	0.051	0.056	0.005	17.841	22.072
0.051	0.0208	0.920	0.062	0.055	0.670	18.172	32.097
0.051	0.0223	0.942	0.073	0.054	2.043	18.457	55.918

VITAE

Name Miss Panita Sumanatrakul

Student ID 5010130008

Educational Attainment

Degree	Name of Institution	Year of Graduation
B.Sc. (Polymer Science)	Prince of Songkla University	2003
Master of Engineering (Chemical Engineering)	Prince of Songkla University	2006

Scholarship Awards during Enrolment

1) Talent of Science (ทุนความสามารถพิเศษทางวิทยาศาสตร์) from faculty of Science, Prince of Songkla University since 1999-2003.
2) Excellent school-record (ทุนผลการเรียนดีเด่น) from Graduate School, Prince of Songkla University since 2003-2006.
3) Prince of Songkla University Graduate Studies Grant Contract 2007 Academic Year (ทุนบัณฑิตศึกษาสงขลานครินทร์) from Graduate School, Prince of Songkla University since 2007-2009.

Work – Position and Address (If Possible)

Scientist in Center for Scientific and Technological Equipments, Walailak University since 2006-2007.

List of Publication and Proceeding (If Possible)

1) Chiraphon Chaibundit, **Panita Sumanatrakool**, Supaporn Chinchew, Proespichaya Kanatharana, Carin E. Tattershall, Colin Booth, and Xue-Feng Yuan. 2005. Association properties of diblock copolymer of ethylene oxide and 1,2-butylene oxide: $E_{17}B_{12}$ in aqueous solution, Journal of Colliod and Interface Science, 283: 544-554.

2) **พนิตา สุมานะตระกูล**, ชญานุช แสงวิเชียร และอรสา ภัทรไพบูลย์ชัย, "อิทธิพลของยางรี-เคลมต่อผลของคุณสมบัติการเชื่อมโยงและคุณสมบัติเชิงกลของของผสมเทอร์โม-พลาสติกอิลาสโตเมอร์", การประชุมวิชาการวิศวกรรมเคมีและเคมีประยุกต์แห่งประเทศไทย ครั้งที่ 15, โรงแรมจอมเทียนปาล์ม บีช รีสอร์ท พัทยา, ชลบุรี, 17-28 ตุลาคม 2548.
3) **พนิตา สุมานะตระกูล**, ชญานุช แสงวิเชียร และอรสา ภัทรไพบูลย์ชัย, "การศึกษาสูตรที่เหมาะสมสำหรับการผลิตเครื่องหมายนำทางจากยางธรรมชาติที่นำกลับมาใช้ใหม่", การประชุมวิชาการทางวิศวกรรมศาสตร์ มหาวิทยาลัยสงขลานครินทร์ ครั้งที่ 4 หาดใหญ่ สงขลา, 8-9 ธันวาคม 2548.
4) Chayanoot Sangwichien, **Panita Sumanatrakool** and Orasa Patarapaiboolchai, Effect of filler loading on curing characteristics and mechanical properties of thermoplastic vulcanizate, Chiang Mai J. Sci. 35(1), (2008), p.141-149.
5) ชญานุช แสงวิเชียร, สุภาพร ราชการกลาง, **พนิตา สุมานะตระกูล**, สุภวรรณ ฏิระวณิชย์กุล, อรสา ภัทรไพบูลย์ชัย, "การออกแบบและทดสอบหลักกั้นเส้นทางจราจรที่ผลิตจากยางธรรมชาติ", การประชุมวิชาการทางวิศวกรรมศาสตร์มหาวิทยาลัยสงขลานครินทร์ ครั้งที่ 6, 8 - 9 พฤษภาคม 2551, คณะวิศวกรรมศาสตร์ มหาวิทยาลัยสงขลานครินทร์ จังหวัดสงขลา.
6) **Panita Sumanatrakool**, Chayanoot Sangwichien, Marc D. Donohue, and Gregory L. Aranovich, "Analysis of adsorption isotherms for greenhouse gases using Ono-Kondo equation", การประชุมวิชาการวิศวกรรมเคมีและเคมีประยุกต์แห่งประเทศไทย ครั้งที่ 19, 26-27 ตุลาคม 2552, เฟลิกซ์ ริเวอร์ แคว รีสอร์ท จังหวัดกาญจนบุรี.
7) **Panita Sumanatrakul**, Chayanoot Sangwichien, Marc D. Donohue, and Gregory L. Aranovich, "Evaluation of adsorbate-adsorbate interaction for supercritical fluids using Ono-Kondo equation", The 2010 International Conference on Chemical Engineering and Applications-CCEA 2010 (Proceeding), Quality Hotel, Singapore, Feb 26-28, 2010.
8) Chayanoot Sangwichien, Arrisa Ruangmee, **Panita Sumanatrakul**, "Separation Efficiency of Oil Palm Shell and Kernel Mixture by using Different Types of Media", The 2010 International Conference on Chemical Engineering and Applications-CCEA 2010 (Proceeding), Quality Hotel, Singapore, Feb 26-28, 2010.